SATELLITE BASED TOP-DOWN APPROACH FOR MODELLING AEROSOL SOURCE STRENGTH AND ITS APPLICATION IN DISCERNING RAINFALL TRENDS
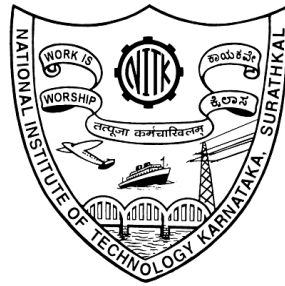
Thesis

Submitted in partial fulfillment of the requirements for the degree of

DOCTOR OF PHILOSOPHY

by

SINAN NIZAR

DEPARTMENT OF WATER RESOURCES & OCEAN ENGINEERING

NATIONAL INSTITUTE OF TECHNOLOGY KARNATAKA

SURATHKAL, MANGALORE - 575025

May, 2021

"In the name of Allah,
The Most Gracious and The Most Merciful"
"By the winds scattering dust,
and the clouds loaded with rain," (Qur'an: 51.1-2)

Dedicated to...

To my parents who helped me in all things great and small,
my wife for her support,
my brothers,
&
all my Teachers and Colleagues...

DECLARATION

By the Ph.D. Research Scholar

I hereby *declare* that the Research Thesis entitled **SATELLITE BASED TOP-DOWN APPROACH FOR MODELLING AEROSOL SOURCE STRENGTH AND ITS APPLICATION IN DISCERNING RAINFALL TRENDS** which is being submitted to the **National Institute of Technology Karnataka, Surathkal** in partial fulfillment of the requirements for the award of the Degree of **Doctor of Philosophy** in **Civil Engineering** is a *bonafide report of the research work carried out by me*. The material contained in this Research Thesis has not been submitted to any University or Institution for the award of any degree.
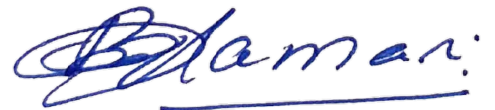
Sinan Nizar

Reg. No.: 155053 AM15F08

Department of Water Resources and Ocean Engineering

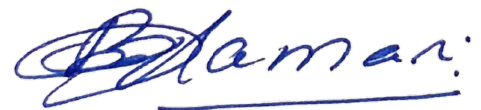Place: NITK, Surathkal.

Date: May, 2021

CERTIFICATE

This is to *certify* that the Research Thesis entitled **SATELLITE BASED TOP-DOWN APPROACH FOR MODELLING AEROSOL SOURCE STRENGTH AND ITS APPLICATION IN DISCERNING RAINFALL TRENDS** submitted by **SINAN NIZAR**, (Reg. No.: 155053 AM15F08) as the record of the research work carried out by him, is *accepted as the Research Thesis submission* in partial fulfillment of the requirements for the award of degree of **Doctor of Philosophy**.

(Prof. B.M. Dodamani)

Research Supervisor

Chairman - DTAC

ACKNOWLEDGMENT

ABSTRACT

This thesis is dedicated to study the possible relationship between the distribution of aerosols and rainfall patterns. The thesis proposes a new approach, wherein aerosol sources are investigated rather than the aerosol loading in a region to understand its variation with rainfall. The study first investigates the influence of meteorological parameters indicating both advection and diffusion on the spatiotemporal distribution of aerosols over the Indian subcontinent and the adjacent Indian Ocean. The research inferences are then used to develop a model to estimate aerosol emissions using satellite data. Further, the spatial aerosol source distribution is used to investigate rainfall variability over southern India.

The prevailing meteorological conditions that influence the advection and diffusion of the atmosphere govern the distribution of atmospheric particles from its sources. The present study first explores the spatiotemporal distribution of atmospheric aerosols over the Indian subcontinent and its dependence on the prevailing meteorological conditions. Eleven years of Aerosol Optical Depth obtained from the Moderate Resolution Imaging Spectroradiometer along with meteorological parameters extracted from reanalysis data are analysed at monthly timescales. Wind speed, wind divergence and planetary boundary layer height are studied as parameters for advection and diffusion of atmospheric aerosols. The result shows the importance of both advection and diffusion in distributing aerosols over the region. The result shows higher aerosol loading during the monsoon season with increased spatial variability.Wind speed and divergence correlate with AOD values both over land (R = 0.75) and ocean (R = 0.82) with increased aerosol loading at higher wind speeds, which are converging in nature. Owing to the varied climatology of the Indian subcontinent, land and ocean areas were classified into subregions. Analysis was carried out over these subregions to infer the influence of meteorological conditions on aerosol loading. Results are indicative of a distinct characteristic in the prevailing meteorological conditions that influence the distribution of

certain aerosol types. Further, the PBLH was analysed as an indicator of atmospheric diffusion to infer its importance in aerosol distribution. The results indicate that PBLH explains almost 30 to 90% of the total variance in AOD over the subregions which is particularly evident during the winter and pre-monsoon seasons.

The study further uses a Lagrangian approach to the Advection Diffusion Equation to estimate the transported aerosols and hence the Aerosol Source Strength using satellite-measured Aerosol Optical Depth (AOD) and reanalysis wind data. This top-down approach is based on the advection and diffusion of atmospheric aerosols considering wind circulation and atmospheric conditions rather than using indicative parameters. To validate the current top down approach, the study first utilises the AOD measurements from the GOES-16 for California and then applies the methodology over southern India using MODIS to identify aerosol hotspots. The results over California are indicative of higher ASS around wildfire locations. The ASS values also show good correlation (R^2 = 0.886) with Fire Radiative Power (FRP) obtained from TerraMODIS fire product. Themethodwas further applied to investigate the spatial correlation of ASS with power plant density, which reveals a steady increase in ASS with power plant density (R^2 = 0.82).

Finally the study investigates the possible relationship between rainfall and aerosol source distribution over southern India during the pre-monsoon season. Aerosol and rainfall trends are computed using Mann Kendall trend test and are correlated spatially with AOD and ASS. To further understand the relationship, cloud microphysics is also investigated. The results indicate that, though the aerosol loading initially supports cloud formation resulting in deeper and wider clouds, higher aerosol loading inhibits cloud formation resulting in narrow and shallow clouds. This in turn decreases rainfall at higher aerosol loading with smaller cloud radius.

Keywords: Aerosols, rainfall, cloud microphysics, AOD, MODIS, aerosol sources, wildfire, power plant, biomass burning.

Contents

List of Figures

List of Tables

Nomenclature and Abbreviations

Symbol		Representation
u	:	Zonal wind
V	:	Meridional wind
w	:	Vertical wind
ϕ	:	Latitude
λ	:	Longitude
r	:	Earth's radius
ρ	:	Aerosol extinction coefficient per unit volume
D	:	Turbulent diffusion coefficient
κ	:	Von Karman constant
u_*	:	Shear velocity
z	:	Depth of flow
f	:	Coriolis parameter
ω	:	Rotation rate of the Earth
L	:	Obukhov length
ψ_m	:	Integrated form of the universal function
ζ	:	Stability parameter
τ_T	:	Columnar transported AOD

Abbreviations and expansions	
AOD : Aerosol Optical Depth	PBLH : Planetary Boundary Layer Height
SS : Sea Salt Aerosol	DU : Dust Aerosol
OC : Organic Carbon	SU : Sulphate Aerosol
PRE : Proportional Reduction in Error	IGP : Indo-Gangetic Plain
ADE : Advection-Diffusion Equation	ASS : Aerosol Source Strength
FRP : Fire Radiating Power	CPCB : Central Pollution Control Board
CF : Cloud Fraction	CTP : Cloud Top Pressure
CTT : Cloud Top Temperature	ER : Cloud Effective Radius

Chapter 1

INTRODUCTION

1.1 INTRODUCTION

Earth is blessed with the priceless gift of life. This life, whether in a single celled organism or in a complex species of animals is dependent on water. To be precise, the cycling of water among various storages is of paramount importance to sustain life. This cycling of water between land, ocean and the atmosphere is called the hydrologic cycle or water cycle. But this cycle is vulnerable to both anthropogenic as well as natural influence. Atmospheric particles such as aerosols that are released from numerous natural and anthropogenic sources are capable of influencing the climate dynamics and hence the water cycle (Ramanathan et al., 2005). Being the second most populated country and a host of varied geographic features, India experiences differential aerosol loading from numerous natural and anthropogenic sources. Cloud, aerosol, and dynamical processes remain at the core of uncertainties about atmospheric aspects of climate and continue to be the subject of detailed research.

1.2 DEFINITIONS

Aerosols are suspended solid or liquid particles in the Earth's atmosphere. Though short lived, their presence is always felt in the atmosphere due to numerous anthropogenic and natural sources. Wind advect these particles from their sources rendering a heterogeneous spatial and temporal distribution over the globe. Though these microscopic particles are not visible to the naked eye, their collective effect is visible in the atmosphere at higher concentrations (eg. haze, smoke plume). Aerosols are mostly pro-

duced near the Earth's surface and hence more concentrated in the lower troposphere near the sources. Aerosols are generally characterized based on the properties of a population of aerosols rather than individual particles. Based on its properties there are several classifications of aerosols.

1. **_Based on Mode of Emission_** - Primary and secondary aerosols. the former is directly emitted into the atmosphere as particles, whereas the later is emitted as gas phase aerosol precursors and undergoes numerous chemical transformations before they condense to particulate phase.

2. **_Based on Emission Environment_** - These includes urban aerosols, continental aerosols, desert aerosols, marine aerosols etc. As the name suggests these classes designate aerosols from a particular environment under the assumption that some of the aerosol properties vary systematically with the environment.

3. **_Based on Origin_** - Natural and anthropogenic aerosols. Emissions from soil, wildfires, ocean, and volcanoes are examples of natural sources. Fossil fuel combustion, agricultural biomass burning, industrial and vehicular effluents etc. which are caused humans are examples of anthropogenic sources.

1.3   AEROSOL SOURCES

Aerosols originate from various sources and have similar characteristics. As the present study tries to estimate aerosol sources this section lists some of the prominent aerosol sources.

1. **_Marine Aerosols_** - These are emitted from ocean surfaces due to wind friction. The sea salt aerosol emission depends on the surface wind speed, sea state, atmospheric stability, sea surface temperature, and seawater composition (Blanchard, 1963; Struthers et al., 2013).

2. **_Desert Dust_** - These are formed by wind friction that detaches soil particles from continental surfaces and suspends them in the atmosphere. Apart from the meteorological conditions, desert dust emission depends on many soil-related parameters such as moisture, texture, and vegetation (Kok, 2011).

2

3. ***Volcanic Aerosols*** - Explosive eruptions from volcanoes emit fragments of rocks and minerals forming volcanic aerosols. Depending on the eruption, these may be injected to various heights in the atmosphere.

4. ***Biomass Burning Aerosols*** - Biomass burning emission is yet another source of trace gases and aerosols and its emission is estimated based on the burned area, biomass fuel load, fraction of biomass burned, and emission factors (Li et al., 2019; Yin et al., 2019). These may be from natural or anthropogenic sources and includes organic carbon, black carbon and aerosol precursors such as sulphur dioxide.

5. ***Fossil Fuel Combustion*** - These are the major sources of air pollution in developing and industrialized countries and stems from the combustion of coal and oil products. Black carbon, organic carbon, and sulphate aerosols from sulphur dioxide are the major constituents of this source.

1.4 AEROSOL-CLOUD-RADIATION INTERACTIONS

The later part of the thesis investigates the cloud microphysics to ascertain its impact on aerosol rainfall interaction. Complex interaction of atmospheric aerosols with electromagnetic radiation have acknowledged their importance in radiation budget and hence climate dynamics (Schwartz, 1996; Ramanathan et al., 2005; Guleria and Kuniyal, 2013, 2016). Depending on their type they may absorb and/or scatter longwave and shortwave radiations (Chyacutelek and Coakley, 1974; Penner et al., 1994). Being cloud condensation nuclei they also influence cloud lifetime and microphysics (Twomey, 1977; Steinfeld, 1998; Li et al., 2017). Water vapour condenses upon these cloud condensation nuclei and controls the size of cloud water droplets.

On the other hand, precipitating clouds also influence aerosol distribution by wet deposition of atmospheric aerosols, thus constituting an important sink for aerosols. Coalescence of coud droplets forms larger droplets thereby mixing aerosols and activates smaller aerosols that can serve as cloud condensation nuclei in other clouds. As the cloud grows they scatter more soar radiation and reflects a significant fraction of solar radiation back to space cooling the atmosphere. Though in small fraction, clouds

also absorbs solar radiation thus heating the atmosphere. The cooling and warming depends on the thickness and height of the cloud and its optical and microphysical properties.

Aerosols influence climate in a number of ways. These effects can be grouped as aerosol-radiation interaction (direct effect and semi-direct effect) and aerosol-cloud interaction (aerosol first and second indirect effect).

1. *Aerosol Direct Effect* - Atmospheric aerosols scatter solar radiation and prevents a portion of it from reaching the Earth's surface. This cools the climate system with a loss of energy. Certain aerosols absorb solar radiation and results in heating of the aerosol layers. But the net effect is to block the absorbed portion of the solar radiation from reaching the Earth's surface. This reduction of solar radiation preferentially during clear sky condition is called the *aerosol direct effect*.

2. *Aerosol Semi-direct Effect* - As the aerosol layers heats up due to absorption of solar radiation, it modifies the vertical temperature profile. This further impacts the atmospheric stability, relative humidity and therefore cloud formation. This is called *aerosol semi-direct effect*.

3. *Aerosol First Indirect Effect* - Aerosols being cloud condensation nuclei, influences cloud optical and microphysical properties. For a fixed cloud liquid water content, an increase in aerosol concentration results in large number of smaller cloud droplets and increased cloud reflectivity. Net effect is to cool the climate system by reflecting more solar radiation back to space. This effect is called the *aerosol first indirect effect*.

4. *Aerosol Second Indirect Effect* - Apart from the first indirect effect, increase in aerosols also enhances cloud lifetime and requires more moisture to generate droplets that are large enough to initiate precipitation. This effect is called *aerosol second indirect effect*.

Besides these atmospheric interactions, aerosols are also associated with adverse impact on human health (Hoek et al., 2002; Pope et al., 2004; Fuzzi et al., 2015) and agriculture (Ainsworth and Long, 2005).

1.5 AEROSOL REMOTE SENSING

Satellite remote sensing has the ability to monitor and quantify aerosol systems on a global scale. Aerosol remote sensing involves the measurement of aerosol properties by virtue of its interaction (scattering and absorption) with electromagnetic radiations. The electromagnetic radiations are either emitted artificially (active remote sensing) or naturally from the shortwave radiations of the Sun or longwave radiations of the Earth (passive remote sensing).

Atmospheric aerosols absorb and scatter electromagnetic radiations and modifies the radiation field. Scattering is the unpredictable diffusion of radiation by particles in the atmosphere, whereas absorption results in effective loss of energy by absorption of energy at a given wavelength. The sum of absorption and scattering is termed as extinction and represents the total effect of a medium in propagating the radiation. The aerosol extinction coefficient is a local property and its vertical integral is called the aerosol optical depth (AOD). AOD is a quantitative estimate of the amount of aerosol present in the atmosphere. The rate of extinction of the light increases as AOD increases. The first satellite instrument capable of crudely monitoring aerosol optical depth from space was the Advanced Very High Resolution Radiometer (AVHRR), which retrieved optical depth from measurements in the visible and near-infrared spectrum, beginning in the late 1970s. Since then, numerous space borne sensors have been used to detect and characterize aerosols.

1.6 MOTIVATION OF THE RESEARCH

Explanation of various possible impacts of atmospheric particles on regional water cycle demands a better understanding and quantification of aerosol processes and interactions. In the case of a developing countries like India, uncontrolled anthropogenic aerosol sources have serious implications on air quality and climate. Therefore, there is an urgent need of measurement and characterisation of aerosol in various parts of India with the focus on understanding the source distribution with respect to space and time. Rapid urbanization and population growth in India has resulted in substantial increase of aerosol emission, most of which is comprised of carbonaceous aerosols from sources

such as industries, thermal power plants and biomass burning. With its importance even in the large scale summer monsoon circulation through the "elevated heat pump mechanism" and the "solar dimming effect" (Lau et al., 2008), there is a need to better understand and estimate aerosol sources and their emissions in India.

This thesis is structured towards the estimation of aerosol emissions using satellite remote sensing. This would provide a better spatial estimate of aerosol source distribution over the Indian subcontinent. This is further utilized to study the impact of emission sources on rainfall variability over the Indian subcontinent.

1.7 RESEARCH GAPS

Traditional bottom-up approach for estimating aerosol source and its emission ia a laborious task. Especially for a country like India, the varying livelihood practices introduces more complexities and parameters which makes it difficult to estimate aerosol emissions. The availability of satellite observations not only enhances the capability of determining various influencing parameters but also provides alternate ways of assessing aerosol sources. Such a satellite based top-down approach was employed by Prijith et al. (2013). Though this approach incorporates the wind factor to estimate aerosol source, huge uncertainties exist as daily sources are estimated based on a single AOD data for a day. This is because as time period increases the wind mass traverse vast distances encountering numerous sources and sinks in its path. An abundant source or sink in its path may be reflected as increased aerosol production or deposition at the computed grid. A better estimate of aerosol sources daily is feasible but at the expense of a coarser resolution. Thus identification of isolated sources is difficult. Moreover the flux continuity equation does not account for the diffusion of aerosols nor the atmospheric stability conditions. Not only the advection of aerosols by wind and its redistribution based on convergence but also the diffusion of these particles during their residence in the atmosphere is an important parameter (Ziomas et al., 1995; Quan et al., 2013; Wang et al., 2016; Su et al., 2018; Nizar and Dodamani, 2019). Hence, the research objectives of the present study have been formulated to address these issues.

1.8 RESEARCH OBJECTIVES

Estimating aerosol sources from satellite remote sensing demands better understanding of various meteorological parameters that influence aerosol distribution. The present study first investigates the influence of meteorological parameters indicating both advection and diffusion on the spatiotemporal distribution of aerosols over the Indian subcontinent and the adjacent Indian Ocean. The research inferences are then used to develop a model to estimate aerosol emissions using satellite data. Further, the spatial aerosol source distribution is used to investigate rainfall variability over southern India. The overall objectives can be summarised as follows:

- To study the spatial and temporal distribution of aerosols over the Indian subcontinent and its dependence on prevailing meteorological conditions.

- To develop a model that incorporates the advection and diffusion of atmospheric particles to ascertain aerosol transportation and hence its source strength.

- To study the influence of various aerosol emission hotspots on rainfall distribution.

1.9 ORGANIZATION AND CONTRIBUTIONS OF THE THESIS

The remaining chapters in this thesis are organized as follows:

Chapter 2: Literature Review

This chapter deals with a critical review of various literature conducted on the distribution of aerosols over the Indian subcontinent, the influence of meteorological parameters on aerosol distribution, its sources and emission quantification, and the impact of aerosols on rainfall.

Chapter 3: Spatio-temporal Distribution of Aerosols Over the Indian Subcontinent and its Dependence on Prevailing Meteorological Conditions

This chapter investigates the influence of meteorological parameters indicating both advection (wind speed and divergence) and diffusion (Planetary Boundary Layer Height, PBLH) on spatiotemporal distribution of aerosols over the Indian subcontinent and the adjacent Indian Ocean. Meteorological parameters such as wind speed, divergence and PBLH from reanalysis data are studied for their possible influence on AOD obtained from MODIS data.

Chapter 4: Satellite-Based Top-Down Lagrangian Approach to Estimate Aerosol Emissions

The availability of satellite observations not only elevates the capability of determining various influencing parameters but also provides alternate ways of assessing aerosol sources. This chapter employs a Lagrangian approach to the Advection Diffusion Equation to estimate the transported aerosols and hence the aerosol source strength using satellite measured aerosol optical depth and reanalysis wind data. This top-down approach is based on the advection and diffusion of atmospheric aerosols considering wind circulation and atmospheric conditions rather than using indicative parameters.

Chapter 5: Investigating the Possible Relationship Between Rainfall and Aerosol Distribution

This chapter presents the variation of aerosols and its association with rainfall trends over southern India.

Chapter 6: Conclusions and Future Directions

This chapter contains the conclusion about the study and future scopes of the developed model.

Chapter 2

LITERATURE REVIEW

2.1 INTRODUCTION

The Indian monsoon (June – September) which can be perceived as a gigantic convection system produced by differential seasonal heating of the continental and the surrounding oceanic areas contributes about 80% of the average annual rainfall in India. With a profound influence of aerosols even on this large-scale circulation (Wang, 2004; Ramanathan et al., 2005; Lau et al., 2008), it is important to understand the spatio-temporal distribution of atmospheric aerosols. Being the second most populated country and a host of varied geographic features, India experiences differential aerosol loading from numerous natural and anthropogenic sources. Cloud, aerosol, and dynamical processes remain at the core of uncertainties about atmospheric aspects of climate and continue to be the subject of detailed research. Studying the impact of aerosols, their distribution, and sources, requires detailed knowledge about the various literatures in this field. In this regard various observational studies and literatures are discussed in this chapter.

2.2 AEROSOL REMOTE SENSING

Satellite aerosol retrievals fundamentally measure the reflected solar radiation at the top-of-the-atmosphere (TOA). This measured up-welling solar radiation at the TOA includes the combined effect of gaseous absorption and molecular scattering, aerosol scattering and absorption, cloud scattering and surface reflection.The first satellite instru-

ment capable of crudely monitoring aerosol optical depth from space was the Advanced Very High Resolution Radiometer (AVHRR), which retrieved optical depth from measurements in the visible and near-infrared spectrum, beginning in the late 1970s. Since then, several algorithms have been applied to satellite datasets to solve the inverse problem of separating the surface and atmospheric scattering contributions. However, these diverse algorithms and approaches do not always give consistent values of the aerosol properties for a given ground scene. Major hurdle in aerosol retrieval is the treatment of bright surfaces whose contribution to the satellite-measured signal is significantly larger than the aerosol contribution. The separation of the small aerosol component from a significantly larger surface term is a large source of error if the surface reflective properties are not accurately characterized. Aerosol retrieval algorithms that use observations of reflected radiance have been based on pre-calculated TOA reflectances assuming aerosol models characterized in terms of aerosol particle size distribution and composition.

The MISR and AATSR uses the multi-angle observations of the same ground scene (Thomas et al., 2005; Grey et al., 2006) making it possible to accurately account for directional surface scattering in the retrieval procedure. The more polarized atmospheric scattering in comparison to surface reflections is employed for aerosol retrieval in some studies eg., POLDER (Deuze et al., 2001). Good agreement between aerosol retrievals from different satellite datasets and algorithms enhances confidence in remotely sensed estimates of AOD, but there is not always consistency between the different aerosol estimates. The MODIS sensors on board the Aqua/Terra platforms (Levy et al., 2010; Hsu et al., 2013) is the first satellite observation plan designed to provide aerosol optical characteristic globally of high spatial resolution. These sensors assumes that the influence of aerosols on the TOA reflectance in the shortwave infrared (SWIR) is negligible and the correlations of reflectances in the visible and SWIR are employed (Kaufman et al., 1997; Remer et al., 2005). It can provide a long time series of AOD products and can be very useful for air quality studies, etc. The operational MODIS AOD product over land is based on two algorithms, namely, the Dark Target (DT) and Enhanced Deep Blue (DB) algorithms. MODIS AOD products have been extensively validated by

numerous researchers (Tripathi et al., 2005; Choudhry et al., 2012; Sayer et al., 2013; Misra et al., 2015). Monthly average AOD (550 nm) from Collection 6.1, level 3 AOD products ($1° \times 1°$) derived from Terra's MODIS measurements are used in this study.

2.3   AEROSOL DISTRIBUTION OVER THE INDIAN SUBCONTINENT

Distribution of aerosols over the Indian subcontinent has been perceived by various observations from multiple platforms such as: ground based, ships, aircrafts, balloons and satellites. Routine measurements of aerosols in India was started in the late 1980's in Trivandrum and a couple of cities in southern India (Sikka, 2002). The Space Physics Laboratory (SPL) group in Trivandrum measured AOD in different wavelengths using multispectral radiometers for over a decade and pointed out some of the aerosol climatology over the region. The SPL group observed a peak AOD during the monsoon season and reported its primary contribution from sea-salt aerosols with occasional contributions from transported desert dust (Moorthy and Satheesh, 2000). They also observed an increasing trend in AOD owing to an increase in urbanization and other anthropogenic sources.

The Indian Space Research Organization established a network of seven stations in India through its Geosphere Biosphere Program for monitoring aerosols using a multi-wavelength solar radiometer. However, a limited number of monitoring stations are not enough to understand the aerosol climatology over the Indian subcontinent owing to its varied meteorological parameters (Singh et al., 2004).

The Indian Ocean Experiment (INDONEX) provided a wider picture of aerosol distribution over the Indian Ocean by integrating simultaneous observations from multiple platforms: ground stations, ships, aircrafts and satellite obervations. The study reports an 80% contribution from anthropogenic sources to the total aerosol loading with influence of long range aerosol transport over the equatorial Indian Ocean (Ramanathan et al., 2001).

Over northern India, a detailed study with continuous measurements using auto-

matic sun and sky radiometers was carried out by Singh et al. (2004). They analysed the spectral, seasonal and interannual variability of aerosols over Kanpur located in the Ganga basin. They reported a mean AOD of 0.6 at 500 nm with prominent seasonal influence. The premonsoon season is clearly distinguished with maximum dust loading, whereas the winter season is dominated by anthropogenic urban-industrial aerosols with an absorbing atmosphere. The diurnal variation of AOD shows maximum variation during the monsoon season with the presence of mixed aerosol type. Overall, they reported an increasing aerosol loading over the region from January 2001 to December 2003.

Though point measurements provide reliable in-depth view of aerosol properties on a local scale, they are not necessarily representative of regional concentration. In this regard, satellites are proved to be a good tool to understand the broad Spatio-temporal characteristics of aerosols and associated effects from global to local scales. The first satellite instrument capable of crudely monitoring aerosol optical depth from space was the Advanced Very High Resolution Radiometer (AVHRR), which retrieved optical depth from measurements in the visible and near-infrared spectrum, beginning in the late 1970s. Satellite based regional distribution of aerosols over the Indian subcontinent and its surrounding oceanic areas has been studied using AVHRR, Polarization and Directionality of the Earth's Reflectance (POLDER), Total Ozone Mapping Spectrometer (TOMS), Moderate Resolution Imaging Spectroradiometer (MODIS), Sea-Viewing Wide Field-of-View Sensor (SeaWiFS), Multi-angle Imaging Spectroradiometer (MISR), and Oceansat Ocean Colour Monitor (IRS-P4-OCM, Rajeev et al. (2004)).

Prasad and Gupta (1998) used the visible and near IR channels of the AVHRR to compute AOD over the Indian Ocean. They compared satellite based estimates from AVHRR and ground based radiometer aerosol data showing comparable results. Their analysis revealed the transportation of dust aerosols from the Thar Desert, displacing the marine aerosols over the Bay of Bengal and the Arabian Sea. The influence of steel plants and other industries on AOD distribution over the east coast was also visible from the AVHRR AOD data. The authors also established the capability of AVHRR data to monitor the intrusion of continental aerosols over the Arabian Sea.

The regional distribution and long-range transport of aerosols over the Indian sub-continent and its surrounding oceanic areas were instigated by Rajeev et al. (2004) using AOD derived from AVHRR and circulation patterns from NCEP reanalysis data. Their study demonstrates the transport of aerosols from continental areas in the northern hemisphere to the oceanic regions from November to April and aerosol transport from the Arabian Desert region to the Arabian Sea from June to September. Thus the northern oceanic regions in general and the Arabian Sea in particular are always under the influence of continental aerosols throughout the year.

AOD computed from AVHRR is limited to oceanic regions whereas sensors such as TOMS and MODIS can produce AOD vales over land surfaces as well. Washington et al. (2003) used TOMS aerosol data to demonstrate the impact of southwest Asian dust storms on aerosol loading over the Indo-Gangetic Plains. Massie et al. (2004) investigated the decadal changes in regional aerosols using TOMS aerosol data from 1979 to 2000. They reported a large increase in aerosol trends between 1979 and 2000 over the Ganga basin. A detailed spatial analysis of AOD climatology over the Indian sub-continent using MISR AOD was provided by Di Girolamo et al. (2004). They examined the regional mean AOD at 558 nm during the winter season (DJF) of 2001-2004. The result shows detailed distribution of high aerosol loading over the Indo-Gangetic basin with higher pollution pool over Bihar.

In general, northern India (20°N-30°N) is subjected to heavier aerosol loading when compared to southern India. The Indo-Gangetic Plains (IGP) in northern India is the major hotspot of aerosol loading (Srivastava et al., 2016). IGP in the south Asian region, where about 16% of the world's population lives is the hub of increasing atmospheric pollution due to urbanization/industrialization and growing energy demands. The Indo-Gangetic plain, which is one of the largest river basins in the world is surrounded by mountain ranges in the north (Himalayas) and south (Vindhya Satpura). The west is bordered by the Thar Desert and the Arabian Sea and the east by the Bay of Bengal. The months from April through early June, which is the premonsoon season in India, witnesses the highest loading of aerosol over the Indo-Gangetic plains and over the elevated slopes of the Himalayas. The westerly air mass that prevail during that time

is responsible for the transport of aerosols. These aerosols have their source in the arid zones of south west Asia namely the Arabian peninsula (Washington et al., 2003). As these mineral aerosols are transported from the Thar Desert, they get mixed with anthropogenic emissions in the Indo-Gangetic plain (Prospero, 2002).

But the prevailing westerlies and the arid sources are not the only reason for such a heavy loading of aerosols over the Indo-Gangetic plain. The Himalayas that borders the Indo-Gangetic plains to the north acts as a barrier that advects the dust aerosols to higher altitudes. Such spatial gradients in aerosol loading with topographical differences near the foothills of Himalayas was observed by Liu et al. (2008). They used CALIPSO lidar observations to investigate the vertical distribution of aerosols over the Tibetan Plateau and the surrounding areas. The transported dust aerosols are found to be vertically advected to elevated altitudes near the Himalayan-Gangetic region primarily driven by atmospheric circulation and guided by the orography of the Himalayas.

Acharya and Sreekesh (2013) presented the spatio-temporal analysis using MODIS level 2 AOD data set. Winter and summer seasons showed the highest aerosol loading whereas the onset of monsoon removes the particles from the atmosphere through precipitation. They inferred that the spatial variability of AOD depends on the source strength of emissions and atmospheric conditions. They also pointed out the necessity of estimating the anthropogenic as well as natural aerosol sources to explain the spatio-temporal variability of aerosols over the Indian subcontinent.

2.4 INFLUENCE OF METEOROLOGICAL PARAMETERS ON AEROSOL DISTRIBUTION

The spatial and temporal distribution of aerosols strongly depends on the distribution of sources/sinks and how these interact with transport. However, aerosol transportation and its distribution is also governed by the prevailing meteorological conditions. Among the various causes of deteriorating air quality, favourable weather conditions are important influencing factors (Zhao et al., 2010). Early studies by SPL group at Trivandrum using ground station data reports that atmospheric stability and wind conditions resulted in a prominent diurnal variation of AOD with increased AOD at higher wind speeds. Moorthy and Satheesh (2000) explored the influence of wind speed on

daily AOD at Minicoy in the Arabian Sea and found an exponentially increasing relationship. Though this remote island is influenced by continental aerosols during certain months, the exponential relation is mainly attributed to higher wind speeds contributing to marine aerosol production. The Indian coastal zones also depicts influence of land sea breeze and relative humidity on aerosol distribution (Sikka, 2002). Using reanalysis wind data and MODIS aerosol product, Aloysius et al. (2008) showed that wind convergence over the Ganga basin is the major factor causing heavy aerosol concentration.

Not only the advection of aerosols by wind and its redistribution based on convergence but also the diffusion of these particles during their residence in the atmosphere is an important parameter. The meteorological conditions that are unfavorable for diffusion causing air pollution in an urban environment were presented by Ziomas et al. (1995). They used meteorological variables such as wind speed, wind direction, and air temperature to forecast pollution episodes and pointed out that meteorological conditions that are unfavorable for dispersion can cause serious air pollution episodes. Tanner and Law (2002) made a substantial study of pollutant gas concentration under various weather systems. They concluded the importance of meteorological conditions rather than changes in emission strength to create pollution episodes in the study area. They also observed the influence of marine air masses on diluting the local pollution during favorable weather systems. In contrast, a continental air mass or a stagnant condition lead to high pollution episodes in the city.

Ding et al. (2004) simulated land sea breeze to understand pollutant transportation. Their simulation indicated a delayed sea breeze onset during pollution episodes due to offshore synoptic winds. The simulation also displayed lower mixing layer height during the pollution episodes. Further they conducted trajectory analysis revealing the transport of pollutants from inland areas.

Demuzere et al. (2009) studied the role of meteorological processes in O_3 and PM_{10} levels in rural mid-latitude sites in the Netherlands. They analyzed rural station measurements of wind speed, wind direction, daily mean, minimum and maximum temperature, and relative humidity to investigate its relation to air quality at a local scale. The study shows various circulation patterns that transport ozone from the free troposphere

towards the surface.

Numerous studies confirms that the synoptic-scale circulation patterns over a region represents a particular atmospheric condition through its relationship with various meteorological parameters. Thus atmospheric circulation patterns can be used instead of individual meteorological parameters to ascertain pollution episodes. Saavedra et al. (2012) characterized atmospheric conditions leading to ozone pollution over the north western Iberian Peninsula. Their analysis revealed the synoptic weather patterns causing pollution episodes in the region.

Xu et al. (2011) found that the mean diurnal patterns of gaseous pollutants are determined by variations of mixing height, vertical turbulence and horizontal wind velocity. They also found the dependence of O_3 concentrations on temperatures higher than 294 K to be linearly increasing.

Csavina et al. (2014) studied the relationship between dust concentration and relative humidity. They pointed out that wind speed and relative humidity are not directly correlating separately, but at higher wind speeds (>4 m/s), a definite trend is observed between relative humidity and dust concentration. They hypothesized that water sorption increases dust concentration up to a relative humidity of 25% beyond which the inter particle cohesive forces reduces dust concentration.

Zheng et al. (2015) used 10 years of MODIS AOD and NCEP reanalysis data to study the relationship between atmospheric circulation and regional pollution over eastern China. Their study showed the role played by low level wind divergence as the region is prevailed by uniformly descending motion, gathering pollutants in the lower layer. The atmosphere is cleaner during strong middle and lower tropospheric circulation favoring horizontal diffusion of air pollutants. They also pointed out that vertical velocity and wind divergence values are good indicators to identify different atmospheric diffusion conditions.

Wang et al. (2016) investigated the influence of atmospheric diffusion conditions on air quality in China. Daily PBLH, surface wind speed and precipitation were used as indicators for air stagnation, describing the atmospheric diffusion capability. Their results showed that favorable atmospheric diffusion conditions contributed to approxi-

mately 40% of the total decreased concentrations during winter.

2.5 AEROSOL SOURCES AND EMISSION QUANTIFICATION

Aerosols originate either from natural or anthropogenic sources. Most of the natural aerosols are emitted from the ocean, soils, vegetation, fires and volcanoes. Anthropogenic sources contribute as much as natural sources to the global aerosol optical depth (Ramanathan et al., 2001). Combustion of fossil fuels, biomass burning, industrial effluents, vehicular pollution and domestic activities are some of the prominent sources of anthropogenic aerosols (Boucher, 2015). Anthropogenic aerosols have higher radiative impacts due to its absorbing properties. Some of the major aerosol sources are discussed the following sections.

2.5.1 Power Plants

With a total installed capacity of around 220 GW (CEA 2018), thermal power plants (TPP) account for about 66% of power generation in India. TPPs, especially coal fired plants comes with fatal cost to air quality and health. Though they are small spatial entities, they contribute heavily in terms of pollutants. Sulphur dioxide (SO_2), nitrogen oxides (NO_x), particulate matter (PM), carbon monoxide (CO), volatile organic compounds (VOCs), and various trace metals like mercury are the likely emissions from a coal fired TPP (Guttikunda and Jawahar, 2014). Prasad et al. (2006) studied the influence of coal based TPPs on aerosol optical properties in Northern India. Aerosol optical depths were found to be high with relatively coarser particles over major TPP locations. Aerosol source strength estimated from satellite imageries also shows higher values in areas with denser TPP concentration (Aloysius et al., 2008). With more than a 100 TPPs and being the third largest producer of coal, it is one of the prominent sources of pollution in India. Knowledge about the emissions from such sources would help to ascertain their impacts on the environment and also help to formulate control measures.

2.5.2 Biomass Burning

Air pollution from biomass burning is a prominent source impacting human health, air quality and climate. Being recognized as one of the countries with significant biomass

burning, a lot of research have been done in India to investigate its impact (Venkataraman et al., 2006; Kumar, 2012; Badarinath et al., 2006; Sahu et al., 2015). Punjab, Uttar Pradesh, Haryana and Maharashtra are the major states in terms of crop residue burning. Large quantities of agricultural wastes are produced in India and is likely to increase in the future. Farmers often burn these residues as an easy way to manage bulk quantities of wastes and to prepare the field for the next crop (Jain et al., 2014). Not only that crop burning deteriorates air quality, but also causes nutrient and resource loss. Jain et al. (2014) identified that residue burning largely contributed by rice and wheat is a matter of serious concern for pollution, health and nutrient loss. Large uncertainties exists in the estimate of these open farm crop residue burning. Accuracy of the conventional bottom-up approach relies extensively on the knowledge of the type of crop, its residue to grain fraction etc. Approximate values of these parameters are often assigned due to lack of data availability. In this regard a satellite based top-down approach would be appropriate.

2.5.3   Marine Aerosols

Apart from oil spills and acoustic pollution, marine traffic is a source of air pollutants. With over 89,000 transport ships at sea (Equasis statistics 2016, (EMSA)), this is an important source of air pollution especially near ports and coastal cities (Endresen et al., 2003; Mueller et al., 2011). The Indian coastline spanning over 7500 km, houses 12 major and 200 minor ports. These ports handles about 95% of India's trading by volume and 68% by value (Ministry of Shipping 2016,(MoCA, 2016)). Ship-borne measurements from the Integrated Campaign for Aerosol, Gases and radiation Budget (ICARB) reported a significant increase in aerosol abundance from heavy shipping in the oceanic region (Nair et al., 2008). Anthropogenic aerosol loading over the adjoining ocean region in the west coast of India was also shown by Srivastava et al. (2016). Thus the Indian peninsula and the surrounding ocean is susceptible to air pollution from marine traffic.

2.5.4   Anthropogenic Sources

Urban areas are characterized by denser population concentrated over large areas in which industries and service activities are the dominant economic activities (Montgomery and Hewett, 2005). Deterioration of air quality in these metropolitan areas are often attributed to vehicular effluents, industries and power sector exhausts (Lewtas, 2007; McDonald et al., 2012; Mahalakshmi et al., 2014). Petroleum refineries, cement factories, fertilizer factories, sugar factories, textile industries, chemical industries and brick kilns are the major industries responsible for air pollution. Categorizing industrial areas in terms of air quality is important for prioritising these areas for planning and management. The Central Pollution Control Board (CPCB) has identified 88 industrial hotspots in India. Emissions of various pollutants are collected in these areas using ground based instruments. Though this gives more reliable estimates of emissions, the process is laborious and are not necessarily representative of regional concentration. In this regard, though satellite based source estimate provide lumped areal values, they provides large spatial data. This will further help to define the spatial boundaries as well as the extent of eco-geological damages.

2.5.5   Aerosol Emissions

Aerosols are emitted into the atmosphere either as primary particulate matter (mineral dust, sea salt, black carbon, and primary biological organic particles) or as secondary particulate matter from gaseous precursors (non-sea-salt sulfate, nitrate, and ammonia). The contribution of various aerosol types to aerosol composition varies from region to region. Knowledge about the distribution of various aerosol sources and their composition is essential in the parameterization of sources for initializing aerosol transport models (Penner et al., 1994; Ginoux et al., 2001). However, different aerosol types are influenced by different parameters and atmospheric conditions. For example, the sea salt aerosol emission depends on the surface wind speed, sea state, atmospheric stability, sea surface temperature, and seawater composition (Blanchard, 1963; Struthers et al., 2013). Desert dust, on the other hand, depends on many soil-related parameters such as moisture, texture, and vegetation (Kok, 2011).

Biomass burning emission is yet another source of trace gases and aerosols and is estimated based on the burned area, biomass fuel load, fraction of biomass burned, and emission factors (Li et al., 2019; Yin et al., 2019). The accuracy of conventional bottom-up approaches to estimate various aerosol emissions depends on the degree to which the influencing parameters are estimated. In fact, the direct measurement of aerosol fluxes is difficult and is often estimated based on laboratory and/or field measurements. However, satellite based top-down approach can tackle such difficulties by estimating biomass emissions using indicative parameters such as FRP (Kaiser et al., 2012).

Fire intensity information contained in FRP has been used to estimate wildfire source strength. Ichoku and Ellison (2014) used MODIS AOD over smoke plumes to estimate source strength. They derived emission factors by dividing AOD by the plume age, calculated from the plume's horizontal extend and advection speed from reanalysis wind data. These emission factors were evaluated over multiple smoke plumes in different ecosystems to ascertain its relationship with FRP. Li et al. (2019) estimated hourly biomass burning emissions using FRP from the GOES satellite. They adjusted and calibrated the GOES FRP against the MODIS FRP prior to estimating the emissions. Their study shows the diurnal variations of smoke emissions over different ecosystems. Yin et al. (2019) used the daily MODIS FRP data to calculate fire radiative energy and combusted biomass. Their study identified the various contributions of smoke aerosols over China with forest fire as the primary contributor.

The availability of satellite observations not only enhances the capability of determining various influencing parameters but also provides alternate ways of assessing aerosol sources. AOD from satellite observations is directly related to light extinction by atmospheric aerosols. Numerous research has been made to bridge a relationship between PM2.5 measurements and AOD so that a regional picture of particulate matter can be inferred from satellite imagery. The relationship have evolved from a simple empirical equation Wang (2003) to one that incorporates the meteorological conditions (Liu et al., 2005; Gupta and Christopher, 2009; Kamarul Zaman et al., 2017) and even the vertical aerosol distribution from LIDAR (light detection and ranging) measurements (Schaap et al., 2009). But this information pertains to total aerosol or particulate matter

at a specified time and fails to distinguish the amount of aerosols produced in a region. The regional aerosol distributions are influenced by local sources as well as from far away production centers which are connected by wind transport. Convergence or divergence of atmospheric wind can sometimes cause large concentrations of aerosols where there are no significant sources and also low concentration in the vicinity of prominent sources (Rashki et al., 2019).

Aloysius et al. (2008) used the wind data to estimate the transported aerosols and hence, the aerosol source/sink strength. The authors estimated the source of aerosols over Ganga basin by incorporating MODIS AOD data and NCEP reanalysis wind data to the aerosol flux continuity equation. The ASS was estimated over $2.5° \times 2.5°$ grids and showed good correlation with the concentration of thermal power plants in the basin. Prijith et al. (2013) used the aerosol flux continuity equation to derive an aerosol source/sink map over the globe. Thus aerosol production or deposition for twenty-four hours was estimated using AOD obtained from MODIS.

2.6   AEROSOL IMPACT ON RAINFALL

Rainfall irrigates more than 65% of the cultivated land in India and is a major factor in agricultural output. For a rain fed agrarian country like India whose gross domestic product is nurtured by agricultural sector, understanding the spatial and temporal patterns in rainfall is a very vital issue with significant implications on water resources and management policies.

Aerosol radiative and microphysical effects suppress precipitation and tends to spin down the hydrological cycle (Ramanathan et al., 2001). Crutzen and Andreae (1990) studied the cloud microphysics and aerosols. Their study shows that aerosols not only enhance precipitation by acting as cloud condensation nuclei, but also suppress the downpour of atmospheric moisture if abundant. Forest fire is one of the prominent natural source of atmospheric aerosol releasing large quantities of smoke. The impact of such heavy smoke on precipitation anomalies was studied by Rosenfeld (1999). Using satellite precipitation data he observed that the effect is to shut off warm air process in convective tropical clouds and explained this suppression as a result of increased cloud

23

condensation nuclei, inhibiting the growth of cloud droplets. He also pointed out that this indirect effect increased the cloud lifetime. The clouds take more time until its depth is increased with colder cloud top temperatures and eventually raining out.

Evidence of aerosol indirect effects on orographic clouds was presented by Givati and Rosenfeld (2004). Their investigation of polluted clouds as it undergoes orographic lifting shows that precipitation is reduced by about 20% upslope of mountains. They explained this decrease as a result of increasing cloud condensation nuclei which increases cloud lifetime. Increased aerosol concentration can not only inhibit precipitation, but in some case enhance too. This is the case when the increased aerosols are supplied with sufficient moisture. The aforementioned scenario explored by Diem and Brown (2003) concluded an enhanced precipitation in Phoenix. This enhancement was acknowledged to an increase in pollution derived cloud condensation nuclei coupled with increased humidity from human irrigation projects.

Chung et al. (2002) inferred that the effect of absorbing aerosols on regional climate can be significant. Their study shows that the dynamical response to aerosol by the south Asian haze increases the average precipitation over the haze area by as much as 20%. This also cools the land surfaces and warms the atmosphere, leading to a reduction of evapotranspiration over the area. Menon et al. (2002) used a global climate model to study the influence of aerosols in cooling effect observed over India and China. They found that the absorbing aerosols are responsible for atmospheric heating, altering atmospheric stability and vertical motions. They inferred that this could have significant regional climate effect by altering the hydrologic cycle. Using satellite observations of aerosols and meteorological parameters from NCEP, Patra et al. (2005) suggested that monsoon rainfall prediction models should include synoptic as well as inter annual variability in both atmospheric dynamics and chemical compositions. Lau and Kim (2006) presented the preliminary observational evidences showing that the Indian subcontinent and surrounding regions are subjected to heavy loading of absorbing aerosols which can impact the Asian summer monsoon.

The impact of black carbon aerosols Indian monsoon was studied by Meehl et al. (2007). They stated that, though the premonsoon months experiences an enhanced pre-

cipitation due to the increased meridional tropospheric temperature, the reduced surface temperatures over India that extends to the Himalayas act to reduce monsoon rainfall over India. Satheesh et al. (2008) found evidence that during pre-monsoon season most of Indian region is characterized by elevated aerosol layers with a substantial fraction (as much as 50 to 70%) of aerosol optical depth above clouds, causing strong tropospheric warming. Further evidence of tropospheric warming due to aerosols and hence the increased land sea thermal gradient was shown by Gautam et al. (2009b). From combined analysis of changes in tropospheric temperatures and summer monsoon rainfall in the past three decades, the authors suggest a future possibility of an emerging rainfall pattern of a wetter monsoon over South Asia in early summer followed by a drier period. Bollasina et al. (2011) provided compelling evidence of the prominent role of aerosols in shaping regional climate change over south Asia. Using a series of climate model experiments, they attributed the decreasing precipitation over south Asia to be mainly due to human influenced aerosol emissions. The influence of anthropogenic emissions on aerosol distribution and the hydrologic cycle was studied by Cherian et al. (2013). They showed that the decreasing precipitation during the south west monsoon is due to a reduction in convective precipitation, where there is an increase in cloud droplet number and solar dimming effect.

Besides the impact on large scale circulations aerosols are also capable of affecting regional precipitation by indirect effect. Numerous researches provides insight to aerosol indirect effect in India. Tripathi et al. (2007) studied the variations in water and ice cloud effective radius with aerosol optical depth using MODIS data. Their study shows that the temporal variation of cloud effective radius follows a negative trend as that of aerosol optical depth for most of the time. But this is also affected by various meteorological factors such as wind, humidity etc. They showed that the relationship is highest in winter when the role of meteorology is the least.

The aerosol indirect effect over India was also studied by Panicker et al. (2010), where they estimated the indirect effect of aerosol over four regions in India. Cloud parameters such as fine mode fraction, ice path, cloud liquid water path (CLWP), water radius and cloud ice radius (CIR), were obtained from MODIS data. These parame-

ters were examined during below normal, normal and above normal rainfall years. It was observed that for years with similar CLWP and CIP, a positive indirect effect was observed during below normal rainfall years. But a negative indirect effect was observed during above normal and normal rainfall. Aerosol–cloud studies have stated a reduction in cloudiness under high AOD for areas with high absorbing aerosol loading (Koren et al., 2004; Small et al., 2011). The interaction of aerosol, rainfall and various cloud parameters over the summer monsoon regions has been presented by Sarangi et al. (2017).

2.7 SUMMARY OF LITERATURE

The aforementioned literature suggests the importance of prevailing meteorological parameters in regulating the transport of atmospheric particles. This provides knowledge in improving the prediction of aerosol concentration over the globe. For a developing economy like India, anthropogenic aerosol sources are rising owing to urbanisation and industrialisation. This necessitates the understanding of spatial redistribution of aerosols from their sources. Various literature have studied the influence of meteorological parameters such as wind speed, direction, and divergence on aerosols distribution over the Indian subcontinent. But these parameters are indicative of atmospheric advection, whereas the diffusion of atmospheric particles is also an important factor. An investigation of the influencing meteorological parameters indicating both advection and diffusion of aerosols over the Indian subcontinent and the adjacent Indian Ocean is of prime importance. This would also facilitate a better estimate of various aerosol emissions using satellite imagery. Besides, most of the aerosol-precipitation studies in India has concentrated in regions of higher aerosol concentration rather than the sources. Identifying various aerosol sources over the Indian subcontinent would provide a different perspective for studying its impact on precipitation.

Chapter 3

SPATIOTEMPORAL DISTRIBUTION OF AEROSOLS OVER THE INDIAN SUBCONTINENT AND ITS DEPENDENCE ON PREVAILING METEOROLOGICAL CONDITIONS

3.1 INTRODUCTION

The prevailing meteorological conditions that influence the advection and diffusion of the atmosphere governs the distribution of atmospheric particles from its sources. Literature suggests the importance of prevailing meteorological parameters in regulating the transport of atmospheric particles. This provides knowledge in improving the prediction of aerosol concentration over the globe (Ziomas et al., 1995; Moorthy and Satheesh, 2000; Rajeev et al., 2000; Tanner and Law, 2002; Ding et al., 2004; Cheng et al., 2007; Aloysius et al., 2008; Zhao et al., 2010; Zheng et al., 2015; Wang et al., 2016). For a developing economy like India, anthropogenic aerosol sources are rising owing to urbanisation and industrialisation. This necessitates the understanding of spatial redistribution of aerosols from their sources. Various literature (Moorthy and Satheesh, 2000; Aloysius et al., 2008; Chitranshi et al., 2015) have studied the influence of meteorological parameters such as wind speed, direction, and divergence on aerosols distribution over the Indian subcontinent. But these parameters are indicative of atmospheric advection whereas the diffusion of atmospheric particles is also an important factor (Ziomas et al., 1995; Wang et al., 2016). This chapter explores the spatio-temporal distribution

of atmospheric aerosols over the Indian subcontinent (5° - 40°N, 65° - 100°E) and its dependence on the prevailing meteorological conditions. Eleven years (2002-2012) of Aerosol Optical Depth (AOD) obtained from the Moderate Resolution Imaging Spectro-radiometer (MODIS) along with meteorological parameters extracted from reanalysis data are analyzed at monthly timescales. Wind speed, wind divergence and PBLH are studied as parameters for advection and diffusion of atmospheric aerosols.

3.2 DATA AND METHODOLOGY

The data used and the methodology adopted for the study are described in this section. The study considers the region between 5°N to 40°N and 65°E to 100°E bounding the Indian mainland and adjacent oceans for 11 years from 2002 – 2012 3.1.
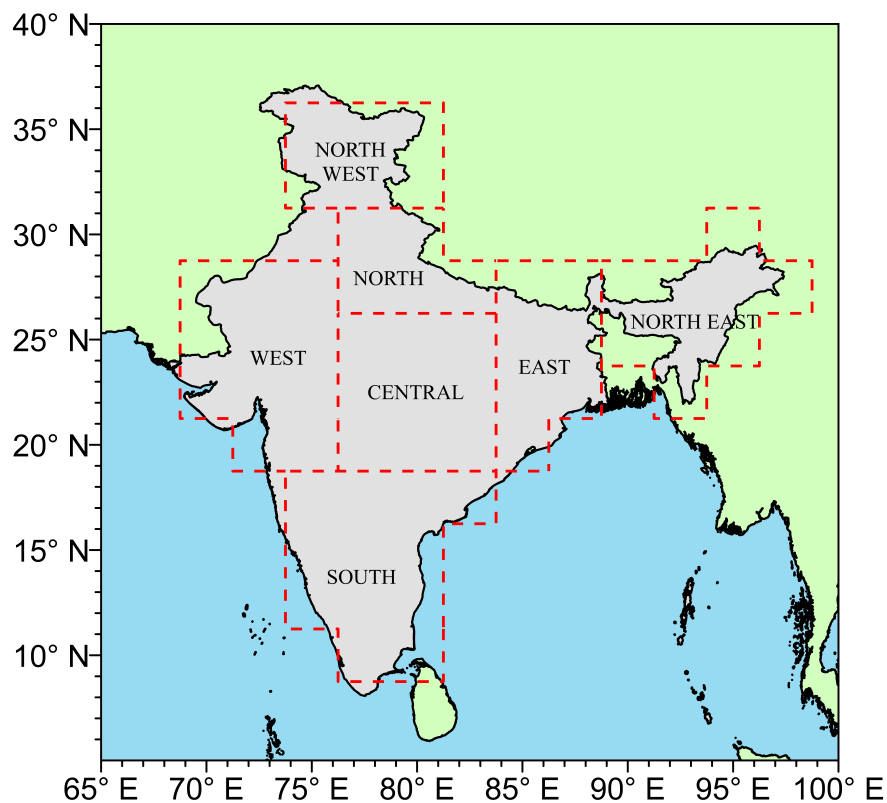
Figure 3.1 Location of different subregions in the study area.

3.2.1 Aerosol Data

Though point measurements provide a refined view of aerosol characteristics on a local scale, they are not necessarily representative of regional concentration. In this regard, satellites were established to be a decent tool to understand the broad spatio-temporal properties of aerosols and their accompanying effects from global to local scales (Misra et al., 2015). Terra and Aqua satellites on-board the Moderate Resolution Imaging Spectroradiometer, provide global observations of AOD (Levy et al., 2010; Hsu et al., 2013). These observations provide daily insight into the global distribution of aerosol columnar content. MODIS AOD products have been extensively validated by numerous researchers (Tripathi et al., 2005; Choudhry et al., 2012; Sayer et al., 2013; Misra et al., 2015). Monthly average AOD (550 nm) from Collection 6.1, level 3 AOD products ($1° \times 1°$) derived from Terra's MODIS measurements are used in this study (Platnick et al., 2017). To ascertain the contribution of different aerosol types, the reanalysis dataset from the Modern-Era Retrospective Analysis for Research and Applications, Version 2 (MERRA 2; Gelaro et al. (2017)) have been used. The AOD at 550 nm from dust (DU), sea salt (SS), black carbon (BC), organic carbon (OC) and sulfate (SU) aerosols are derived from the monthly mean aerosol diagnostics dataset (GMOA 2015b).

3.2.2 Meteorological Data

The corresponding meteorological analyses implemented in this paper are based on the results of meteorological reanalysis products provided by the National Centre for Environmental Prediction (NCEP), Reanalysis 2 (https://www.esrl.noaa.gov/psd/data/ gridded/data.ncep.reanalysis2.pressure.html). For a complete understanding, we consider both the upper-air and surface circulation patterns. Wind field at various vertical levels was extracted from the NCEP Reanalysis data set on a $2.5° \times 2.5°$ latitude/longitude grid on a monthly basis. As the PBLH has strong diurnal variation, its value during the time of passage of Terra over the Indian Subcontinent was extracted at a spatial resolution of $1° \times 1°$ from the MERRA 2 dataset (Global Modeling Assimilation, 2015). Since the wind fields were available at $2.5°$ resolution, the present study was done at

$2.5° \times 2.5°$ with all data resampled to this resolution.

3.2.3 Methodology

The present study first focusses on the spatio-temporal distribution of 550nm AOD and then analyses various meteorological parameters to investigate their possible influence. As evident from the literature, the atmospheric transportation and the distribution of aerosols are governed by advection and diffusion. Thus, wind speed and divergence are used as indicators for advection, whereas the PBLH is used as an indicator of atmospheric stability and hence atmospheric diffusion. 11 years (2002 – 2012) of aerosol climatology during the winter (January-February), pre-monsoon (March-May), monsoon (June-September) and post-monsoon (October-December) season is presented in this paper. Spatial plots of mean seasonal AOD was derived from monthly AOD over the Indian subcontinent bounded between $5°$ and $40°$ north latitudes and $65°$ and $100°$ east latitudes. The mean seasonal AOD for each grid was derived from the AOD for a month m in the year $yAOD_{m,y}$ in a given season for that particular grid as:

$$AOD_{season} = \frac{\sum_{m=1}^{n} AOD_{m,y}}{n} \tag{3.1}$$

Where n is the total number of months of MODIS data during a given season over all the 11 years of data. Pixels with missing data values during the period was left as no data pixels. As the land areas inhibited higher aerosol loading in comparison to the oceanic areas, all the proceeding analysis were carried out separately over the land and ocean. Temporal variation of AOD was plotted from the spatially averaged AOD ($\overline{AOD}_{month}$) for each month over the land and ocean separately as:

$$\overline{AOD}_{month} = \frac{\sum AOD}{n} \tag{3.2}$$

Where AOD is the AOD value at each pixel with data value and n is the total number of pixels with data value over the land or ocean in that particular month. Each pixel was classified as land if 50% or more area of the pixel corresponded to land or else as the ocean. Temporal variations of AOD_{month} for over 132 months starting from January 2002 is presented in this study. To study the monthly spatial variation of AOD, standard deviations were also plotted along with each monthly values. This represents the spatial

variations of AOD during each month.

Meteorological parameters derived from reanalysis data were then analyzed. Monthly values of zonal (u) and meridional (v) wind components were extracted at different vertical levels and the resultant wind speeds were calculated for every $2.5° \times 2.5°$ pixel. To account for the inflow and outflow of air masses, the wind divergence was also studied. The wind divergence was computed from the horizontal wind components as described by McNoldy (2004) using the formula

$$Divergence = \frac{\partial u}{r\,cos\phi\,\partial\lambda} + \frac{\partial\,(v\,cos\phi)}{r\,cos\phi\,\partial\phi} \qquad (3.3)$$

Where ϕ and λ are latitude and longitude and r is the Earth's radius. Similar to the wind speed, the wind divergence was also computed at different vertical levels at the same spatial resolution. As the horizontal length scale of each grid (≈ 277 km) is much larger than the vertical perturbations over the land (≈ 10 km), this equation is applied both over the land and ocean. Temporal variation of these meteorological parameters and their correlation with AOD was then investigated.

The Indian subcontinent being a host of varied climatology is further divided into subregions for further analysis. The whole Indian region is thus subdivided into seven sub-regions. The division is in accordance with Ramachandran and Cherian (2008) where he classified the region according to its geographic location. The locations and their bounds are shown in Figure 3.1. Correlation analysis was then carried out over each subregion between AOD and each of the meteorological parameters. For the correlation analysis, only those grids where collocated values were available for each parameter were considered. These values of wind speed, divergence, and PBLH were then sorted as a function of AOD and averaged to create a total of 50 scatter points. These values were then used for Multiple Regression analysis to ascertain their contribution to aerosol loading.

As the Indian subcontinent hosts a variety of aerosol types, AOD values for sea salt aerosol (SS), dust aerosol (DU), organic carbon aerosol (OC), black carbon aerosol (BC), and Sulphate aerosol (SU) were derived from the MERRA-2 dataset to analyse the contribution of different aerosol types to the total AOD. The total AOD (AOD_{Total})

31

values could roughly be fitted using the equation

$$AOD_{Total} = DU + BC + OC + SS + SU \tag{3.4}$$

Thus the contribution of each aerosol type ($AOD_{contribution}$) can be calculated as

$$AOD_{contribution} = \frac{AOD_s}{AOD_{Total}} \tag{3.5}$$

where, AOD_s is the aerosol optical depth of each aerosol type (DU, BC, OC, SS, and SU) obtained from MERRA 2. The contribution of each aerosol type in difference meteorological conditions are analysed. In addition to this, Proportional Reduction in Error (PRE; Judd et al. (2017)) was also calculated from the residuals of regression analysis.

$$PRE = \frac{\sum E(B) - \sum E(A)^2}{\sum E(B)^2} \tag{3.6}$$

Where $E(B)$ is the residual in a model excluding PBLH and $E(A)$ is the residual in a model involving all the three parameters (wind speed, wind divergence, and PBLH). The PRE helps to identify the contribution of PBLH in defining the variations in AOD.

Multiple trajectories at different locations over the land and ocean were computed using the PC-Windows based NOAA HYSPLIT model. The HYSPLIT model computes air trajectories, dispersion and deposition simulations by a hybrid between Lagrangian and Eulerian approach (Stein et al., 2015; Rolph et al., 2017). The locations over the land and ocean were selected based on the aerosol loading and four day multiple backward trajectories were computed at different vertical levels. As the Terra overpass the study region around 12:00 IST, trajectories were calculated starting at every 12:00 IST for a year. The daily NCEP reanalysis data with a resolution of $2.5° \times 2.5°$ was used for this analysis. Trajectory frequency was then computed from these 365 backward trajectories to investigate further how frequently the air masses are drawn from a region. The frequencies are computed over an arbitrary grid over the computational domain by counting the number of trajectory intersections over each grid cell and normalizing by the number of trajectories. Further, trajectory clusters for the highest loaded month for these locations were also computed. Both the locations experienced highest AOD load-

ing during May 2011 and trajectories during this month was clustered to show potential aerosol transport pathways.

3.3   RESULTS AND DISCUSSION

3.3.1   Spatial Distribution of AOD

Before investigating the link between aerosols concentration and prevailing meteorological conditions, it is necessary to study its spatio-temporal distribution over the region. The spatial distribution of AOD highlighting the spatial variability over the Indian subcontinent is presented in Figure 3.2. As mentioned in the literature (Washington et al., 2003; Dey, 2004) the dominance of aerosols over northern India especially the IGP is visible. Heavy aerosol loading over the Thar Desert in western India and eastern Pakistan is transported over northern India along the IGP and is eventually spread over the Bay of Bengal in the eastern Indian Ocean. Thus a vivid picture of aerosol transportation from the arid regions is depicted. Similar to the observations by Gautam et al. (2009b,a), a significant reduction in aerosol concentration in contrast to IGP is observed over the foothills of the Himalayas and the Tibetan Plateau. Such spatial gradients with topographical differences are also visible over the Aravali, Eastern Ghats and the Western Ghats mountain ranges. Apart from the IGP, certain regions of central India (19°N, 76°E) shows high aerosol loading when compared to the surrounding areas. It is interesting to note that these regions are bounded by the Western Ghats to the west and south, Satpura ranges to the north and the Eastern Ghats to the east. Hindrance to flow caused by the surrounding mountain ranges transporting aerosols to higher altitudes near its foothills could be a factor for increasing the aerosol loading.

The influence of continental aerosols on the adjacent oceanic regions can be inferred as most of the heavier aerosol concentrations are observed along the coast and weaken as the distance from the land increases. Over the Bay of Bengal, aerosol loading along the east coast can be seen as an extension of the IGP aerosol loading. Thus most of the aerosols are dust mixed with anthropogenic aerosols from IGP (Guttikunda et al., 2003; Monkkonen, 2004). Though not as heavy as the east coast, the west coast shows wider aerosol loading over the Arabian Sea. Apart from the continental sources, the
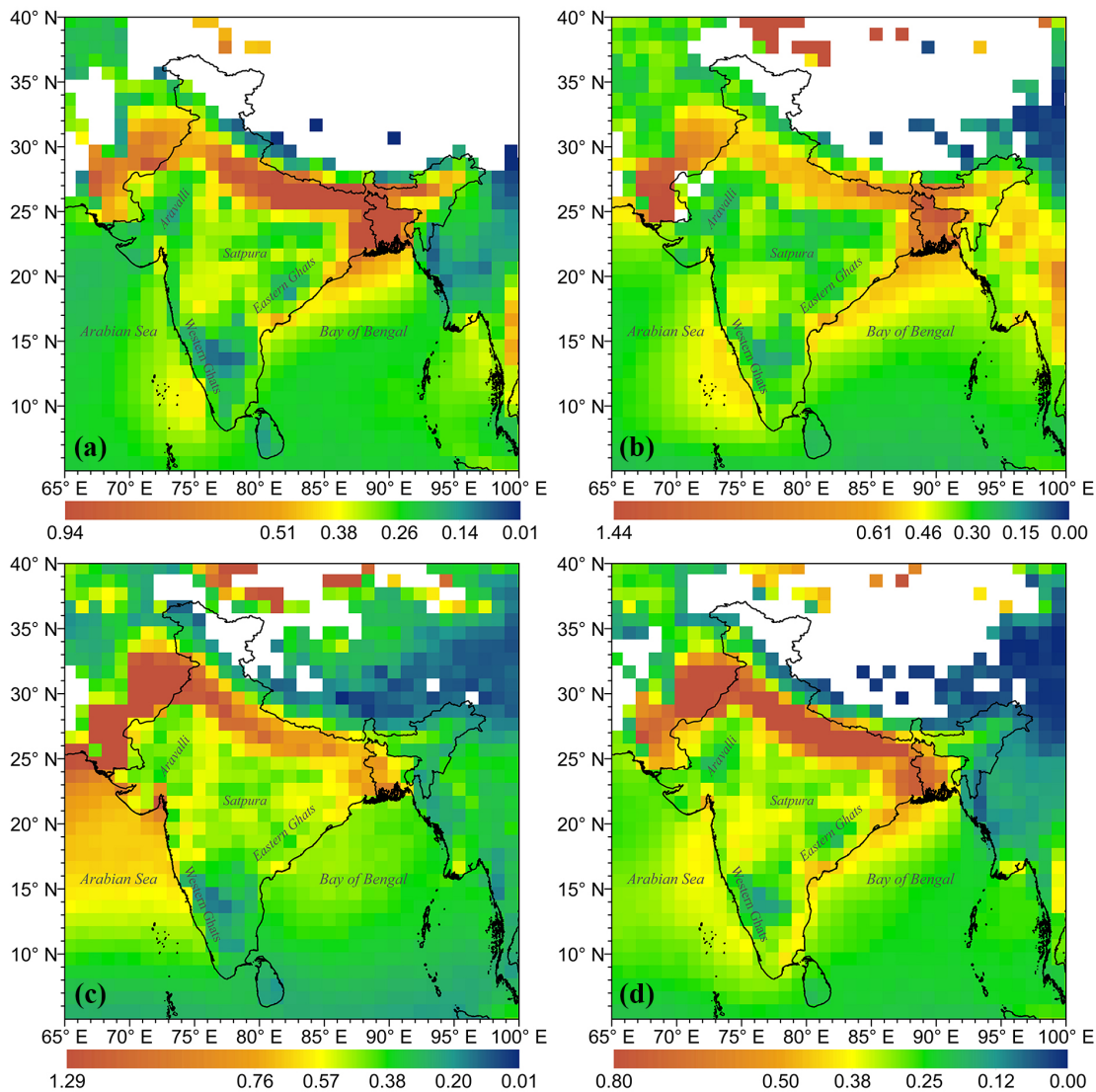
Figure 3.2 Spatial distribution of seasonal AOD from MODIS averaged during 2002–2012. (**a**) Winter. (**b**) Pre-monsoon. (**c**) Monsoon. (**d**) Post-monsoon

oceanic regions are also influenced by marine traffic (Nair et al., 2008). The Indian coastline spanning over 7500 km, houses 12 major and 200 minor ports. These ports handle about 95% of India's trading by volume and 68% by value (Ministry of Shipping 2016, MoCA (2016)). Ship-borne measurements from the Integrated Campaign for Aerosol, Gases and Radiation Budget (ICARB) reported a significant increase in aerosol abundance from heavy shipping in the oceanic region (Nair et al., 2008). Anthropogenic aerosol loading over the adjoining ocean region in the west coast of India was also shown by Srivastava et al. (2016). Thus marine traffic along with continental aerosols

is responsible for aerosol loading over the oceanic regions. Though a general picture of the seasonal climatological mean of AOD is depicted in Figure 3.2, there also exists annual variations in spatial distributions.

Owing to increased aerosol sources of natural and anthropogenic origin, land areas are heavily loaded in comparison to the surrounding ocean. Not only the distribution of sources but also the variety topography influences the aerosol distribution over land, whereas such influences are absent over the ocean. The results indicate that average AOD values over land (0.40) are almost 30% more than those over the ocean (0.30) for the 11 years under consideration.

3.3.2 Temporal Distribution of AOD

Apart from the spatial variability, there also exists a temporal variation in AOD. The spatial averages over land and oceanic regions were calculated for each month. This enables to study the temporal changes in average aerosol concentrations. The monthly variation in the average daily AOD over land and ocean along with the standard deviation are given in Figure 3.3. Both land and ocean show a strong seasonal variation of AOD with increased aerosol loading during the monsoon months of June, July and August. Standard deviations about the monthly spatial means are also plotted to show its spatial variation. It can be observed that there is not only an increase in average AOD but also an increase in the spatial variability among the pixels during the monsoon season. This suggests that the increased aerosol loading during the monsoon season is concentrated in particular locations. The AOD over the oceanic areas is substantially lower than those over land areas. Moreover, the oceanic areas also experience less spatial variability as shown by the standard deviation bars.

3.3.3 Meteorological Characteristics

Given the spatio-temporal distribution of AOD, knowledge about the variations in meteorological characteristics is required to link their relationship. Thus the monthly variation in the meteorological parameters such as wind speed and divergence are presented in this section.
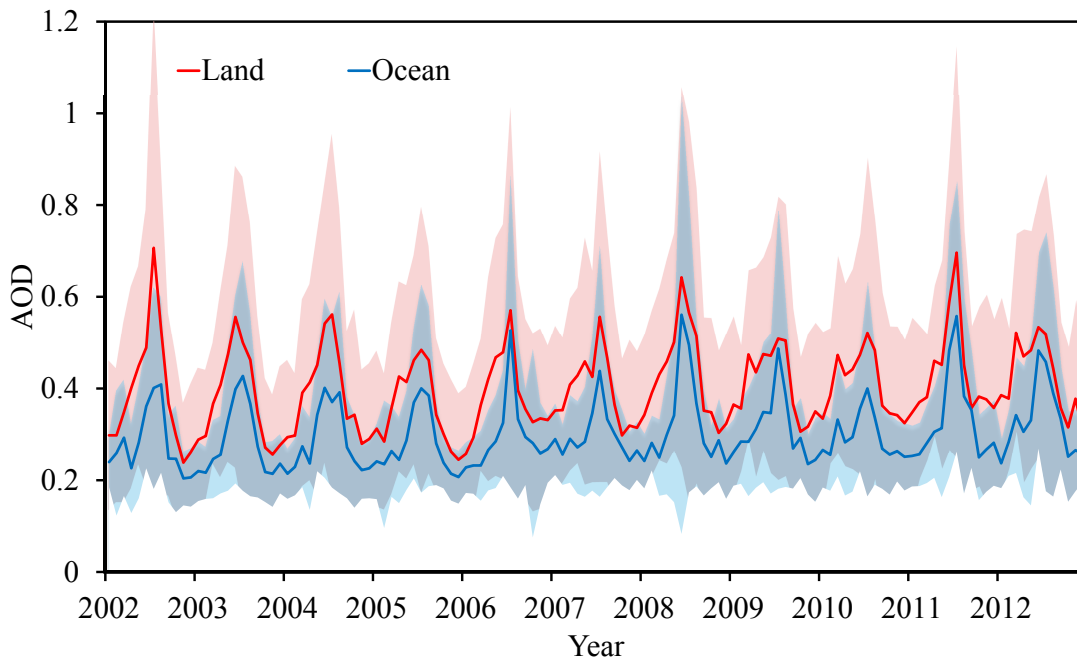
Figure 3.3 Monthly variation of average daily AOD over the land and ocean from 2002 to 2012

Wind Speed

Due to the vertical gradient of horizontal wind speed in the atmosphere, the wind speeds at different vertical levels have been studied. The temporal distribution of the average wind speed at different vertical levels over land is shown in Figure 3.4a. Though the wind speed increases with altitude, there is a similar seasonal pattern up to 850 hPa with higher wind speeds during the monsoon season similar to the AOD distribution. It is also observed that during the monsoon season the difference in wind speeds at the different levels increases compared to that in other months similar to the variation in the standard deviation of AOD. Thus, the monsoon season witnesses stronger wind speeds with distinct vertical gradients. The wind speed over the ocean is relatively higher compared to that over land but shows a similar seasonal variation (Figure 3.4b). This is due to the lesser surface roughness over the oceanic areas. Unlike land, ocean shows similar patterns in wind speed even up to 700 hPa.

36
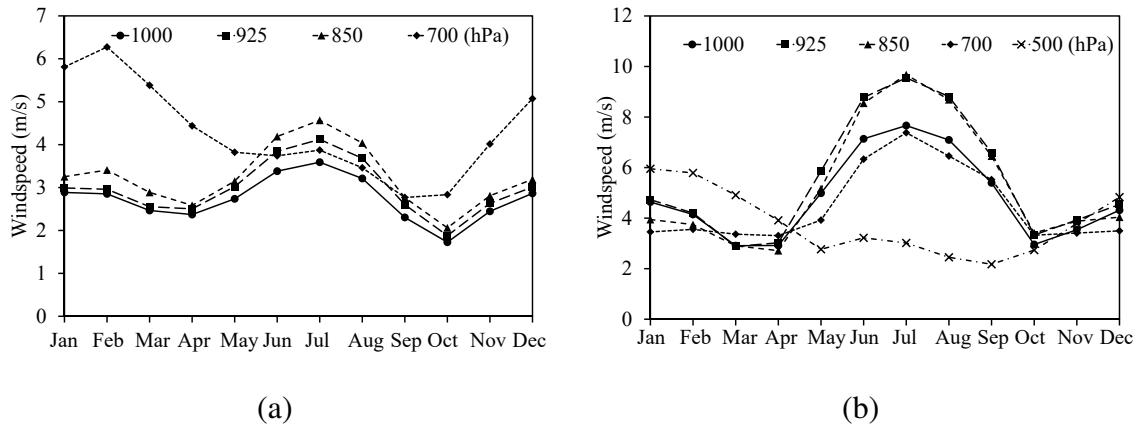
Figure 3.4 Monthly variation of average wind speed at different pressure levels (hPa) over the land (**a**) and ocean (**b**) from 2002 to 2012.

Divergence

Wind divergence is indicative of the accumulation or dispersion of atmospheric parti-cles in a region. Temporal distribution of wind divergence at different vertical levels is shown in Figure 3.5. Over the land, divergence during the winter season decreases towards the summer and eventually becomes convergence (negative divergence) dur-ing the monsoon season. Similar to wind speed, the divergence over the land up to a height of 850 hPa shows similar patterns. Unlike land, the ocean experiences increasing divergence during the monsoon season. Overall, the wind speed and divergence over the land and ocean are characterised with seasonal variations with the monsoon season witnessing higher wind speeds with converging air masses over the land and diverging air masses over the ocean.

3.3.4 Variation of AOD With Meteorological Parameters

Having said that both AOD and meteorological parameters such as wind speed and di-vergence exhibit seasonal variation, their correlation was investigated. Figure 3.6 shows the monthly variation in AOD along with wind speed over the land. Wind speed and AODs show similar temporal variation with higher values during the monsoon season. Thus AOD values over land increase with an increase in wind speed. The variation of AOD along with wind divergence is shown in Figure 3.6. The monsoon season with
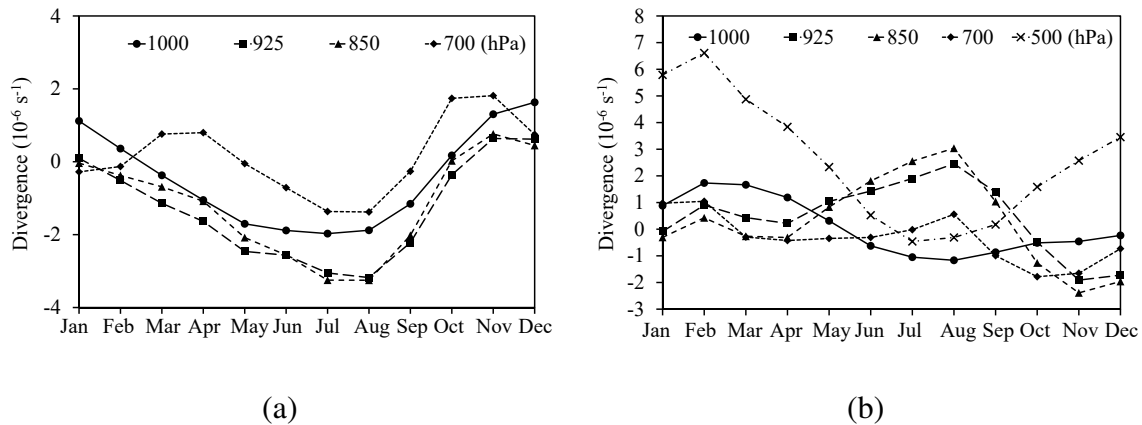
Figure 3.5 Monthly variation of average wind divergence at different pressure levels (hPa) over the land (**a**) and ocean (**b**) from 2002 to 2012.

higher AOD values is characterized by negative wind divergence. A multiple regression analysis of wind speed and divergence with AOD using the 11 years of monthly data (132 data points) shows a good correlation as indicated by the correlation coefficient (R). The correlation varies at different vertical levels with a maximum of 0.75 at 850 hPa.

Over the ocean a more vivid relationship is observable. AOD and wind speed (850 hPa) exhibits a higher correlation ($R = 0.82$), whereas a clear divergence can be seen during the monsoon season (Figure 3.7). This increased correlation is due to the relatively pristine ocean areas which are loaded mostly by transported continental aerosols in comparison to the numerous aerosol sources over the land.

Both land and ocean show an increasing correlation of wind speed and AOD at higher vertical levels with a maximum occurring at 850 hPa. This expresses the importance of wind direction and air mass trajectories with different areal influence. This was further investigated by running multiple backward trajectories at different vertical levels. Previous studies have also used trajectory analysis to infer the sources and locations of aerosols (Nair et al., 2008; Giles et al., 2011; Kedia et al., 2014). The frequency of backward trajectories at near surface (1000 hPa) and mid-tropospheric (850 hPa) levels over the land and ocean were plotted (Figure 3.8). The locations for computing trajectories were decided from among regions of heavy aerosol loading. Thus over the land

38
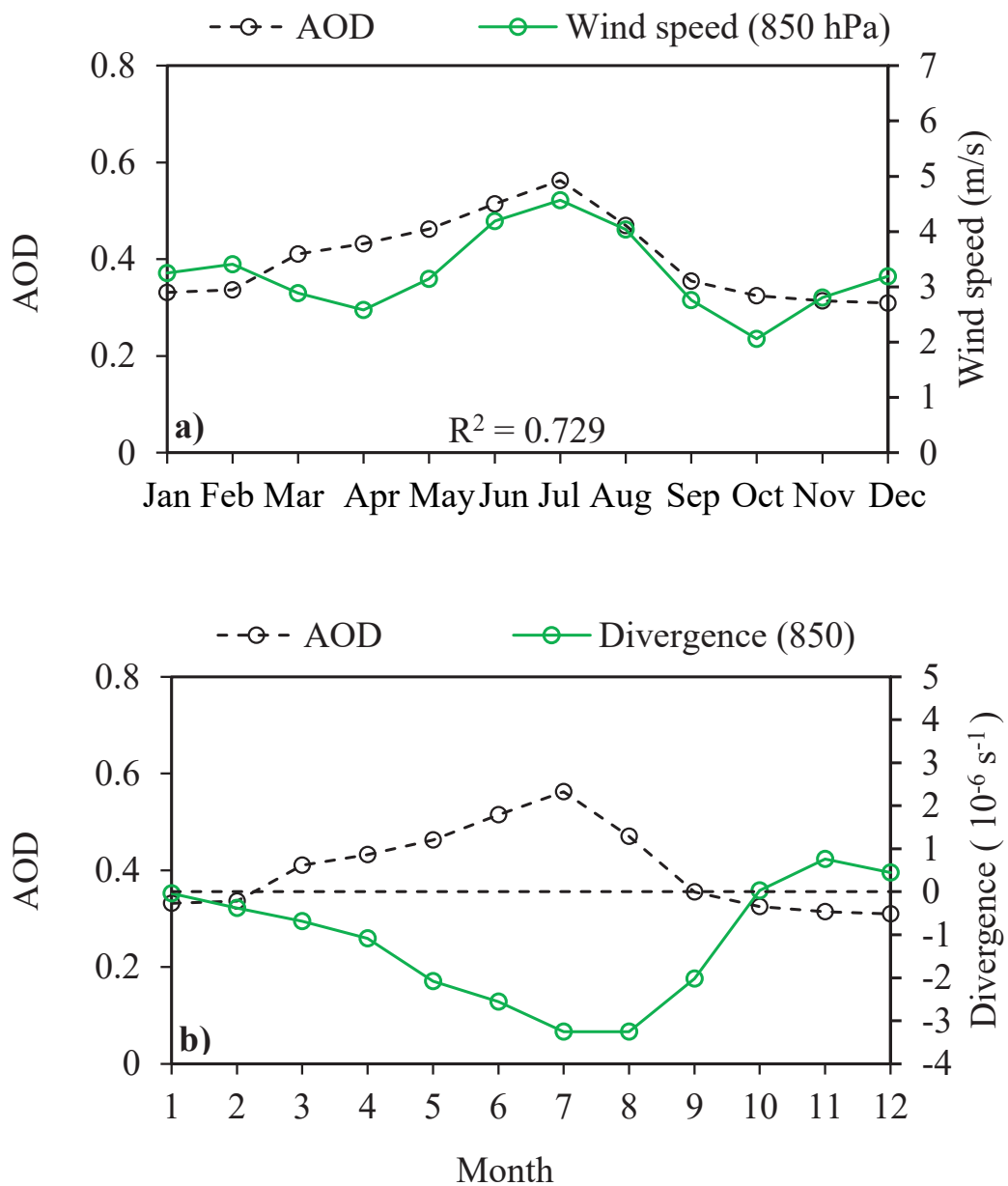
Figure 3.6 Temporal variation of average daily AOD with (**a**) wind speed and (**b**) divergence at 850 hPa over the land from 2002 to 2012.

a location at IGP (26°N, 83°E) and over the ocean a location near east coast (20°N, 88°E) was selected as shown in figure 3.6. Though both near surface (Figure 3.8a) and mid-tropospheric (Figure 3.8b) trajectories shows similar frequencies over IGP, the 850 hPa trajectories are more frequently driven from the arid regions such as the Thar
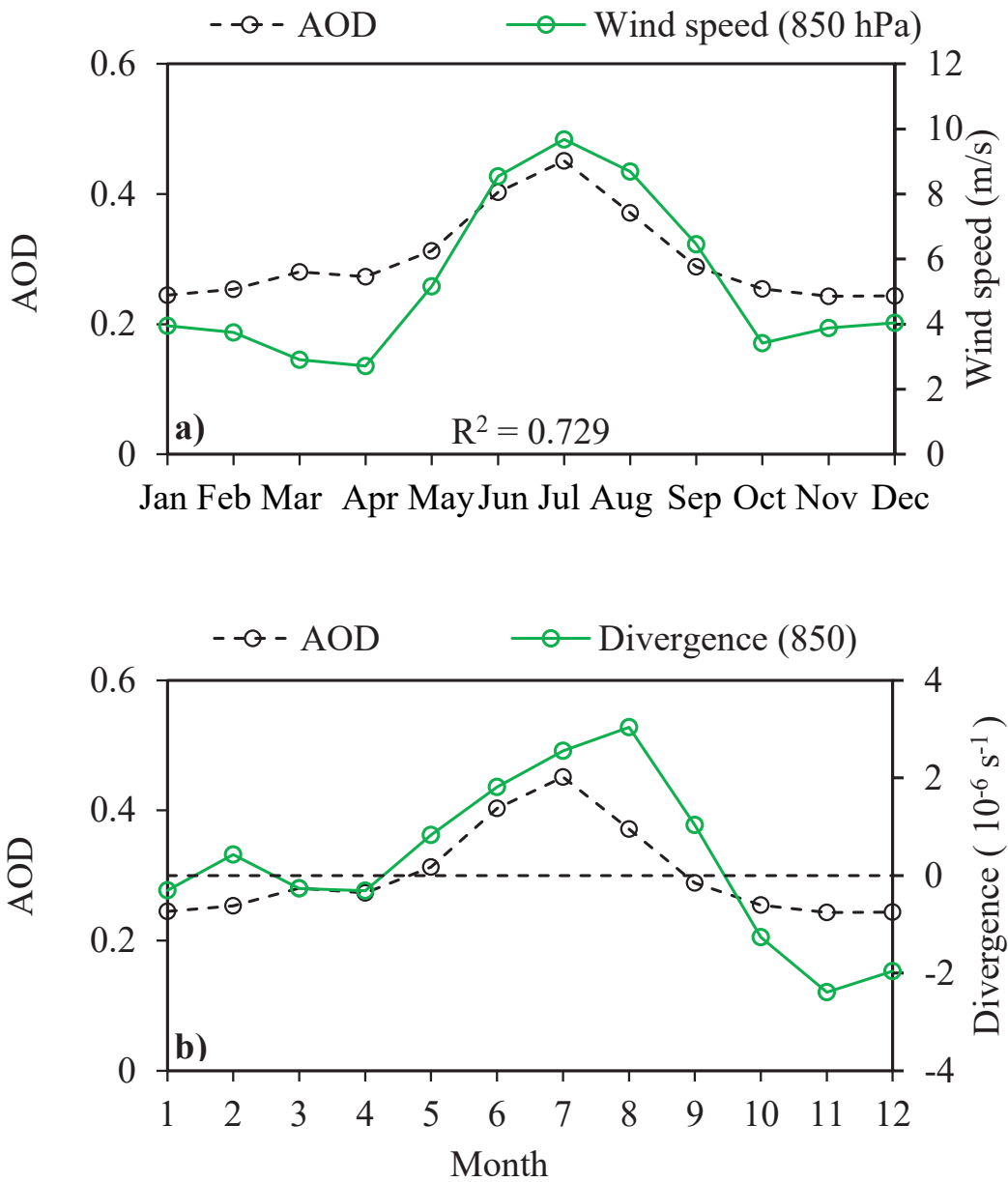
Figure 3.7 Temporal variation of average daily AOD with (**a**) wind speed and (**b**) divergence at 850 hPa over the ocean from 2002 to 2012.

desert. Thus the 850 hPa trajectories not only accounts for surface aerosol movement but also for the elevated mid-tropospheric aerosols from farther areas. Over the ocean there is more frequency of winds blowing from the adjacent land areas at 850 hPa when compared to 1000 hPa (Figure 3.8c-3.8d). To further validate the importance of mid-tropospheric wind, multiple backward trajectories at these locations were carried out

for the month with the highest aerosol loading. Both the locations experienced highest AOD during May of 2011. Daily backward trajectories during this month were clustered and the results are presented in Figure 3.9. It is evident that the trajectories at 850 hPa are driven from the arid regions bringing in dust aerosols and resulting in heavier aerosol loading. Over the ocean, the backward trajectories at 1000 hPa are confined over the ocean whereas the 850 hPa are driven over the land surface. Thus an increase in correlation with altitude can be inferred as the trajectories extending to land masses contributing to most of the oceanic aerosols.

3.3.5 Meteorological Characteristics Over Regions of High and Low AOD

Apart from the seasonality in overall aerosol loading, there is also evidence of large spatial variability as seen in previous sections. This suggests that the increased aerosol loading over the Indian subcontinent is concentrated to particular locations within the region. Thus aerosol concentrations were analyzed to understand its dependence on meteorological conditions. For this purpose, the land and oceanic regions were classified into subregions, and the variation of meteorological parameters with AOD was analysed. As the literature suggests the importance of atmospheric diffusion in aerosol redistribution, PBLH has also been studied as an indicator of atmospheric stability. Thus wind speed, divergence, and PBLH were analyzed as an indicative parameter for atmospheric advection and diffusion.

The figures showing the seasonal variation of wind speed, divergence and PBLH with AOD over the subregions are shown in figures 3.10 to 3.13. The trends of each parameter along with the P-value is summarised in Tables 3.1 to 3.3. The northwest sub-region has been omitted due to a large amount of missing data. The parameters exhibit distinct patterns not only over different subregions but also over the same sub-
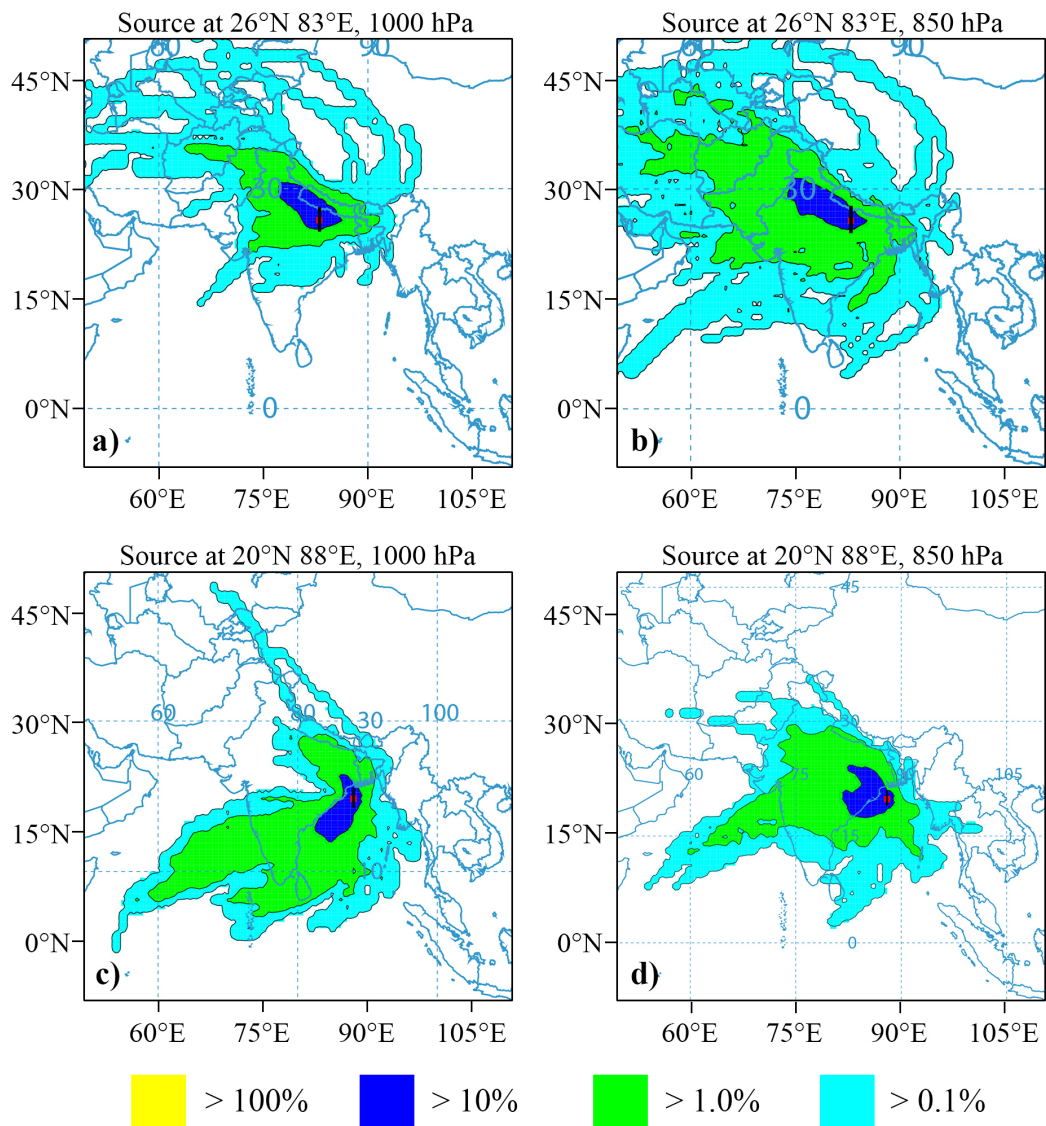
Figure 3.8 Trajectory frequency for 2013 over the land and ocean at different vertical levels.

region during different seasons. For example, the wind speed over the south subregion shows a decreasing trend with increasing AOD during the winter whereas the monsoon witness increasing wind speed with AOD. Thus winter season over the south subregion is characterized by heavier aerosol loading over regions of lower wind speed whereas regions with high wind speed experience heavier aerosol loading during monsoon. This is because the Indian subcontinent hosts different aerosol types with each aerosol type
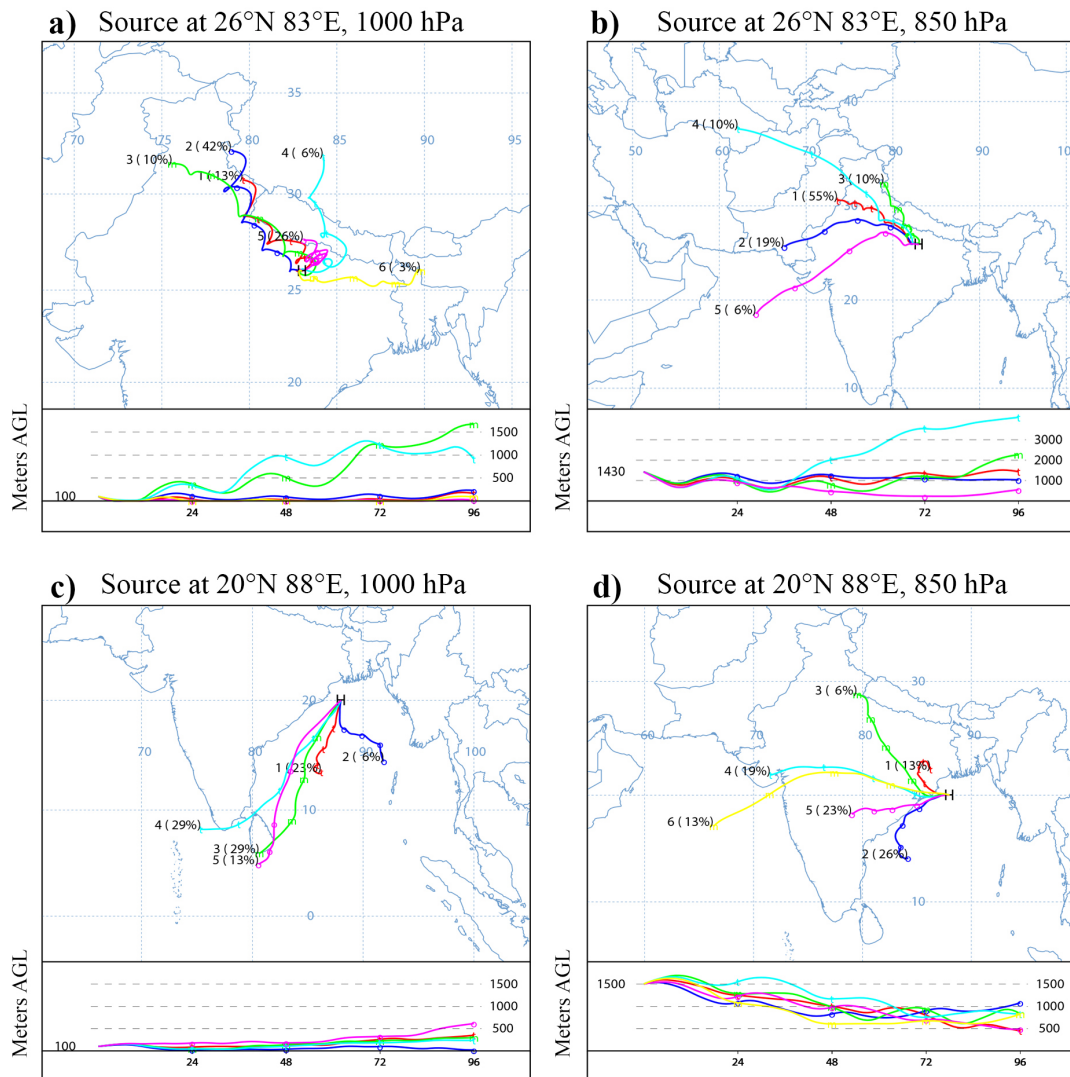
Figure 3.9 Trajectory cluster for May 2011 over the land and ocean at different vertical levels.

having different climatology.

The AOD over the sub-regions experience varying contributions from each aerosol type during the seasons. The contribution of each aerosol type towards the total AOD over the subregions during different seasons are shown in Table 3.4. The south sub-region during the winter season is characterized by significantly decreasing PBLH, significantly increasing divergence and significantly decreasing wind speed with increasing aerosol loading. Thus the south sub-region during the winter experiences heavier
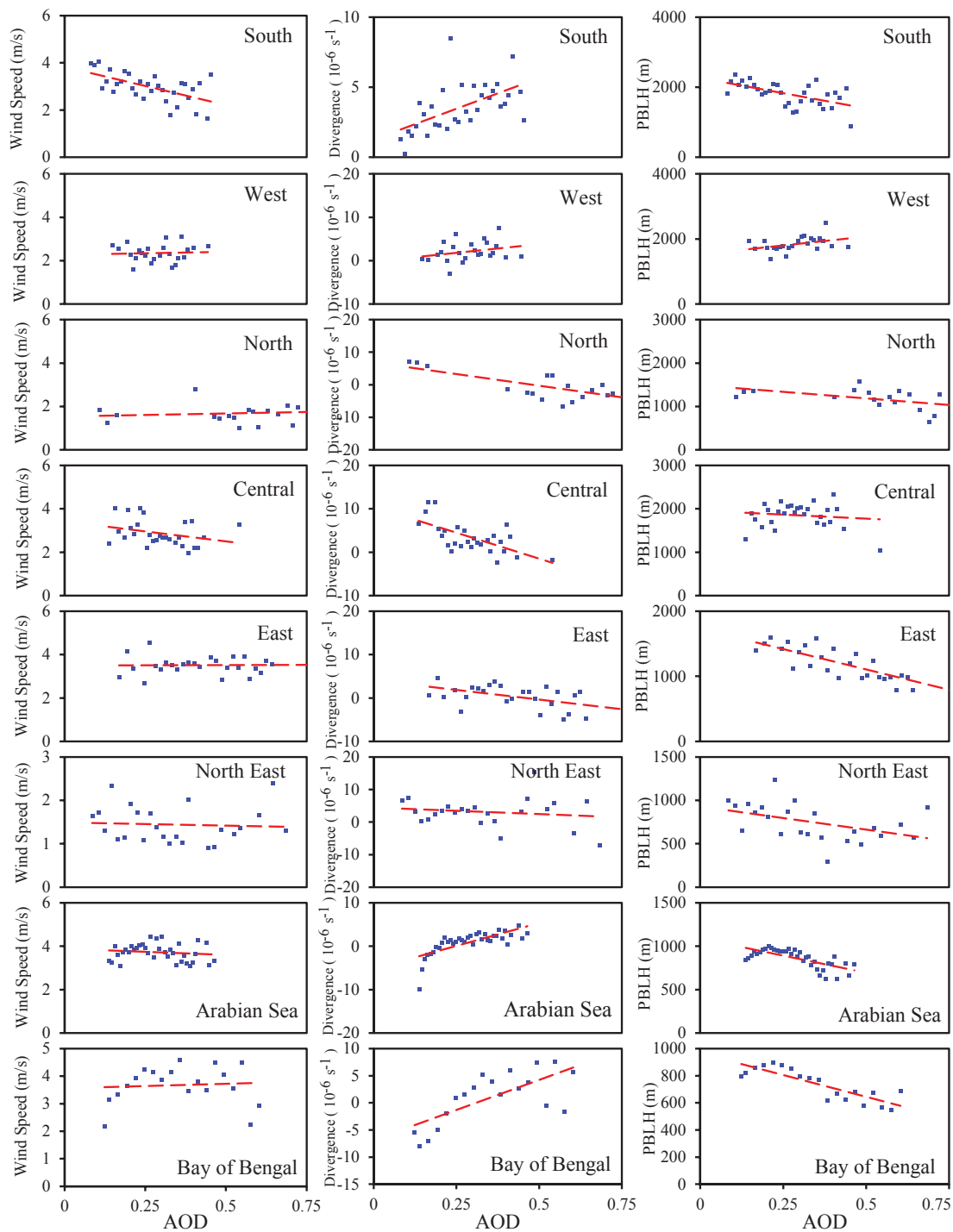
Figure 3.10 Variation of meteorological parameters with MODIS AOD over the sub regions during the winter season.
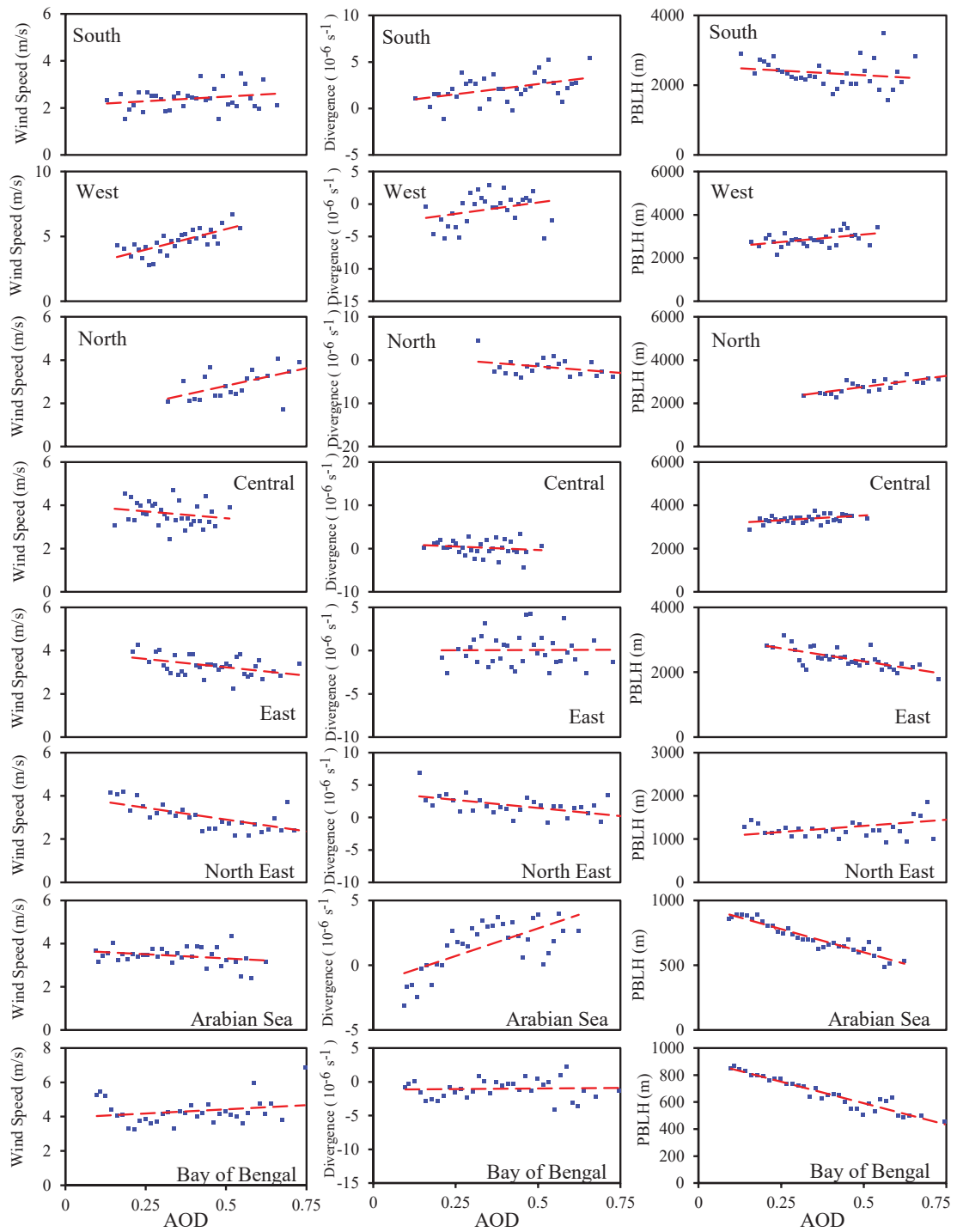
Figure 3.11 Variation of meteorological parameters with MODIS AOD over the sub regions during the pre-monsoon season.
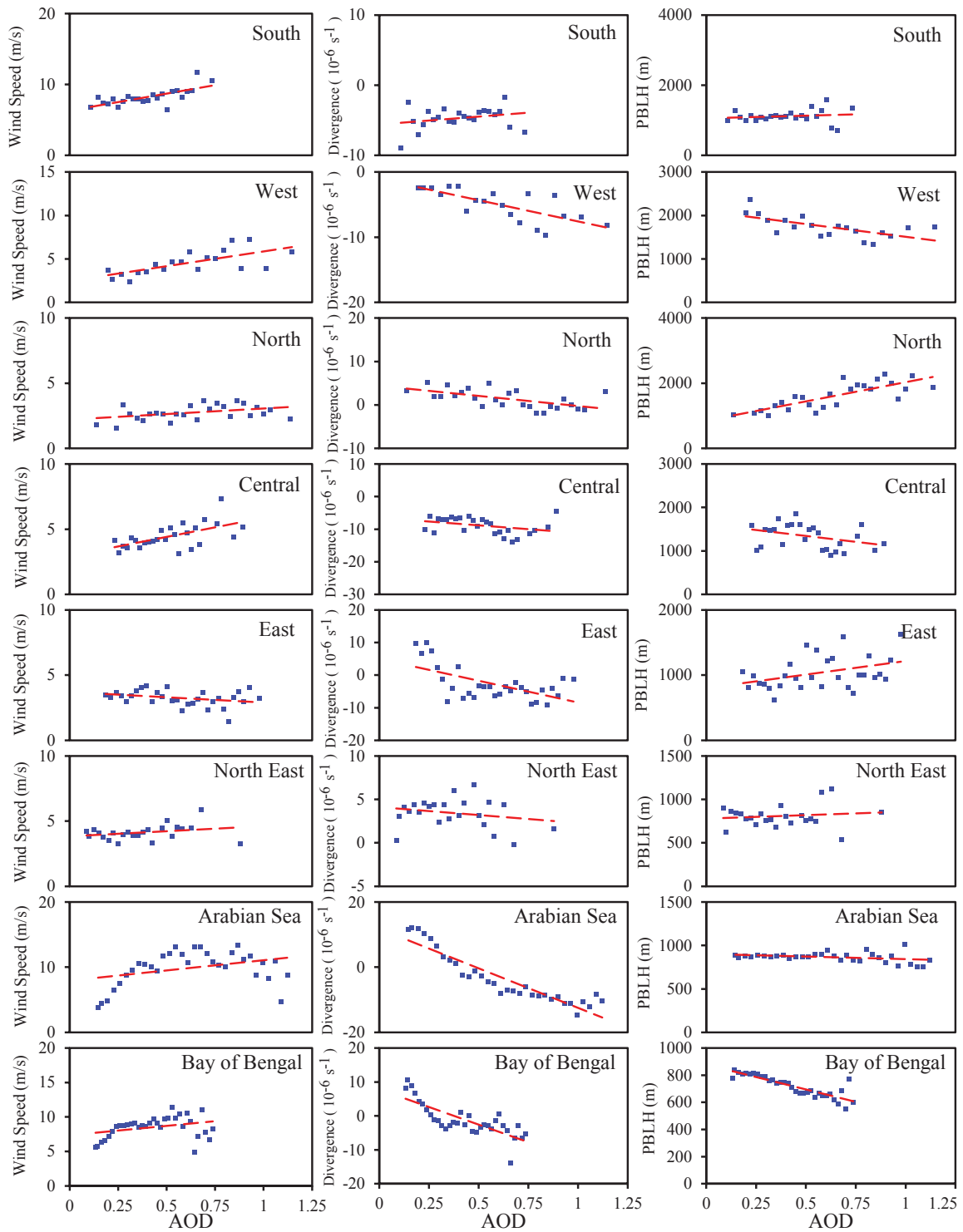
Figure 3.12 Variation of meteorological parameters with MODIS AOD over the sub regions during the monsoon season.

46
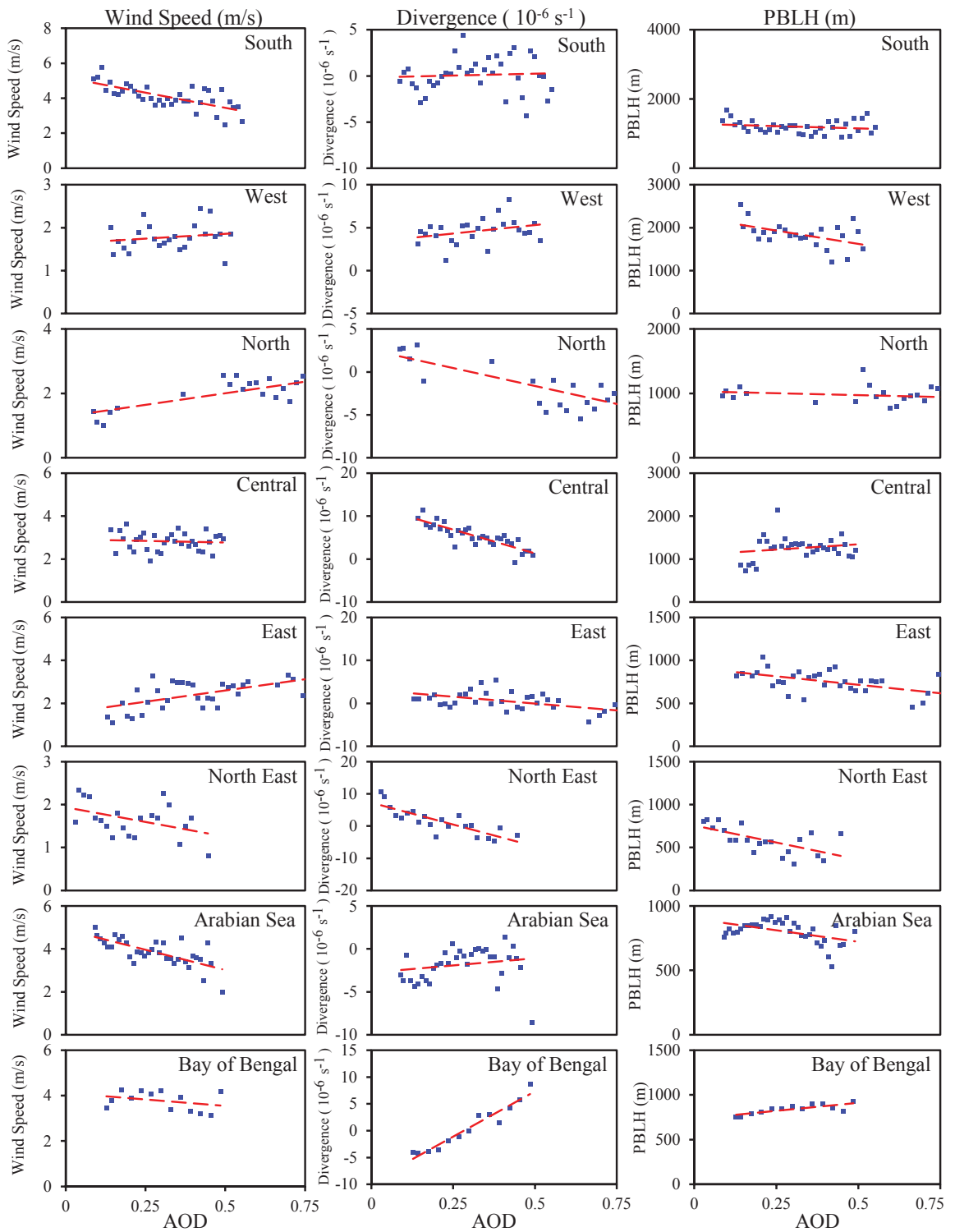
Figure 3.13 Variation of meteorological parameters with MODIS AOD over the sub regions during the post-monsoon season.

47

Region	Winter		Pre-monsoon		Monsoon		Post-monsoon	
	Trend	P-value	Trend	P-value	Trend	P-value	Trend	P-value
S	-3.25	0.01	0.78	0.17	4.81	0.01	-3.44	0.01
W	0.25	0.82	6.33	0.01	3.38	0.01	0.46	0.41
N	0.27	0.63	3.26	0.01	0.86	0.03	1.44	0.01
C	-1.83	0.12	-1.28	0.22	2.93	0.01	-0.30	0.68
E	0.04	0.95	-1.54	0.01	-0.80	0.10	2.11	0.01
NE	-0.14	0.79	-2.17	0.01	0.78	0.20	-1.37	0.06
AS	-0.57	0.43	-0.77	0.08	3.14	0.05	-3.78	0.01
BoB	0.34	0.76	0.95	0.20	2.75	0.06	-1.14	0.28

Table 3.1 Trends in wind speed over the sub regions during each season.

aerosol loading in locations with lower PBLH and low wind speed which is diverging. However, it should be noted that the winter season has larger contribution from SU, BC and OC aerosols (84%) and less contribution from DU and SS aerosols (16%). AOD variation during the pre-monsoon is characterized by decreasing PBLH but is not significant as in winter. The wind divergence is increasing and is coupled with an increasing wind speed. The contribution of DU and SS aerosols (38%) during this season is increased drastically along with a decrease in SU, BC and OC aerosols (62%). The variation of PBLH completely reverses with a significantly increasing trend with AOD during the monsoon season. Though the wind divergence during the monsoon is increasing as in the previous seasons the wind speeds are significantly increasing with AOD. The contribution of DU and SS aerosols during this season is increased to 47% of the total AOD. Thus there exists a pattern wherein lower PBLH and low wind speeds aids SU, BC and OC aerosols and higher PBLH and increased wind speeds aids DU and SS aerosols. This pattern can also be seen during the post-monsoon season. Though not significant, the PBLH and wind speeds experiences decreasing trends with AOD and is characterised by lower contribution by DU and SS aerosols (12%) and larger contribution from SU, BC and OC aerosols (88%).

The west sub-region during the winter season is characterised by increasing PBLH, insignificant but increasing divergence and significantly increasing wind speed with increasing aerosol loading. This is similar to the conditions over the south during the monsoon season and exhibits similar contributions of aerosol types. With increasing

Region	Winter		Pre-monsoon		Monsoon		Post-monsoon	
	Trend	P-value	Trend	P-value	Trend	P-value	Trend	P-value
S	8.80	0.01	4.41	0.01	2.24	0.23	0.83	0.72
W	7.97	0.21	7.02	0.10	-6.51	0.01	3.97	0.12
N	-14.3	0.01	-6.00	0.08	-4.65	0.01	-8.34	0.01
C	-23.9	0.01	-3.26	0.33	-4.68	0.09	-22.10	0.01
E	-8.83	0.01	0.15	0.95	-13.40	0.01	-6.37	0.01
NE	-4.13	0.45	-4.98	0.01	-1.81	0.31	-27.02	0.01
AS	21.15	0.01	8.50	0.01	-24.31	0.01	3.32	0.27
BoB	22.23	0.01	0.34	0.81	-20.63	0.01	33.76	0.01

Table 3.2 Trends in wind divergence over the sub regions during each season.

PBLH and higher wind speeds, the DU and SS aerosols contribute about 35% of the total AOD. The increase in PBLH and wind speed becomes significant during the pre-monsoon season and results in an increased contribution from DU and SS aerosols (72%). Though the wind speed continues to be significantly increasing the PBLH and wind divergence shows a decreasing trend during the monsoon season. As a result, the contribution of DU and SS aerosols (63%) can be seen to deteriorate. As the post-monsoon season approaches the wind speeds become insignificant with significantly decreasing PBLH. As a result, the season witnesses decreased contribution from DU and SS aerosols (24%) when compared to the previous seasons. The results contribute more validity to the dependence of aerosol types on meteorological condition wherein, lower PBLH and low wind speed aids SU, BC and OC aerosols and higher PBLH and increased wind speed aid DU and SS aerosols.

Similar patterns can also be observed over the north sub-region. The winter season is characterised by decreasing PBLH, significantly increasing convergence and insignificantly varying wind speed with increasing aerosol loading. With decreasing PBLH and converging wind, the DU and SS aerosols contributions are low (23%) compared to other seasons. The PBLH and wind speed during the pre-monsoon season becomes significantly increasing with AOD and as expected the contributions of DU and SS aerosols are drastically increased (59%). The PBLH continues to be significantly increasing during the monsoon season but the wind speed though increasing becomes insignificant. This is reflected as a decrease in DU and SS aerosol contribution (46%). As the post-

Region	Winter		Pre-monsoon		Monsoon		Post-monsoon	
	Trend	P-value	Trend	P-value	Trend	P-value	Trend	P-value
S	-1747	0.01	-536	0.25	145	0.53	-273	0.24
W	1077	0.07	1379	0.01	-587	0.01	-1250	0.01
N	-599	0.03	2031	0.01	1179	0.01	-123	0.40
C	-364	0.53	864	0.01	-545	0.07	494	0.28
E	-1250	0.01	-1607	0.01	419	0.03	-392	0.01
NE	-535	0.03	564	0.01	81	0.55	-794	0.01
AS	-791	0.01	-714	0.01	-58	0.07	-356	0.01
BoB	-641	0.01	-639	0.01	-365	0.01	360	0.01

Table 3.3 Trends in PBLH over the sub regions during each season.

monsoon approaches, the PBLH becomes decreasing with decreased contribution from DU and SS aerosols (18%). Similar patterns can be observed over the central, east and north-east regions. Thus in general over the land higher PBLH and higher wind speed supports DU and SS aerosols whereas lower PBLH and low wind speed support SU, BC and OC aerosols. This may be because increased wind speed and higher PBLH results in increased surface wind stress and an unstable atmosphere with increased turbulence in turn supporting DU and SS aerosol production.

The oceanic regions show a different character. Both the AS and BoB are characterised by significantly decreasing PBLH with increasing AOD during the winter and pre-monsoon seasons. Thus the increased aerosols concentrate over relatively stable atmospheric regions over the ocean. The contribution of SS aerosols (approx. 20%) remains low whereas the continental aerosols have a higher contribution to the total AOD. These continental aerosols are mostly transported from the adjacent land areas and concentrate over stable oceanic regions with lower PBLH. As the monsoon season approaches the wind speeds starts to increase causing an increase in SS contribution both over the AS and BoB (39% and 41%).

Both the land and oceanic regions depicts that not only the advection but also the diffusion of atmospheric particles is an important factor in aerosol distribution as indicated by the influence of PBLH. Further, the influence of atmospheric diffusion is quantified by evaluating the PRE of a multiple linear regression model. The results are tabulated

Region		S	W	N	C	E	NE	AS	BoB
Winter	BC	6	6	7	7	7	7	4	5
	DU	9	33	22	16	13	12	16	5
	OC	23	18	22	22	23	28	18	30
	SS	7	2	1	2	1	1	22	19
	SU	55	40	48	53	54	52	39	41
Pre-monsoon	BC	4	2	3	4	4	4	3	4
	DU	27	65	56	46	37	28	36	17
	OC	18	7	12	15	18	28	12	22
	SS	11	7	3	5	5	5	20	23
	SU	41	19	25	31	35	35	29	34
Monsoon	BC	3	2	3	3	4	5	1	2
	DU	31	45	38	30	23	21	36	16
	OC	10	6	10	11	13	17	5	11
	SS	16	18	8	10	9	9	39	41
	SU	41	29	41	47	51	49	20	29
Post-monsoon	BC	5	7	8	7	7	7	5	5
	DU	6	22	17	12	8	8	13	3
	OC	23	22	25	24	26	29	18	21
	SS	6	2	1	1	1	1	21	26
	SU	59	47	50	56	58	55	44	44

Table 3.4 Contribution of various aerosol types to the total AOD inferred from MERRA 2 data.

Location	Winter		Pre-monsoon		Monsoon		Post-monsoon	
	R2	PRE	R2	PRE	R2	PRE	R2	PRE
South	0.79	0.60	0.35	0.11	0.57	0.02	0.52	0
West	0.39	0.07	0.69	0.29	0.62	0.08	0.28	0.18
North	0.78	0.54	0.66	0.45	0.67	0.47	0.75	0.23
Central	0.57	0.01	0.40	0.33	0.48	0.14	0.76	0.06
East	0.66	0.54	0.57	0.46	0.53	0.25	0.55	0.04
North East	0.23	0.20	0.77	0.42	0.13	0.03	0.76	0.24
Arabian Sea	0.78	0.47	0.92	0.83	0.94	0.18	0.66	0.27
Bay of Bengal	0.81	0.46	0.92	0.92	0.83	0.56	0.96	0.43

Table 3.5 Proportion of variations in AOD by the PBLH as inferred by the PRE.

in Table 3.5. The inclusion of PBLH in addition to wind speed and divergence shows significant PRE in most of the cases. This is visible during the winter and pre-monsoon seasons. Higher temperature during the pre-monsoon season results in an unstable atmosphere with more influence on AOD. The PBLH during this season explains almost 30 to 90% of the variance in AOD over various regions. However, the PRE during the monsoon and post-monsoon seasons are lower and is due to the substantial reduction in the spatial variation of PBLH during these seasons. Thus the atmospheric diffusion influences aerosol distribution especially during the winter and pre-monsoon seasons.

3.4 CONCLUSIONS

In this chapter, spatio-temporal distribution of AOD over the Indian sub-continent and the surrounding Indian Ocean ($5°N$ to $40°N$ and $65°E$ to $100°E$) was studied to understand the possible influence of prevailing meteorological conditions. Eleven years (2002-2012) of MODIS AOD data along with wind speed, wind divergence, and PBLH were investigated as parameters for advection and diffusion of atmospheric particles. These parameters derived from reanalysis data sets along with satellite measured AOD values reveals distinctive characteristics over the land and ocean. Further, the study pertains to the influence of meteorology in redistributing atmospheric particles over the region. The main conclusions are summarised as follows.

The distribution of aerosols shows large spatial variability with heavier loading over the IGP. Dust aerosols from the arid regions of Thar Desert are blown over northern India and are eventually spread over the Bay of Bengal. Similar to the foothills of the Himalayas and Tibetan Plateau, mountain ranges such as the Aravali, Eastern Ghats, and the Western Ghats also exhibits spatial gradients with topographical differences. A region in central India bordered by mountain ranges on all four sides shows heavier aerosol loading suggesting the possibility of vertically advected aerosol layers due to surface hindrance but requires further analysis.

Meteorological parameters such as wind speed and divergence show seasonality with increased wind speed and convergence during the monsoon season. Monthly wind speeds and divergence correlates with AOD values both over the land and ocean suggesting an increased aerosol loading at higher wind speed which is converging to the

region. However, there is an increased correlation in wind speeds at higher altitude with a maximum correlation at 850 hPa. The higher correlation was further investigated with backward trajectories at near surface (1000 hPa) and mid-tropospheric (850 hPa) levels describing the importance of wind direction and areal influence of wind trajectories. Apart from the seasonality in AOD, there is also evidence of increasing spatial variability suggesting the accumulation of increased aerosols to particular locations within the region. The Indian subcontinent being a host of varied climatology was further divided into sub-regions for the analysis. Correlation analysis between AOD and the meteorological parameters were carried out over each sub-region. The results depict the influence of prevailing meteorological conditions on distributing various aerosol types over the sub-regions. In general, over the land, higher PBLH and higher wind speed supports DU and SS aerosols whereas lower PBLH and low wind speed supports SU, BC and OC aerosols. This may be because increased wind speed and higher PBLH results in increased surface wind stress and an unstable atmosphere with increased turbulence in turn supporting DU and SS aerosol production. Over the ocean the transported continental aerosols are concentrated over regions of stable atmosphere as denoted by lower PBLH. Increasing wind speeds over the ocean results in an increased SS aerosol concentration over the region. Further, the influence of atmospheric diffusion is quantified by evaluating the PRE of a multiple linear regression model. The inclusion of PBLH in addition to wind speed and divergence shows significant PRE in most of the cases. This is particularly evident during the winter and pre-monsoon seasons where the PBLH explains almost 30 to 90% of the total variance in AOD over the sub-regions.

Chapter 4

A SATELLITE BASED TOP-DOWN APPROACH TO QUANTIFY AEROSOL EMISSIONS

4.1 INTRODUCTION

Accurate forecasting of air quality demands better estimates of aerosol emissions. The accuracy of conventional bottom-up approaches to estimate aerosol emissions depends on the degree to which various influencing parameters are estimated. The availability of satellite observations not only enhances the capability of determining various influencing parameters, but also provides alternate ways of assessing aerosol sources. Aloysius et al. (2008) used the wind data to estimate the transported aerosols and hence, the aerosol source/sink strength. The authors estimated the source of aerosols over Ganga basin by incorporating MODIS AOD data and NCEP reanalysis wind data to the aerosol flux continuity equation. The ASS was estimated over $2.5° \times 2.5°$ grids and showed good correlation with the concentration of thermal power plants in the basin. Prijith et al. (2013) used the aerosol flux continuity equation to derive an aerosol source/sink map over the globe. Thus aerosol production or deposition for twenty-four hours was estimated using AOD obtained from MODIS. Though this approach incorporates the wind factor to estimate aerosol source, huge uncertainties exist as daily sources are estimated based on a single AOD data for a day. This is because as time period increases the wind mass traverse vast distances encountering numerous sources and sinks in its path. An abundant source or sink in its path may be reflected as increased aerosol production or deposition at the computed grid. A better estimate of aerosol sources daily

is feasible but at the expense of a coarser resolution. Thus identification of isolated sources is difficult. Moreover the flux continuity equation does not account for the diffusion of aerosols nor the atmospheric stability conditions. Not only the advection of aerosols by wind and its redistribution based on convergence but also the diffusion of these particles during their residence in the atmosphere is an important parameter (Ziomas et al., 1995; Quan et al., 2013; Wang et al., 2016; Su et al., 2018; Nizar and Dodamani, 2019). This chapter uses a Lagrangian approach to the Advection Diffusion Equation (ADE) to estimate the transported aerosols and hence the Aerosol Source Strength (ASS) using satellite-measured Aerosol Optical Depth (AOD) and reanalysis wind data. This top-down approach is based on the advection and diffusion of atmospheric aerosols considering wind circulation and atmospheric conditions rather than using indicative parameters.

Daily measurements of AOD over the Indian subcontinent is available from the MODIS sensor on board Terra and Aqua satellites. Terra and Aqua overpass the study domain roughly at around 06:00 (UTC) and 09:00 (UTC). Thus a three hour ASS can be computed between 06:00 and 09:00 (UTC). Though the aerosol sources computed for three hours have better accuracy than a 24 hour source (Prijith et al. 20013), this represents the source strength only for a very small fraction of the day. In this regard geostationary satellites with timely measurements can provide ASS estimates throughout the day. Though the indigenous geostationary satellite such as INSAT3D/3DR provides AOD measurements every 30 minutes, these images have limitations for AOD estimation due to only one channel for aerosol detection. Thus to validate the current top down approach, the study first utilizes the AOD measurements from the GOES-16 for California and then applies the methodology over southern India using MODIS to identify aerosol hotspots. Conventional emission estimations employ a bottom-up approach wherein, the ground parameters (e.g., amount of fuel burned, duration, type of fuel, and its spatial extend etc.) are collected and estimates of atmospheric emissions are prepared. In contrast, the top-down approach employed in this study utilizes the remotely sensed data pertaining to the total atmospheric pollution and prepares estimates of ground emissions based on the meteorological parameters and spatio-temporal dis-

tribution of these pollutants. Being a Lagrangian approach, the present ASS algorithm tracks wind masses as it traverses during a certain time. Computations are carried out at each grid separately rather than a large fixed spatial extend.

4.2 WILDFIRE AEROSOL EMISSIONS OVER CALIFORNIA

California is one of the most innovative State in terms of pollution control strategies with strong environmental standards (Vogel, 2019). But the State has witnessed numerous wildfires resulting in prolonged public exposure to poor air quality. The 2018 wildfire season was the most destructive, with July seeing some of the most widespread fires such as the Mendocino Complex and Carr fire. Understanding the potential source regions of air pollutants and their relative contributions are of great importance for air pollution control strategies. The present study thus focusses on the aerosol emissions over California during July 2018. ASS is computed every three hours at at $0.25° \times 0.25°$ grids across California during July 2018 using AOD retrievals from the GOES-16 with observations every 15 min. As the proposed method does not involve indicative parameters such as FRP, this method can be extended to applications that do not involve fire, such as estimation of power plant emissions, dust emissions, etc. Of course the distinction of various sources contributing to the aerosol emission is ambiguous and could have contribution from multiple sources. However, an ASS map of a region would be helpful in investigating the correlation of aerosol emissions with the spatial distribution of potential sources such as power plants, industries, and deserts dust, etc. The computed ASS is thus compared with the distribution of power plants over California.

4.2.1 Methodology
GOES AOD

The Geostationary Operational Environmental Satellite (GOES)-16, hosts on-board the Advanced Baseline Imager (ABI; Schmit et al. (2005, 2017)), which measures radiances in multiple wavelengths at high spatial and temporal resolution. With over 16 different spectral bands ranging from the UV through IR, the aerosol optical depth products derived from ABI can potentially have statistical qualities similar to those from MODIS and VIIRS Zhou et al. (2018). The ABI L2+ aerosol optical depth product at 550 nm

over the full disk available every 15 minutes is used in this study. To reduce computational time, aerosol source strength was computed every three hours at a spatial resolution of $0.25°$. Thus a $0.25° \times 0.25°$ AOD data was compiled every three hours (starting from 0:00 UTC) from the 2 km AOD data. Before resampling the data, missing data values were filled from adjacent time periods. For this, the AOD at a particular time t (AOD_t), was compared with AOD_{t-1}, AOD_{t+1}, and AOD_{avg} $\left(\frac{AOD_{t-1}+AOD_{t+1}}{2}\right)$. The results indicate a better correlation of AOD_t with AOD_{avg} ($R^2 = 0.87$) than AOD_{t-1} ($R^2 = 0.78$) and AOD_{t+1} ($R^2 = 0.81$; Figure 4.1). Thus the missing AOD values were filled based on the availability of adjacent data.

$$\text{Missing } AOD_t = \begin{cases} AOD_{avg} & \text{; if both } AOD_{t\pm1} \text{ are available} \\ AOD_{t\pm1} & \text{; which ever is available} \\ \text{No data} & \text{; if none are available} \end{cases} \quad (4.1)$$
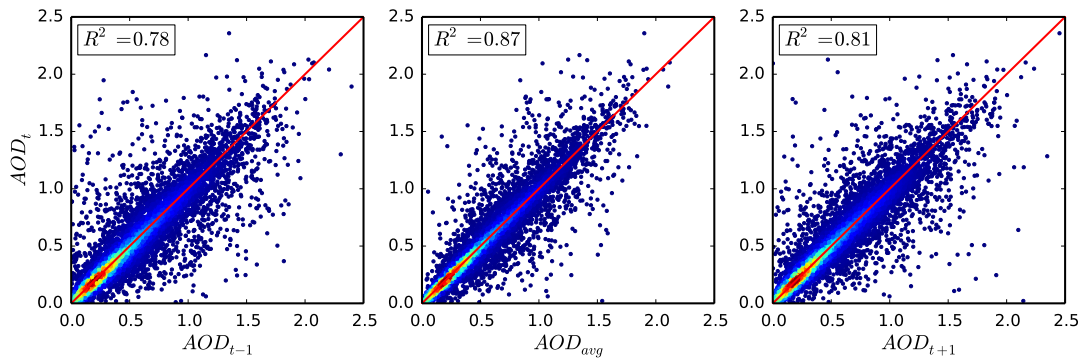
Figure 4.1 Comparison of GOES-16 AOD at adjacent times over California during July 2018.

Advection-Diffusion equation

Aerosol transportation is strongly influenced by wind which may enhance or diminish its concentration by convergence or divergence (Aloysius et al., 2008; Prijith et al., 2013). The present study proposes a lagrangian approach to the ADE to estimate the transported aerosol and hence the ASS using satellite measured AOD and reanalysed

58

wind data. The three dimensional ADE is given by:

$$\frac{\partial \rho}{\partial t} + u\frac{\partial \rho}{\partial x} + v\frac{\partial \rho}{\partial y} + w\frac{\partial \rho}{\partial z} = D_x\frac{\partial^2 \rho}{\partial x^2} + D_y\frac{\partial^2 \rho}{\partial y^2} + D_z\frac{\partial^2 \rho}{\partial z^2} \qquad (4.2)$$

Where ρ is the aerosol extinction coefficient per unit volume, u, v, and w are the wind velocities in the x, y, and z direction and D_x, D_y, and D_z are the turbulent diffusion coefficients in the respective directions. For an instantaneous volumetric source over a range $\left(\frac{-L}{2} < x < \frac{L}{2}\right), \left(\frac{-L}{2} < y < \frac{L}{2}\right)$, and $\left(\frac{-d}{2} < z < \frac{d}{2}\right)$, the solution is given by:

$$
\begin{aligned}
\rho\,(x,y,z,t) = &\frac{\rho_o}{8}\left(erf\left(\frac{\left(x+\frac{L}{2}\right)-ut}{\sqrt{4D_xt}}\right) - erf\left(\frac{\left(x-\frac{L}{2}\right)-ut}{\sqrt{4D_xt}}\right)\right) \times \\
&\left(erf\left(\frac{\left(y+\frac{L}{2}\right)}{\sqrt{4D_yt}}\right) - erf\left(\frac{\left(y-\frac{L}{2}\right)}{\sqrt{4D_yt}}\right)\right) \times \\
&\left(erf\left(\frac{\left(z+\frac{d}{2}\right)}{\sqrt{4D_zt}}\right) - erf\left(\frac{\left(z-\frac{d}{2}\right)}{\sqrt{4D_zt}}\right)\right)
\end{aligned}
\qquad (4.3)
$$

The vertical atmospheric column at each grid was divided into different layers to account for the vertical gradient of horizontal wind speed and direction. To decide the layer depth, cluster analysis was performed at various locations along a central section of California based on wind speed and direction of vertical atmospheric layers. The K mean clustering was employed which partitions each atmospheric layer to a cluster with the closest mean. Basically it tries to minimise the variances or Squared Euclidean Distances within each cluster. The number of clusters at each location was decided based on elbow method wherein, the variations explained is plotted as a function of the number of clusters. The number of clusters corresponding to the bend (Elbow) in the plot represents the optimum number of cluster which in this case varied from three to five depending on the ground elevation of the location. The result of the cluster analysis is plotted in Figure 4.2, which reveals a vertical structure of the atmosphere based on wind speed and direction. The present study adopted a total of 5 vertical layers centered at 750, 1500, 2000, and 3500 m above mean sea level.

The total columnar AOD at a grid was converted to normalized aerosol extinction profile at each vertical layer, assuming an exponentially decreasing vertical profile with a scale height of 2 km. Since the depth (d), of these 3D grids is very small as compared
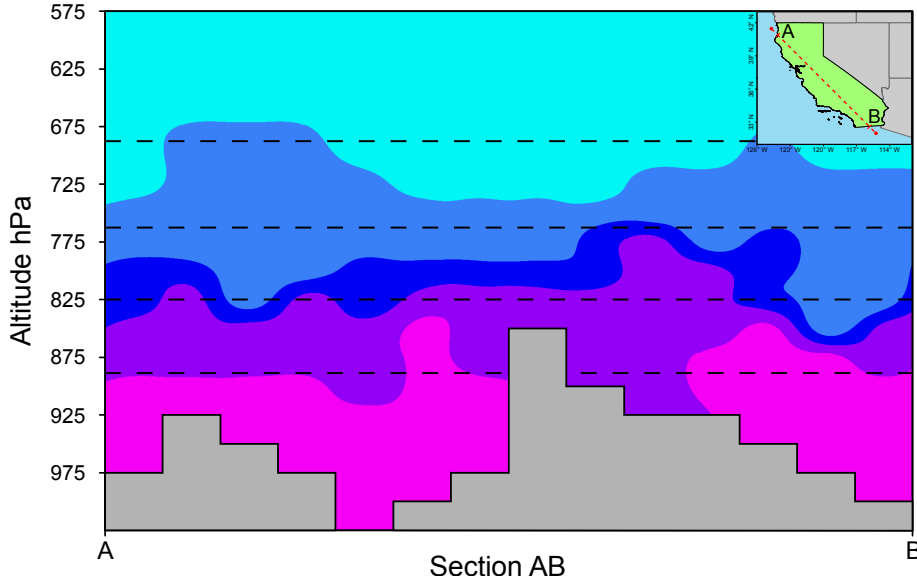
Figure 4.2 Clusters of atmospheric wind over a section across California during July 2018.

to the other two dimensions ($L \approx 25d$), the diffusion in the longitudinal and lateral direction will be minimal compared to the vertical direction for a given period. The eddy diffusion coefficient (D_z) for pollutants is usually assumed to equal K_h (eddy diffusivity for heat) and experimental evidence tends to support this (Lodge, 1983). A common characteristic of K_h is that it has a linear variation near ground, a constant value at mid mixing depth and a decreasing trend as the top of the mixing layer is approached. Shir (1973) gave such an expression based on theoretical analysis of neutral boundary layer, in the form:

$$D_z = \kappa u_* z \times exp \left(\frac{-4fz}{u_*} \right) \tag{4.4}$$

Where, κ is the Von Karman constant, u_* is the shear velocity, z is the depth of flow, and f is the coriolis parameter given by $f = 2\Omega sin\varphi$. Where, Ω is the rotation rate of the earth in radians/s, and Ω is the latitude in degree decimals. To compute u_* under different stability conditions, the wind profile is used.

$$u(z) = \frac{u_*}{\kappa} \left(ln \left(\frac{z}{z_0} \right) - \psi_m(\zeta) \right) \tag{4.5}$$

Where ψ_m is the integrated form of the universal function given as,

$$\psi_m(\zeta) = \begin{cases} -6\zeta & ; \text{stable} \\ ln\left(\left(\frac{1+x^2}{2}\right)\left(\frac{1+x}{2}\right)^2\right) - 2tan^{-1}x + \frac{\pi}{2} & ; \text{unstable} \end{cases} \qquad (4.6)$$

Where $x = (1 - 19.3\zeta)^{\frac{1}{4}}$, and the stability parameter is defined as $\zeta = \frac{z-d}{L}$, where L is the Obukhov length (m).
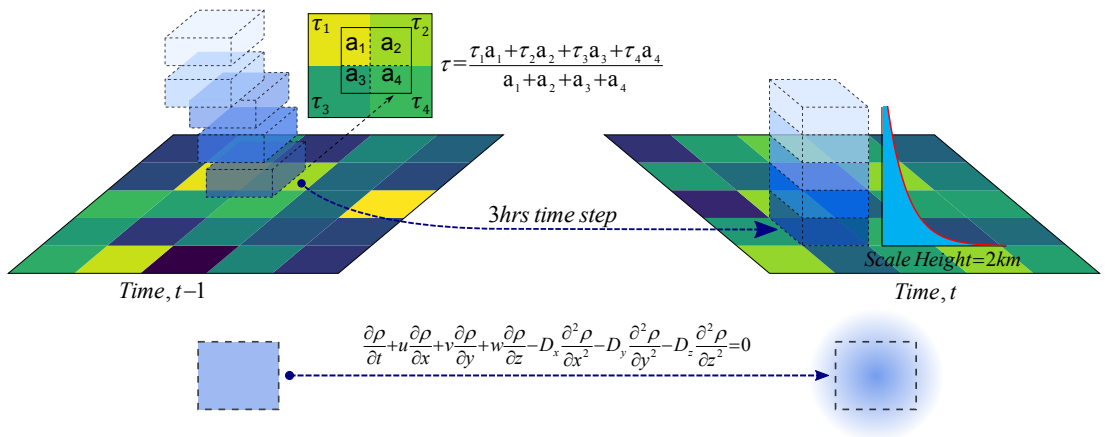
Figure 4.3 Schematic of the proposed methodology.

For each grid point, the transported aerosol extinction coefficient ρ is calculated from the initial aerosol extinction coefficient ρ_o using the advection-diffusion equation. A three-hour backward trajectory is computed using the PC-Windows-based NOAA HYSPLIT model (Stein et al., 2015; Rolph et al., 2017) to find the grid location at time $t-1$. ρ_o is the aerosol extinction coefficient over this location at this time. Similarly, ρ is computed for each vertical layer and its vertical integration at a grid, gives the columnar transported AOD (τ_T).

$$\tau_T(x,y) = \int_0^H \rho(x,y,z)dz \qquad (4.7)$$

The column integrated source strength $S(x,y)$ can thus be expressed per unit area per unit time as the difference between the actual columnar AOD at time t, and the columnar transported AOD.

$$S(x,y) = \tau(x,y) - \tau_T(x,y) \tag{4.8}$$

MODIS FRP

The temporal integration of satellite retrieved FRP is directly proportional to the total amount of fuel consumed by fire (Li et al., 2018), which in turn is directly proportional to aerosol emissions from the fire. Thus, the computed ASS at fire locations is compared with MODIS MaxFRP. The MODIS sensor onboard Terra satellite provides daily fire products at a spatial resolution of 1 km. The MaxFRP values from MOD14A1 level 3 – version 6 data product (Giglio et al., 2016) is used in this study. The daily MaxFRP at each $0.25° \times 0.25°$ grids are resampled by taking the summation of MaxFRP values within each grid. The collocated MaxFRP values for July are then sorted as a function of ASS and is averaged into equal bins of 5 percentiles each. The average value of MaxFRP for each bin is plotted against mean ASS values to illustrate the correlation between AOD-based and FRP-based approach for estimating biomass emissions.

Power plant concentration

A quantitative comparison between the concentration of thermal power plants and ASS over California is also performed. The power plant shapefile data was acquired from the US energy information administration (EIA) website. In order to give equal weight to the aerosol pollution from the power plants lying in all directions, their concentration in each $0.25° \times 0.25°$ grid was determined by defining a circle of influence with radius $0.25°$ and centre in the middle of the grid. The variation of average ASS in this influence zone with the corresponding power plant concentration is then studied.

4.2.2 Results

The spatial distribution of AOD, along with surface wind pattern, is shown in Figure 4.4. The state experiences a maximum AOD of 0.55 with considerable spatial variation (CV = 35%) from a mean value of 0.23. The wind pattern shows steady inflow of marine air into the Central Valley through the San Francisco Bay. The Central Valley shows a

higher concentration of AOD towards the downwind regions indicating the advection of aerosol particles from their sources by the prevailing winds. Moreover, this flat valley experiences higher aerosol loading when compared to the surrounding mountain ranges. This is due to the surrounding mountainous topography that obstructs wind, trapping pollutants within the valley (De Young et al., 2005). Thus the spatial distribution of aerosols does not necessarily reflect the spatial distribution of its sources.
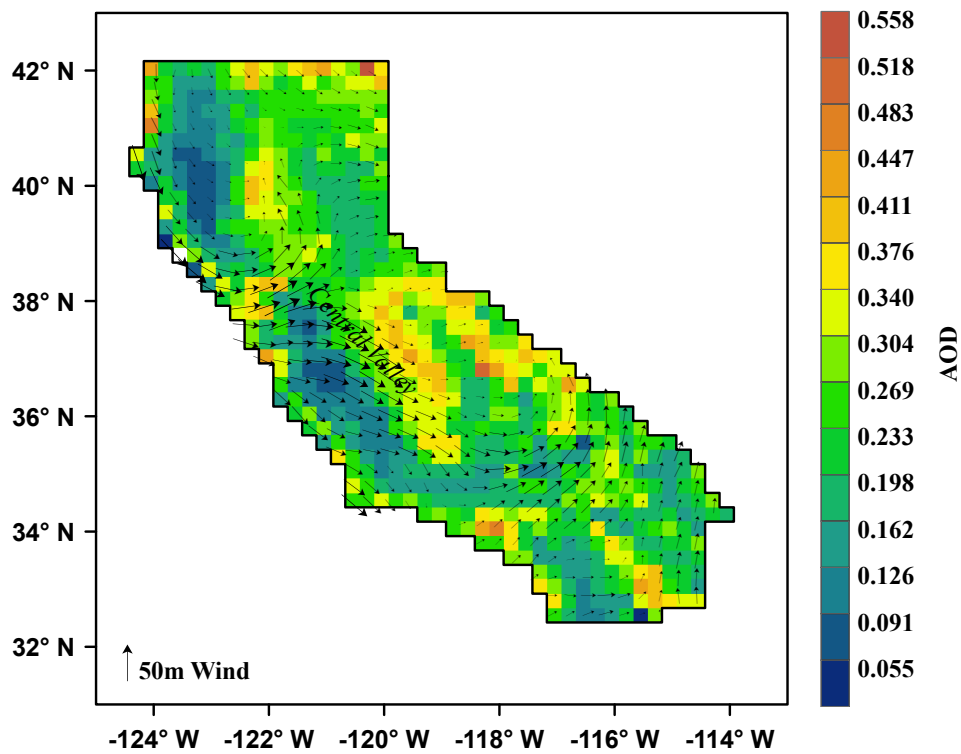
Figure 4.4 AOD over California during July 2018 along with surface wind pattern.

The ASS distribution over the State computed using the proposed methodology is presented in Figure 4.5. Major sources of aerosols such as power plants and wildfire locations are also located in the figure. The State exhibits a maximum ASS of 0.14 AOD/hr and an average ASS of 0.02 AOD/hr. Aerosol sources are prominent around densely populated regions such as San Francisco, Los Angeles and Orange County. The Coastal ranges are seen devoid of significant aerosol sources except along a narrow strip

of low lying coastal areas. Aerosol sources in the Central valley are distinctly visible between mountain ranges. The major population centers within the valley (Bakersfield, Fresno, Sacramento, and Redding) appears as clusters of aerosol sources. Unlike northern California where most of the aerosol sources are anthropogenic, southern California, especially the Mojave Desert, inhibits natural aerosols. Desert dust is the primary source of aerosols, wherein the emissions vary depending on surface roughness, sediment availability, and friction velocity (Sweeney et al., 2011). The spatial occurrence of low dust emitting (desert pavements) and high dust emitting landforms (sand dunes, dry washes, etc.) influences the spatial distribution of aerosol sources within the region.
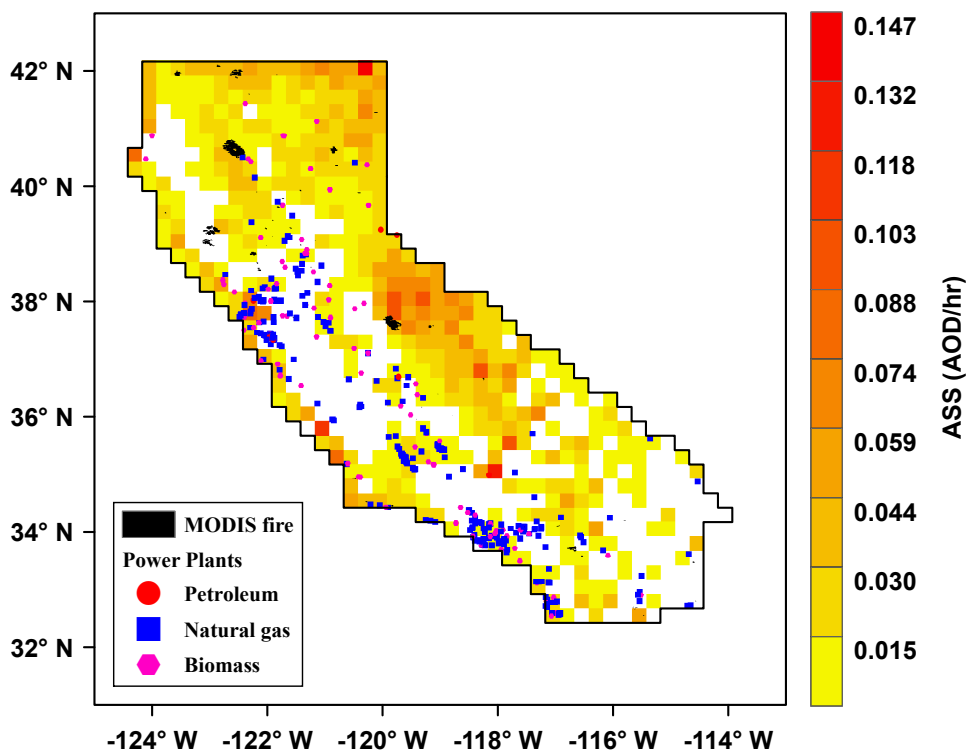
Figure 4.5 ASS over California during July 2018 along with prominent sources.

Another major source of atmospheric aerosols is wildfire biomass burning emissions. The State witnessed numerous wildfires during July, burning over 721,794 acres of land. The major fires are shown in Figure 4.5. As expected, the result shows higher

ASS around fire locations. Starting from the north, the Klamathon Fire recorded over 230 fire pixels with a mean FRP of 10.21 MW. The Klamathon Fire produced an ASS of 0.035 AOD/hr. The Carr Fire, being the most massive fire in terms of area, burned over 929 fire pixels with a mean FRP of 38.635 MW, and is characterized by an ASS of 0.023 AOD/hr. Though the Mendocino Complex Fire started by the end of July, it burned over 474 fire pixels in 5 days with a mean FRP of 17.61 MW. The fire exhibits an ASS of 0.034 AOD/hr during July. Finally, the Ferguson Fire near the Sierra National Forest burned over 572 fire pixels starting from 13th of July with a mean FRP of 20.56 MW, exhibiting an ASS of 0.065 AOD/hr.

Figure 4.6 Variation of ASS with MODIS MaxFRP over California during July 2018.

The temporal integration of satellite retrieved FRP is directly proportional to the total amount of fuel consumed by fire (Li et al., 2018), which in turn, is directly proportional to aerosol emissions from the fire. In other words, FRP should be linearly related to the ASS computed using the proposed methodology. Figure 4.6 plots the variation

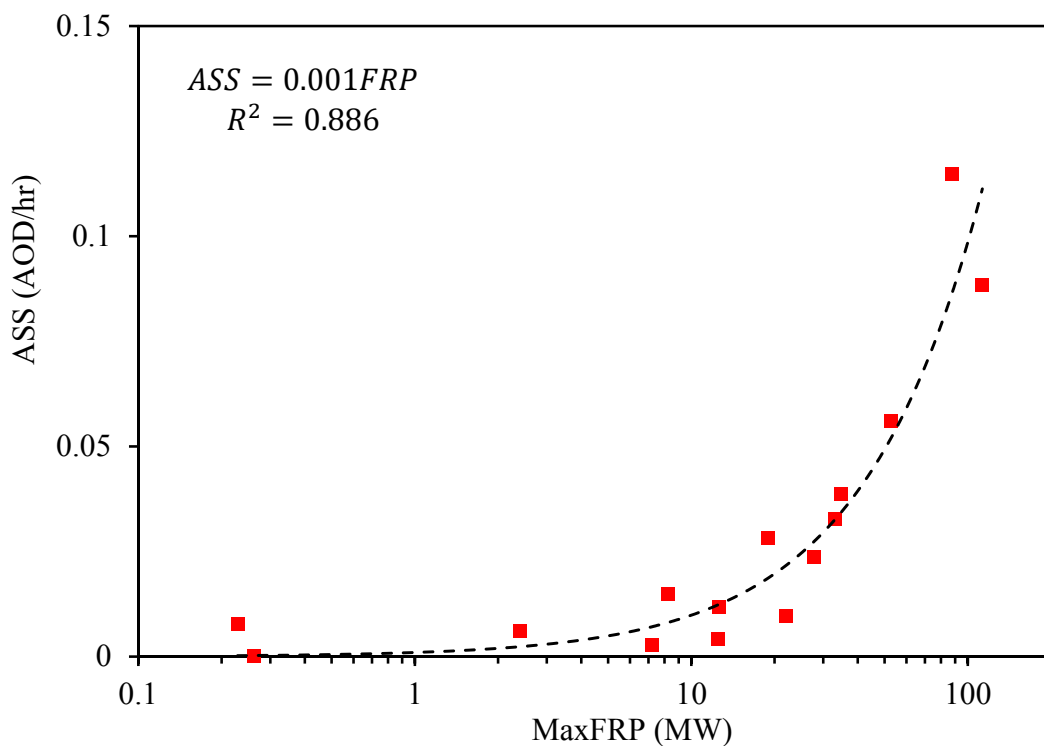of the computed ASS with the MODIS retrieved MaxFRP. Since MaxFRP value ranges from one to several 100s, a logarithmic scale is applied. The plot shows a high linear correlation ($R^2 = 0.886$) between ASS and FRP. A scalar multiplication factor of 0.001 AOD/MW-hr can be obtained from the relationship. Satellite FRP has been proved to provide reliable estimates of biomass burning emissions (Wooster et al., 2005; Freeborn et al., 2008). Thus, a linear relationship validates that the ASS computed using the proposed methodology reflects the actual aerosol production rather than the residual or transported aerosols.

As the proposed method is based on advection and diffusion of atmospheric aerosols rather than using indicative parameters such as FRP, this method can be applied to estimate sources that do not involve fire. The distribution of non-renewable power plants in the State correlates spatially with ASS as evident from Figure 4.5. This spatial correlation was further explored, and the variation of ASS with power plant density is shown in Figure 4.7. The graph shows a steady increase in ASS with power plant density. However, it should also be noted that these power plants are located near populated areas which can have vehicular and other anthropogenic aerosol contributions. Nevertheless, such a high correlation with power plant density ($R^2 = 0.82$) implies the contribution of power plant emissions. The results also help to infer the significance of anthropogenic sources in comparison to natural emissions. In fact the results indicates that, the region of highest power plant density (20 $powerplants/2400km^2$) records an ASS of 0.021 AOD/hr, which is similar to the emissions from the Carr fire.

4.3 AEROSOL EMISSION HOTSPOTS OVER SOUTHERN INDIA

In this study, aerosol production or deposition during the time between the passage of MODIS on board Aqua and Terra was estimated using the AOD obtained from these satellites. Terra and Aqua overpass the study domain roughly at around 06:00 (UTC) and 09:00 (UTC) respectively. Thus a three hour aerosol source strength was computed for each day rather than for 24 hours using AOD values of adjacent days. The
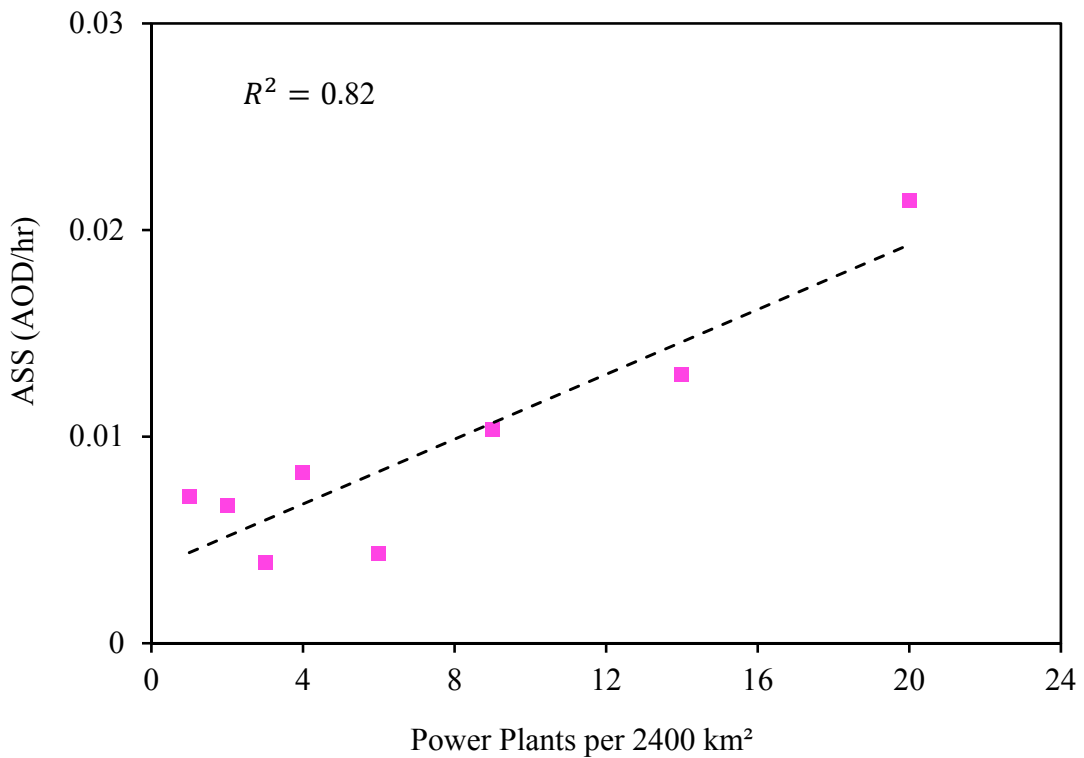
Figure 4.7 Variation of ASS with power plant concentration over California during July 2018.

methodology is explained in section 4.2.1

4.3.1 Results

Aerosol distribution

Before investigating the aerosol emission sources, it is necessary to study its spatial distribution over the region. The spatial distribution of AOD highlighting its spatial variability over sourthern India during the premonsoon along with prominent sources are presented in Figure 4.8.

Large concentration of aerosols are found over the Bay of Bengal along the eastern coast. As discussed in Chapter 3, this is an extension of the IGP aerosol loading. Heavy aerosol loading over the Thar Desert in western India and eastern Pakistan is transported over northern India along the IGP and is eventually spread over the Bay of Bengal in the eastern Indian Ocean (Washington et al., 2003; Dey, 2004). The influence of continental aerosols on the adjacent oceanic regions can be inferred as most of the heavier aerosol
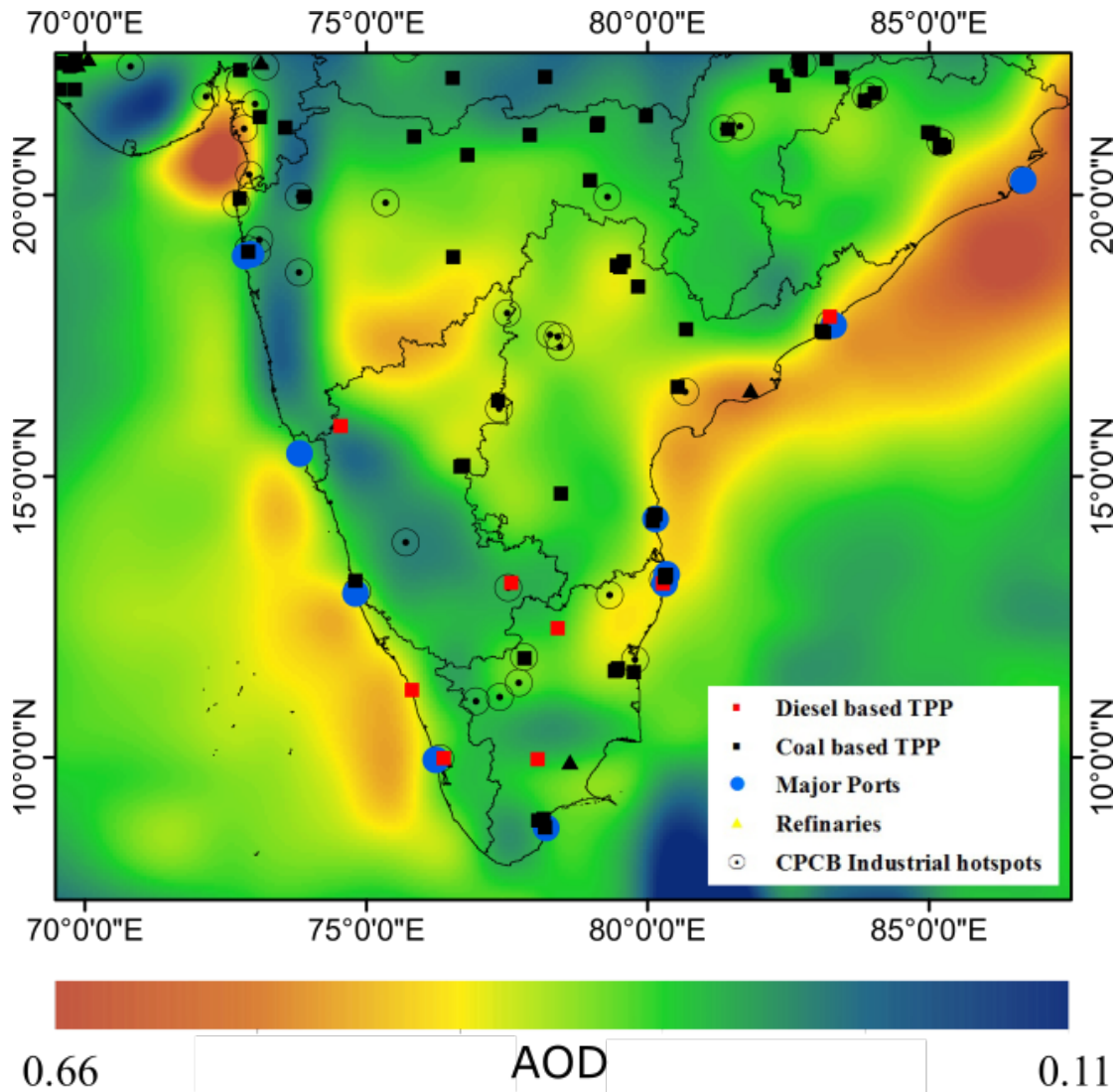
Figure 4.8 AOD distribution during the premonsoon season along with prominent sources.

concentrations are observed along the coast and weaken as the distance from the land increases. Along the west coast, aerosols are concentrated near the Kerala-Karnataka coast. The southern coast of Gujarat is another major location of aerosol concentration. As discussed in Chapter 3, these concentrations are dependent on various meteorological conditions and the distribution of sources and sinks and does not necessarily reflect the distribution of aerosol sources over the region. This is evident from the figure as most of the sources such as thermal power plants and CPCB industrial hotspots shows lower AOD. Especially the clusters of coal based thermal power plants along the 20°N
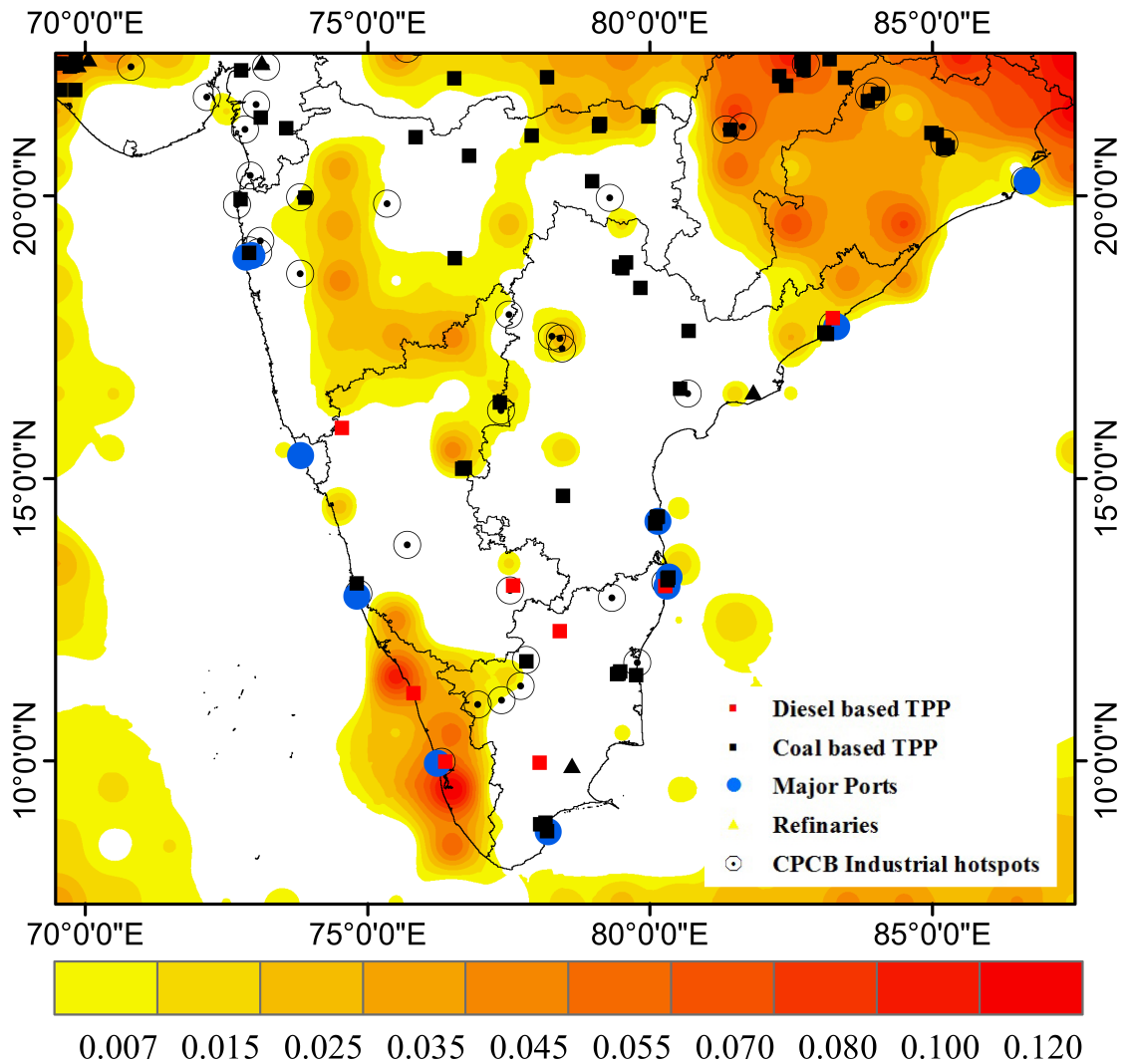
Figure 4.9 ASS (AOD/hr) during the premonsoon season computed using the proposed method.

latitude shows low aerosol concentration but are actually one of the major sources.

Aerosol sources

The average aerosol source computed during the premonsoon season over southern India is shown in Figure 4.9. Though the AOD map shows higher concentration over the Bay of Bengal, the ASS computed using the proposed method shows low aerosol emission. Thus the model is able to identify BoB AOD as transported aerosol. In contrast, though the AOD map shows low values over the clusters of coal power plants in central India, the model clearly simulates aerosol emissions. In fact, these are regions of high

aerosol production. similar results can be seen over the west coast where the aerosols are emitted from the adjacent land towards the sea. Emissions are high over the land and is transported over to the sea. However, certain location of Maharashtra shows higher aerosol emissions, even though not associated with any major sources. This could be due to various other sources such as vehicles, arid lands, industries, biomass burning, etc. Though ASS is estimated only for a short time of the day, the average ASS during the premonsoon season can identify the major hotspots in the study area during the season. Apart from providing prior knowledge about the major pollution centres, the study also provides a new perspective of studying the influence of aerosols on rainfall. This is explored in the next chapter.

4.3.2 Conclusions

In this chapter a top-down lagrangian approach is proposed to quantify aerosol emissions using satellite AOD data. The study employs the ADE to estimate the transported aerosols and hence the ASS. ASS is first computed over California during July 2018 and is then applied over southern India.

The distribution of aerosols over California is influenced by the prevailing wind pattern and topography, with higher AOD concentration towards downwind regions. Though AOD data reveals the spatial distribution of aerosols, it does not necessarily represent the emission sources. The ASS generated using the proposed methodology reveals distinct aerosol emission hotspots over California. The distribution of aerosol sources vary depending on the geographic features within the State, with prominent aerosol sources around densely populated regions. The computed ASS shows higher values around wildfire regions, which is a significant source of atmospheric aerosols. The Ferguson Fire near the Sierra National Forest exhibited the highest aerosol emission (0.065 AOD/hr) followed by the Klamathon Fire (0.035 AOD/hr), the Mendocino Complex Fire (0.034 AOD/hr), and the Carr Fire (0.023 AOD/hr).

As the temporal integration of satellite retrieved FRP is proportional to aerosol emissions from the fire, the computed ASS at fire locations was compared with MODIS MaxFRP. The results indicate a high linear correlation (R2 = 0.886) between ASS and FRP with a scalar multiplication factor of 0.001 AOD/MW-hr. A linear relationship

validates that the ASS computed using the proposed methodology reflects the actual aerosol production rather than the residual or transported aerosols. As the proposed method is based on advection and diffusion of atmospheric aerosols rather than using indicative parameters such as FRP, this method was applied to investigate the spatial correlation of ASS with power plant density. There is a steady increase in ASS with power plant density, with the region of highest power plant density recording an ASS of 0.021 AOD/hr, which is similar to the aerosol emission from the Carr Fire. The study thus aids to infer the relative importance of various emission sources in the region. Application of the methodology over the Indian subcontinent reveals its aerosol source hotspots during the premonsoon season. The model is able to distinguish the transported aerosols and hence points out the actual aerosol production centres. The clusters of coal based thermal power plants along the $20°$ N latitude exhibits higher source strength apart from various CPCB industrial hotspots.

Chapter 5

INVESTIGATING THE POSSIBLE RELATIONSHIP BETWEEN RAINFALL AND AEROSOL DISTRIBUTION

5.1 INTRODUCTION

Rainfall irrigates more than 65% of the cultivated land in India and is a major factor in agricultural output. For a rain fed agrarian country like India whose gross domestic product is nurtured by agricultural sector, understanding the spatial and temporal patterns in rainfall is a very vital issue with significant implications on water resources and management policies.

Aerosol radiative and microphysical effects suppress precipitation and tends to spin down the hydrological cycle (Ramanathan et al., 2005). Crutzen and Andreae (1990) studied the cloud microphysics and aerosols. Their study shows that aerosols not only enhance precipitation by acting as cloud condensation nuclei, but also suppress the downpour of atmospheric moisture if abundant. Forest fire is one of the prominent natural source of atmospheric aerosol releasing large quantities of smoke. The impact of such heavy smoke on precipitation anomalies was studied by Rosenfeld (1999). Using satellite precipitation data he observed that the effect is to shut off warm air process in convective tropical clouds and explained this suppression as a result of increased cloud condensation nuclei, inhibiting the growth of cloud droplets. He also pointed out that this indirect effect increased the cloud lifetime. The clouds take more time until its depth is increased with colder cloud top temperatures and eventually raining out.

5.2 DATA AND METHODOLOGY

5.2.1 Aerosol and Cloud Data

Terra and Aqua satellites boarding the Moderate Resolution Imaging Spectroradiometer, provide global observations of aerosol optical depth. These observations provide daily insight into the global distribution of column integrated aerosols. Various MODIS AOD products over the Indian region has been validated by numerous researchers (Tripathi et al., 2005; Choudhry et al., 2012; Misra et al., 2015). Daily AOD from Collection 6.1, level 2 AOD products derived from Terra's MODIS measurements are used in this study (https://ladsweb.modaps.eosdis.nasa.gov/). For analysing the impact of aerosol variations on cloud, various cloud properties such as cloud fraction (CF), cloud top pressure (CTP), and cloud top temperature (CTT) was also retrieved from Terra observations.

5.2.2 Rainfall Data

The Indian Meteorological Department's (IMD) Gridded Rainfall Dataset of $0.25°$ resolution is utilized. This enables to study the possible connection between rainfall trends at a finer resolution. The dataset has been compiled from more than 6955 rain gauge stations, temporal period covering longer than 110 years over India. The detailed description of the dataset has been discussed by Pai et al. (2014). They have also compared the Gridded dataset with other existing datasets showing comparable results.

5.2.3 Methodology

Mann-Kendall trend test

The Mann-Kendall (MK) trend test (Mann, 1945; Kendall, 1955) is adopted in this paper. This test is frequently used to distinguish monotonic inclinations in hydrological, environmental or climate data series. This is a non-parametric approach and so does not necessitate any assumption about the form of distribution of the data. The null hypothesis H_0 for the test that there is no trend in the series is tested against the alternate hypothesis H_A , that the data tracks a monotonic trend. The computations assume that the observations are independent.

The Mann-Kendall test statistics is calculated according to:

$$S = \sum_{k=1}^{n-1} \sum_{j=k+1}^{n} sgn\left(X_j - X_k\right) \qquad (5.1)$$

where,

$$sgn(x) = \begin{cases} +1 & if \quad x > 0 \\ 0 & if \quad x = 0 \\ -1 & if \quad x < 0 \end{cases} \qquad (5.2)$$

The mean and variance of S is given by:

$$\text{Mean, } E[S] = 0 \qquad (5.3)$$

$$\text{Variance, } \sigma^2 = \frac{\left\{n(n-1)(2n+5) - \sum_{j=1}^{p} t_j(t_j-1)(2t_j+5)\right\}}{18} \qquad (5.4)$$

Where, p is the number of tied groups in the dataset and t_j is the number of data points in the jth tied group. The statistic S is approximately normally distributed provided the following Z transform is applied.

$$Z = \begin{cases} \frac{S-1}{\sqrt{Var(S)}} & if \quad S > 0 \\ 0 & if \quad S = 0 \\ \frac{S+1}{\sqrt{Var(S)}} & if \quad S < 0 \end{cases} \qquad (5.5)$$

The null hypothesis (H_0) is rejected at a significance level α, if $|Z|$ is greater than the value of standard normalized distribution $(Z_{(1-\frac{\alpha}{2})})$ with a probability of $\frac{\alpha}{2}$. A significance level of is 0.05 used to test the null hypothesis H_0. A positive (negative) Z value means increasing (decreasing) trend.

Rainfall and cloud association with aerosol loading

To study the possible correlation between aerosol, cloud and rainfall only those data points were used where a concurrent values where available for each of the two variables under consideration. These variables where then sorted as a function of AOD and

averaged to create a total of 50 scatter points.

5.3   RESULTS AND DISCUSSION

5.3.1   Trend Analysis

Rainfall Trend

The trends in rainfall time series were computed using the Mann Kendall trend test at a grid level of $0.25°$. To assess the magnitudes of rainfall trends, Sen's slope analysis was performed at each grid. The results of trend analysis over the study area is shown in Figure 5.1
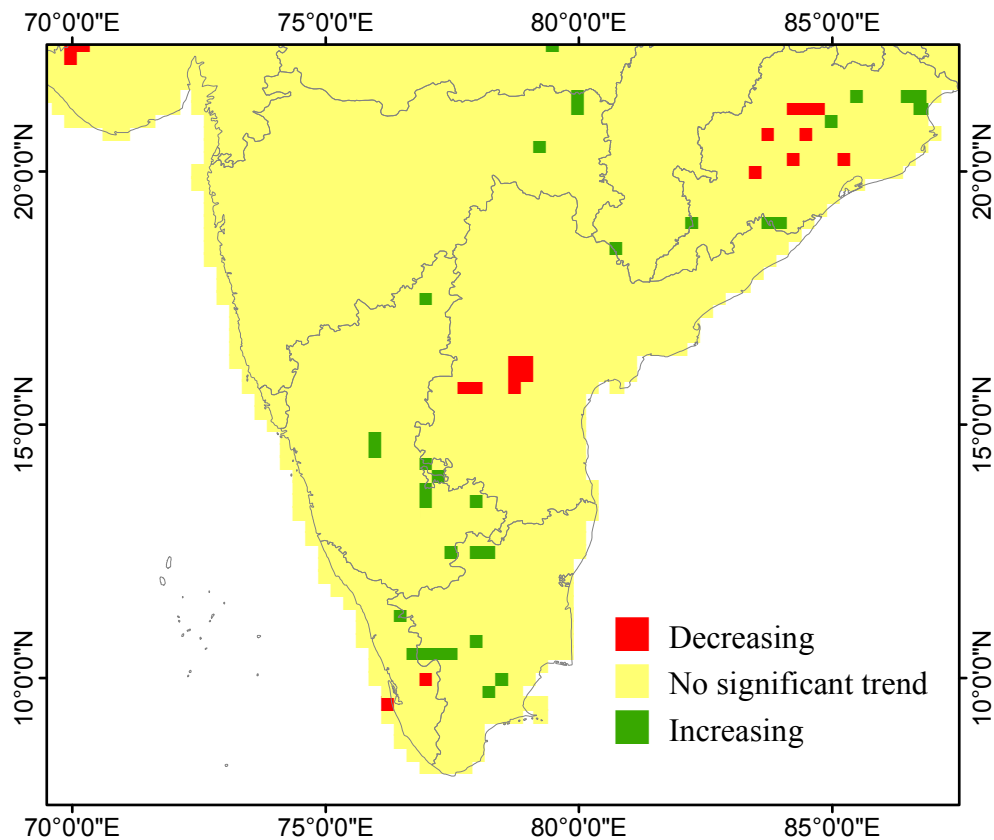
Figure 5.1 Pre Monsoon rainfall trends over the study region from 2002-2013.

Though most of the locations show trends in rainfall, only 63 locations out of 2716 experiences significant trend in rainfall. Out of these, 38 locations are significantly increasing, whereas the rest 25 are significantly decreasing. The figure also shows that

the significant trends are clustered over certain regions. This is studied in details with respect to aerosol sources, wind pattern, and cloud microphysics in the next section. As the trends are computed for the premonsoon season, the influence of other factors such as the Indian Ocean dipole etc. are minimal, which are most profound during the monsoon season. Thus we hypothesise that the trends are mostly due to local influences such as aerosol emissions.

Aerosol Trend

Before investigating the trends in rainfall with respect to aerosol sources, the trends in aerosols over the significantly trending rainfall locations are studied. Figure 5.2
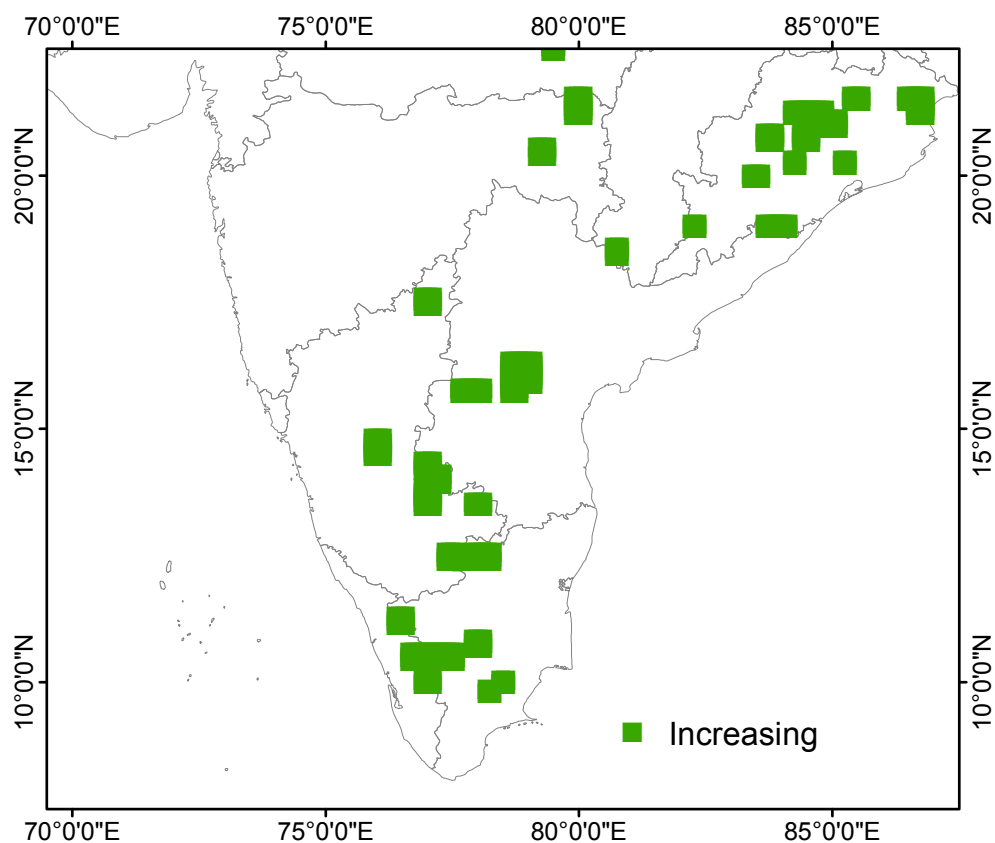
Figure 5.2 Pre Monsoon aerosol trends over significantly trending rainfall locations from 2002-2013.

shows the aerosol trends. However, in contrast to rainfall trends, all the locations shows significantly increasing trends in aerosol. This is a consequence of the increase in air

pollution and dust activities. This necessitates a detailed study of the various cloud microphysics to understand the role of aerosols in rainfall variations.

5.3.2 Aerosol Sources and Rainfall Trends
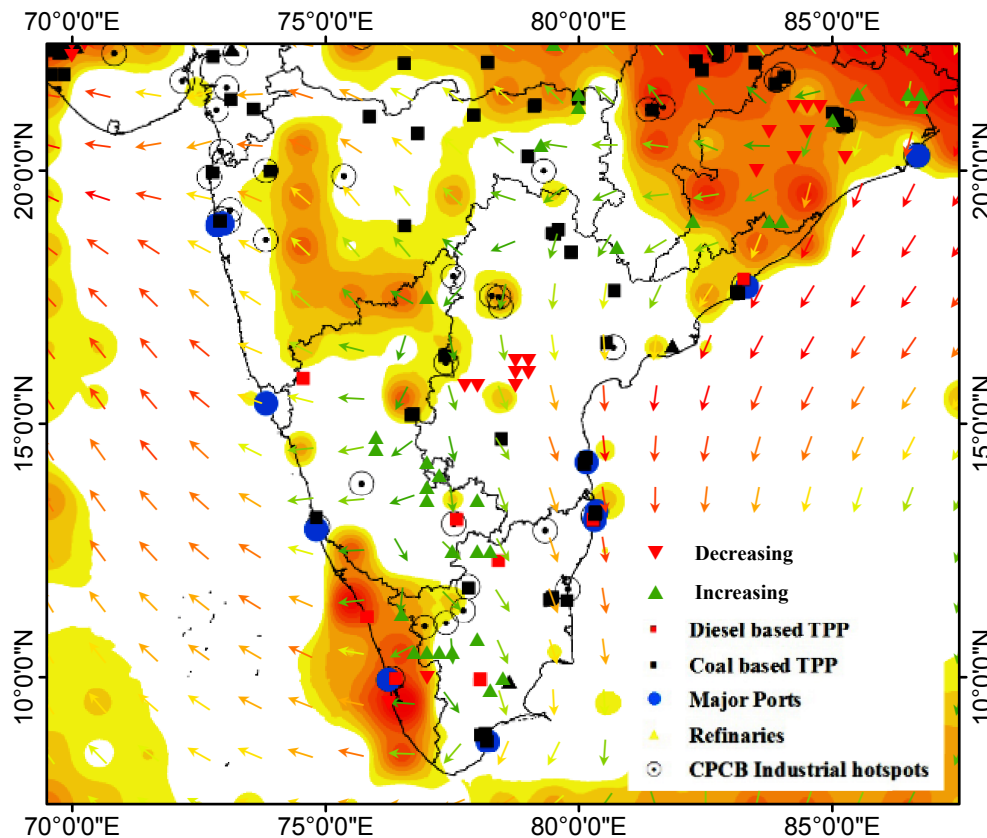
Figure 5.3 ASS (AOD/hr) and rainfall trends from 2002-2013.

Most of the rainfall trends are observed near regions of aerosol sources(Figure 5.3). Along the eastern coast significantly decreasing trends are found at the centre of the aerosol sources and the trend becomes increasing away from the centre. The centre of the ASS is also a wind stagnations point and the wind masses can been seen diverging. As the distance from the ASS increases the rainfall becomes predominantly increasing. A similar result can be observed near the strong ASS regions along the west coast. However this is just an observational perspective and requires further studies to ascertain the relationship. Thus the cloud microphysics has been investigated.

5.3.3 Aerosol Microphysics
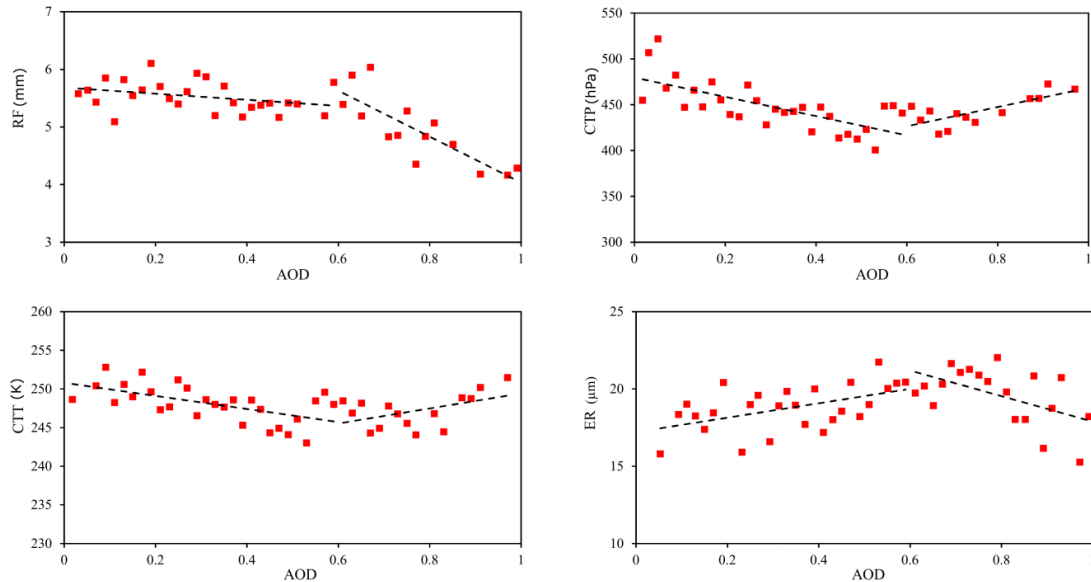
Figure 5.4 Variation of (a) daily rainfall (RF (mm)), (b) cloud top pressure (CTP (hPa)), (c) cloud top temperature (CTT (K)), and (d) cloud effective radius (ER(μm)) with AOD.

Variation of rainfall with aerosol loading is shown in Figure 5.4. Initially as AOD increases the rainfall decreases but is a flat curve upto an AOD value of 0.6 after which the rainfall decreases steeply with further increase in AOD. A similar analysis of aerosol and cloud properties showed the aerosol induced modifications in cloud microphysics. Initially with an increase in AOD up to 0.6 there is deep cloud as evident by the decrease in cloud top pressure. A further increase in AOD reflects an increasing pattern in cloud top pressure. Thus there is a shallower cloud. Not only there is a decrease in cloud height but also there is an increase in its temperature as observed by the variation of CTP and CTT with AOD. Moreover, the increasing cloud radius up-to an AOD of 0.6 becomes a steep decrease there after. Thus, though the aerosol loading initially supports cloud formation resulting in deeper and wider clouds, higher aerosol loading inhibits cloud formation resulting in narrow and shallow clouds. This in turn decreases rainfall at higher aerosol loading with smaller cloud radius. Similar situations wherein aerosols cause a reduction in cloudiness under heavier aerosol loading in regions with higher concentration of absorbing aerosols are reported by Koren et al. (2004).

5.4 CONCLUSIONS

This chapter investigates the possible relationship between rainfall and aerosol source distribution over southern India during the pre monsoon season. Aerosol and rainfall trends are computed using Mann Kendall trend test and are correlated spatially with AOD and ASS. To further understand the relationship, cloud microphysics was also investigated.

The $0.25°$ rainfall trends shows both decreasing as well as increasing significant trends over the study area. The regions of significant trends are clustered spatially with most of the rainfall trends near regions of aerosol sources. Significant decreasing trends are found at the centre of ASS. As the distance from the ASS increases, the rainfall becomes predominantly increasing.

In contrast, the aerosol trends are significantly increasing in all the regions necessitating a detailed study of various cloud microphysics. Initially as AOD increases rainfall decreases but is a flat curve up-to an AOD value of 0.6 after which the rainfall decreases steeply with further increase in AOD. Upto an AOD value of 0.6 there is deep clouds but beyond which the cloud gets shallow. Not only there is a decrease in cloud height but also there is an increase in its temperature as observed by the variation of CTP and CTT with AOD. Thus, though the aerosol loading initially supports cloud formation resulting in deeper and wider clouds, higher aerosol loading inhibits cloud formation resulting in narrow and shallow clouds. This in turn decreases rainfall at higher aerosol loading with smaller cloud radius. Similar situations wherein aerosols cause a reduction in cloudiness under heavier aerosol loading in regions with higher concentration of absorbing aerosols.

Chapter 6

CONCLUSION AND FUTURE SCOPE

6.1 CONCLUDING REMARKS

An advection diffusion based top down Lagrangian approach has been proposed as a part of this thesis. The study first investigates the influence of meteorological parameters indicating both advection and diffusion on the spatiotemporal distribution of aerosols over the Indian subcontinent and the adjacent Indian Ocean. The research inferences are then used to develop a model to estimate aerosol emissions using satellite data. Further, the spatial aerosol source distribution is used to investigate rainfall variability over southern India.

In Chapter 3, spatio-temporal distribution of AOD over the Indian sub-continent and the surrounding Indian Ocean (5°N to 40°N and 65°E to 100°E) was studied to understand the possible influence of prevailing meteorological conditions. Eleven years (2002-2012) of MODIS AOD data along with wind speed, wind divergence, and PBLH were investigated as parameters for advection and diffusion of atmospheric particles. These parameters derived from reanalysis data sets along with satellite measured AOD values reveals distinctive characteristics over the land and ocean. Further, the study pertains to the influence of meteorology in redistributing atmospheric particles over the region. The results depict the influence of prevailing meteorological conditions on distributing various aerosol types over the sub-regions. In general, over the land, higher PBLH and higher wind speed supports DU and SS aerosols whereas lower PBLH and low wind speed supports SU, BC and OC aerosols. This may be because increased wind speed and higher PBLH results in increased surface wind stress and an unstable

atmosphere with increased turbulence in turn supporting DU and SS aerosol production. Over the ocean the transported continental aerosols are concentrated over regions of stable atmosphere as denoted by lower PBLH. Increasing wind speeds over the ocean results in an increased SS aerosol concentration over the region. Further, the influence of atmospheric diffusion is quantified by evaluating the PRE of a multiple linear regression model. The inclusion of PBLH in addition to wind speed and divergence shows significant PRE in most of the cases. This is particularly evident during the winter and pre-monsoon seasons where the PBLH explains almost 30 to 90% of the total variance in AOD over the sub-regions.

Chapter 4 employs a Lagrangian approach to the Advection Diffusion Equation to estimate the transported aerosols and hence the aerosol source strength using satellite measured aerosol optical depth and reanalysis wind data. This top-down approach is based on the advection and diffusion of atmospheric aerosols considering wind circulation and atmospheric conditions rather than using indicative parameters. ASS is first computed over California during July 2018 and is then applied over southern India. The method not only accounts for the advection of aerosols but also considers aerosol diffusion based on atmospheric stability conditions. The computed ASS shows higher values around wildfire regions, which is a significant source of atmospheric aerosols.As the temporal integration of satellite retrieved FRP is proportional to aerosol emissions from the fire, the computed ASS at fire locations was compared with MODIS MaxFRP. The results indicate a high linear correlation (R2 = 0.886) between ASS and FRP with a scalar multiplication factor of 0.001 AOD/MW-hr. A linear relationship validates that the ASS computed using the proposed methodology reflects the actual aerosol production rather than the residual or transported aerosols. As the proposed method is based on advection and diffusion of atmospheric aerosols rather than using indicative parameters such as FRP, this method was applied to investigate the spatial correlation of ASS with power plant density. There is a steady increase in ASS with power plant density, with the region of highest power plant density recording an ASS of 0.021 AOD/hr, which is similar to the aerosol emission from the Carr Fire. The study thus aids to infer the relative importance of various emission sources in the region. Application of the

methodology over the Indian subcontinent reveals its aerosol source hotspots during the premonsoon season. The model is able to distinguish the transported aerosols and hence points out the actual aerosol production centres. The clusters of coal based thermal power plants along the $20°$ N latitude exhibits higher source strength apart from various CPCB industrial hotspots.

Chapter 5 investigates the possible relationship between rainfall and aerosol source distribution over southern India during the pre monsoon season. Aerosol and rainfall trends are computed using Mann Kendall trend test and are correlated spatially with AOD and ASS. To further understand the relationship, cloud microphysics was also investigated. The $0.25°$ rainfall trends shows both decreasing as well as increasing significant trends over the study area. the regions of significant trends are clustered spatially with most of the rainfall trends near regions of aerosol sources. Significant decreasing trends are found at the centre of ASS. As the distance from the ASS increases, the rainfall becomes predominantly increasing.

6.2 LIMITATIONS OF THE RESEARCH

The najor limitations of the study are:

1. Hourly ASS is computed which assumes that each grid has a constant emission of aerosol during the time period. This is not the case of actual scenario where the emissions are varying in time.

2. For ASS computations over the Indian subcontinent, daily measurements of AOD available from the MODIS sensor on board Terra and Aqua satellites are used. Terra and Aqua overpass the study domain roughly at around 06:00 (UTC) and 09:00 (UTC). Thus a three hour ASS can be computed between 06:00 and 09:00 (UTC). Though the aerosol sources computed for three hours have better accuracy than a 24 hour source (Prijith et al., 2013), this represents the source strength only for a very small fraction of the day.

3. The methodology assumes an exponentially decreasing vertical profile with a scale height of 2 km for the vertical distribution of aerosols. Though this assump-

tion holds good for monthly profiles of aerosol, smaller timescales may vary especially in the case of long range aerosol transport in the upper troposphere. This study is constrained by the lack of remote sensing data on the vertical distribution of aerosols at the desired spatio-temporal resolutions.

4. Remote sensing of aerosols, clouds, and precipitation require very different wavebands and methods for each of these three components. These widely varying measurement requirements make it very difficult to observe simultaneously aerosols, clouds and precipitation for understanding their interactions. Hence only separate observational evidences of rainfall variations around aerosol sources are carried out. Further verification requires climate modeling which is beyond the scope of this study.

6.3   FUTURE SCOPE OF THE RESEARCH

In this thesis, a satellite based top-down Lagrangian approach is employed to estimate ASS over the Indian subcontinent. However, due to the lack of quality AOD data from indigenous geostationary satellites, ASS are computed only for a small window of three hours in a day. This could be improved by incorporating INSAT3D/3DR AOD data with MODIS and MISR data for better temporal resolution. Further, the model outputs aerosol emissions in terms of optical depth but further work can be done to convert these values into PM2.5 and can be used to estimate the spread of pollutants especially the PM2.5 distribution during wildfires and other hazards.

Bibliography

Acharya, P. and Sreekesh, S. (2013). Seasonal variability in aerosol optical depth over India: A spatio-temporal analysis using the MODIS aerosol product. *International Journal of Remote Sensing*, 34(13), 4832–4849.

Ainsworth, E. A. and Long, S. P. (2005). What have we learned from 15 years of free-air CO2 enrichment (FACE)? A meta-analytic review of the responses of photosynthesis, canopy properties and plant production to rising CO2. *New Phytologist*, 165(2), 351–372.

Aloysius, M., Mohan, M., Parameswaran, K., George, S. K., and Nair, P. R. (2008). Aerosol transport over the Gangetic basin during ISRO-GBP land campaign-II. *Annales Geophysicae*, 26(3), 431–440.

Badarinath, K. V., Kiran Chand, T. R., and Krishna Prasad, V. (2006). Agriculture crop residue burning in the Indo-Gangetic Plains - A study using IRS-P6 AWiFS satellite data. *Current Science*, 91(8), 1085–1089.

Blanchard, D. C. (1963). The electrification of the atmosphere by particles from bubbles in the sea. *Progress in Oceanography*, 1(C), 73–202.

Bollasina, M. A., Ming, Y., and Ramaswamy, V. (2011). Anthropogenic aerosols and the weakening of the south asian summer monsoon. *Science*, 334(6055), 502–505.

Boucher, O. (2015). *Atmospheric Aerosols: Properties and Climate Impacts*, 1005. Springer.

Cheng, S., Chen, D., Li, J., Wang, H., and Guo, X. (2007). The assessment of emission-source contributions to air quality by using a coupled MM5-ARPS-CMAQ modeling

system: A case study in the Beijing metropolitan region, China. *Environmental Modelling & Software*, 22(11), 1601–1616.

Cherian, R., Venkataraman, C., Quaas, J., and Ramachandran, S. (2013). GCM simulations of anthropogenic aerosol-induced changes in aerosol extinction, atmospheric heating and precipitation over India. *Journal of Geophysical Research Atmospheres*, 118(7), 2938–2955.

Chitranshi, S., Sharma, S. P., and Dey, S. (2015). Satellite-based estimates of outdoor particulate pollution (PM10) for Agra City in northern India. *Air Quality, Atmosphere & Health*, 8(1), 55–65.

Choudhry, P., Misra, A., and Tripathi, S. N. (2012). Study of MODIS derived AOD at three different locations in the Indo Gangetic Plain: Kanpur, Gandhi College and Nainital. *Annales Geophysicae*, 30(10), 1479–1493.

Chung, C. E., Ramanathan, V., and Kiehl, J. T. (2002). Effects of the South Asian absorbing haze on the northeast monsoon and surface-air heat exchange. *Journal of Climate*, 15(17), 2462–2476.

Chyacutelek, P. and Coakley, J. A. (1974). Aerosols and Climate. *Science*, 183(4120), 75–77.

Crutzen, P. J. and Andreae, M. O. (1990). Biomass Burning in the Tropics: Impact on Atmospheric Chemistry and Biogeochemical Cycles. *Science*, 250(4988), 1669–1678.

Csavina, J., Field, J., Félix, O., Corral-Avitia, A. Y., Sáez, A. E., and Betterton, E. A. (2014). Effect of wind speed and relative humidity on atmospheric dust concentrations in semi-arid climates. *Science of the Total Environment*, 487(1), 82–90.

De Young, R. J., Grant, W. B., and Severance, K. (2005). Aerosol Transport in the California Central Valley Observed by Airborne Lidar. *Environmental Science & Technology*, 39(21), 8351–8357.

Demuzere, M., Trigo, R. M., De Arellano, J. V. G., and Van Lipzig, N. P. (2009). The impact of weather and atmospheric circulation on O3 and PM10 levels at a rural mid-latitude site. *Atmospheric Chemistry and Physics*, 9(8), 2695–2714.

Dey, S. (2004). Influence of dust storms on the aerosol optical properties over the Indo-Gangetic basin. *Journal of Geophysical Research*, 109(D20), D20211.

Di Girolamo, L., Bond, T. C., Bramer, D., Diner, D. J., Fettinger, F., Kahn, R. A., Martonchik, J. V., Ramana, M. V., Ramanathan, V., and Rasch, P. J. (2004). Analysis of multi-angle Imaging SpectroRadiometer (MISR) aerosol optical depths over greater India during winter 2001-2004. *Geophysical Research Letters*, 31(23), 1–5.

Diem, J. E. and Brown, D. P. (2003). Anthropogenic Impacts on Summer Precipitation in Central Arizona, U.S.A. *The Professional Geographer*, 55(3), 343–355.

Ding, A., Wang, T., Zhao, M., Wang, T., and Li, Z. (2004). Simulation of sea-land breezes and a discussion of their implications on the transport of air pollution during a multi-day ozone episode in the Pearl River Delta of China. *Atmospheric Environment*, 38(39), 6737–6750.

EMSA. Equasis - The world merchant fleet - statistics from Equasis - EMSA - European Maritime Safety Agency.

Endresen, Ø., Sørgård, E., Sundet, J. K., Dalsøren, S. B., Isaksen, I. S., Berglen, T. F., and Gravir, G. (2003). Emission from international sea transportation and environmental impact. *Journal of Geophysical Research: Atmospheres*, 108(17).

Freeborn, P. H., Wooster, M. J., Hao, W. M., Ryan, C. A., Nordgren, B. L., Baker, S. P., and Ichoku, C. (2008). Relationships between energy release, fuel mass loss, and trace gas and aerosol emissions during laboratory biomass fires. *Journal of Geophysical Research*, 113(D1), D01301.

Fuzzi, S., Baltensperger, U., Carslaw, K., Decesari, S., Denier van der Gon, H., Facchini, M. C., Fowler, D., Koren, I., Langford, B., Lohmann, U., Nemitz, E., Pandis, S., Riipinen, I., Rudich, Y., Schaap, M., Slowik, J. G., Spracklen, D. V., Vignati,

E., Wild, M., Williams, M., and Gilardoni, S. (2015). Particulate matter, air quality and climate: lessons learned and future needs. *Atmospheric Chemistry and Physics*, 15(14), 8217–8299.

Gautam, R., Hsu, N. C., Lau, K.-M., and Kafatos, M. (2009a). Aerosol and rainfall variability over the Indian monsoon region: distributions, trends and coupling. *Annales Geophysicae*, 27(9), 3691–3703.

Gautam, R., Hsu, N. C., Lau, K.-M., Tsay, S.-C., and Kafatos, M. (2009b). Enhanced pre-monsoon warming over the Himalayan-Gangetic region from 1979 to 2007. *Geophysical Research Letters*, 36(7), n/a–n/a.

Gelaro, R., McCarty, W., Suárez, M. J., Todling, R., Molod, A., Takacs, L., Randles, C. A., Darmenov, A., Bosilovich, M. G., Reichle, R., Wargan, K., Coy, L., Cullather, R., Draper, C., Akella, S., Buchard, V., Conaty, A., da Silva, A. M., Gu, W., Kim, G. K., Koster, R., Lucchesi, R., Merkova, D., Nielsen, J. E., Partyka, G., Pawson, S., Putman, W., Rienecker, M., Schubert, S. D., Sienkiewicz, M., and Zhao, B. (2017). The modern-era retrospective analysis for research and applications, version 2 (MERRA-2). *Journal of Climate*, 30(14), 5419–5454.

Giglio, L., Schroeder, W., and Justice, C. O. (2016). The collection 6 MODIS active fire detection algorithm and fire products. *Remote Sensing of Environment*, 178, 31–41.

Giles, D. M., Holben, B. N., Tripathi, S. N., Eck, T. F., Newcomb, W. W., Slutsker, I., Dickerson, R. R., Thompson, A. M., Mattoo, S., Wang, S. H., Singh, R. P., Sinyuk, A., and Schafer, J. S. (2011). Aerosol properties over the Indo-Gangetic Plain: A mesoscale perspective from the TIGERZ experiment. *Journal of Geophysical Research Atmospheres*, 116(18), 1–19.

Ginoux, P., Chin, M., Tegen, I., Prospero, J. M., Holben, B., Dubovik, O., and Lin, S.-J. (2001). Sources and distributions of dust aerosols simulated with the GOCART model. *Journal of Geophysical Research: Atmospheres*, 106(D17), 20255–20273.

Givati, A. and Rosenfeld, D. (2004). Quantifying precipitation suppression due to air pollution. *Journal of Applied Meteorology*, 43(7), 1038–1056.

Global Modeling Assimilation (2015). MERRA2 tavg1_2d_flx_Nx: 2d,1-Hourly,Time-Averaged,Single-Level,Assimilation,Surface Flux Diagnostics V5.12.4.

GMOA 2015b. MERRA-2 tavgM_2d_aer_Nx: 2d,Monthly mean,Time-averaged,Single-Level,Assimilation,Aerosol Diagnostics V5.12.4.

Guleria, R. P. and Kuniyal, J. C. (2013). Aerosol climatology in the northwestern Indian Himalaya: a study based on the radiative properties of aerosol. *Air Quality, Atmosphere & Health*, 6(4), 717–724.

Guleria, R. P. and Kuniyal, J. C. (2016). Characteristics of atmospheric aerosol particles and their role in aerosol radiative forcing over the northwestern Indian Himalaya in particular and over India in general. *Air Quality, Atmosphere & Health*, 9(7), 795–808.

Gupta, P. and Christopher, S. A. (2009). Particulate matter air quality assessment using integrated surface, satellite, and meteorological products: Multiple regression approach. *Journal of Geophysical Research*, 114(D14), D14205.

Guttikunda, S. K., Carmichael, G. R., Calori, G., Eck, C., and Woo, J.-h. (2003). The contribution of megacities to regional sulfur pollution in Asia. *Atmospheric Environment*, 37(1), 11–22.

Guttikunda, S. K. and Jawahar, P. (2014). Atmospheric emissions and pollution from the coal-fired thermal power plants in India. *Atmospheric Environment*, 92, 449–460.

Hoek, G., Brunekreef, B., Goldbohm, S., Fischer, P., and van den Brandt, P. A. (2002). Association between mortality and indicators of traffic-related air pollution in the Netherlands: a cohort study. *The Lancet*, 360(9341), 1203–1209.

Hsu, N. C., Jeong, M.-J., Bettenhausen, C., Sayer, A. M., Hansell, R., Seftor, C. S., Huang, J., and Tsay, S.-C. (2013). Enhanced Deep Blue aerosol retrieval algorithm: The second generation. *Journal of Geophysical Research: Atmospheres*, 118(16), 9296–9315.

Ichoku, C. and Ellison, L. (2014). Global top-down smoke-aerosol emissions estimation using satellite fire radiative power measurements. *Atmospheric Chemistry and Physics*, 14(13), 6643–6667.

Jain, N., Bhatia, A., and Pathak, H. (2014). Emission of air pollutants from crop residue burning in India. *Aerosol and Air Quality Research*, 14(1), 422–430.

Judd, C. M., McClelland, G. H., and Ryan, C. S. (2017). *Data Analysis*. Routledge, Third Edition. | New York : Routledge, 2017. | Revised edition.

Kaiser, J. W., Heil, A., Andreae, M. O., Benedetti, A., Chubarova, N., Jones, L., Morcrette, J.-J., Razinger, M., Schultz, M. G., Suttie, M., and van der Werf, G. R. (2012). Biomass burning emissions estimated with a global fire assimilation system based on observed fire radiative power. *Biogeosciences*, 9(1), 527–554.

Kamarul Zaman, N. A. F., Kanniah, K. D., and Kaskaoutis, D. G. (2017). Estimating Particulate Matter using satellite based aerosol optical depth and meteorological variables in Malaysia. *Atmospheric Research*, 193, 142–162.

Kedia, S., Ramachandran, S., Holben, B., and Tripathi, S. (2014). Quantification of aerosol type, and sources of aerosols over the Indo-Gangetic Plain. *Atmospheric Environment*, 98, 607–619.

Kendall, M. G. (1955). *Rank correlation methods, 2nd ed.* Hafner Publishing Co., Oxford, England.

Kok, J. F. (2011). A scaling theory for the size distribution of emitted dust aerosols suggests climate models underestimate the size of the global dust cycle. *Proceedings of the National Academy of Sciences of the United States of America*, 108(3), 1016–1021.

Koren, I., Kaufman, Y. J., Remer, L. A., and Martins, J. V. (2004). Measurement of the Effect of Amazon Smoke on Inhibition of Cloud Formation. *Science*, 303(5662), 1342–1345.

Kumar, A. (2012). Statistical Models for Long-range Forecasting of Southwest Monsoon Rainfall over India Using Step Wise Regression and Neural Network. *Atmospheric and Climate Sciences*, 02(03), 322–336.

Lau, K. M. and Kim, K. M. (2006). Observational relationships between aerosol and Asian monsoon rainfall, and circulation. *Geophysical Research Letters*, 33(21), 1–5.

Lau, K. M., Ramanathan, V., Wu, G. X., Li, Z., Tsay, S. C., Hsu, C., Sikka, R., Holben, B., Lu, D., Tartari, G., Chin, M., Koudelova, P., Chen, H., Ma, Y., Huang, J., Taniguchi, K., and Zhang, R. (2008). The joint aerosol-monsoon experiment: A new challenge for monoon climate research. *Bulletin of the American Meteorological Society*, 89(3), 369–383.

Levy, R. C., Remer, L. A., Kleidman, R. G., Mattoo, S., Ichoku, C., Kahn, R., and Eck, T. F. (2010). Global evaluation of the Collection 5 MODIS dark-target aerosol products over land. *Atmospheric Chemistry and Physics*, 10(21), 10399–10420.

Lewtas, J. (2007). Air pollution combustion emissions: Characterization of causative agents and mechanisms associated with cancer, reproductive, and cardiovascular effects.

Li, F., Zhang, X., Kondragunta, S., and Roy, D. P. (2018). Investigation of the Fire Radiative Energy Biomass Combustion Coefficient: A Comparison of Polar and Geostationary Satellite Retrievals Over the Conterminous United States. *Journal of Geophysical Research: Biogeosciences*, 123(2), 722–739.

Li, F., Zhang, X., Roy, D. P., and Kondragunta, S. (2019). Estimation of biomass-burning emissions by fusing the fire radiative power retrievals from polar-orbiting and geostationary satellites across the conterminous United States. *Atmospheric Environment*, 211(April), 274–287.

Li, Z., Rosenfeld, D., and Fan, J. (2017). Aerosols and Their Impact on Radiation, Clouds, Precipitation, and Severe Weather Events. In *Oxford Research Encyclopedia of Environmental Science*, 1, 1–36. Oxford University Press.

Liu, Y., Sarnat, J. A., Kilaru, V., Jacob, D. J., and Koutrakis, P. (2005). Estimating Ground-Level PM 2.5 in the Eastern United States Using Satellite Remote Sensing. *Environmental Science & Technology*, 39(9), 3269–3278.

Liu, Z., Liu, D., Huang, J., Vaughan, M., Uno, I., Sugimoto, N., Kittaka, C., Trepte, C., Wang, Z., Hostetler, C., and Winker, D. (2008). Airborne dust distributions over the Tibetan Plateau and surrounding areas derived from the first year of CALIPSO lidar observations. *Atmospheric Chemistry and Physics*, 8(16), 5045–5060.

Lodge, J. P. (1983). Handbook on atmospheric diffusion. *Atmospheric Environment (1967)*, 17(3), 673–675.

Mahalakshmi, D. V., Sujatha, P., Naidu, C. V., and Chowdary, V. M. (2014). Contribution of vehicular emission on urban air quality: Results from public strike in Hyderabad. *Indian Journal of Radio and Space Physics*, 43(6), 340–348.

Mann, H. B. (1945). Nonparametric Tests Against Trend. *Econometrica*, 13(3), 245–259.

Massie, S. T., Torres, O., and Smith, S. J. (2004). Total Ozone Mapping Spectrometer (TOMS) observations of increases in Asian aerosol in winter from 1979 to 2000. *Journal of Geophysical Research Atmospheres*, 109(18), 1–14.

McDonald, B. C., Dallmann, T. R., Martin, E. W., and Harley, R. A. (2012). Long-term trends in nitrogen oxide emissions from motor vehicles at national, state, and air basin scales. *Journal of Geophysical Research Atmospheres*, 117(17).

McNoldy, B. D. (2004). Surface winds, divergence, and vorticity in stratocumulus regions using QuikSCAT and reanalysis winds. *Geophysical Research Letters*, 31(8), L08105.

Meehl, G. A., Arblaster, J. M., and Tebaldi, C. (2007). Contributions of natural and anthropogenic forcing to changes in temperature extremes over the United States. *Geophysical Research Letters*, 34(19), 1–5.

Menon, S., Hansen, J., Nazarenko, L., and Luo, Y. (2002). Climate effects of black carbon aerosols in China and India. *Science*, 297(5590), 2250–2253.

Misra, A., Jayaraman, A., and Ganguly, D. (2015). Validation of Version 5.1 MODIS Aerosol Optical Depth (Deep Blue Algorithm and Dark Target Approach) over a Semi-Arid Location in Western India. *Aerosol and Air Quality Research*, 15(1), 252–262.

MoCA (2016). Ministry of Civil Aviation, Governement of India.

Monkkonen, P. (2004). Relationship and variations of aerosol number and PM10 mass concentrations in a highly polluted urban environment - New Delhi, India. *Atmospheric Environment*, 38(3), 425–433.

Montgomery, M. R. and Hewett, P. C. (2005). Urban poverty and health in developing countries: Household and neighborhood effects. *Demography*, 42(3), 397–425.

Moorthy, K. K. and Satheesh, S. K. (2000). Characteristics of aerosols over a remote island, Minicoy in the Arabian Sea: Optical properties and retrieved size characteristics. *Quarterly Journal of the Royal Meteorological Society*, 126(562), 81–109.

Mueller, D., Uibel, S., Takemura, M., Klingelhoefer, D., and Groneberg, D. A. (2011). Ships, ports and particulate air pollution - An analysis of recent studies.

Nair, V. S., Suresh Babu, S., and Krishna Moorthy, K. (2008). Spatial distribution and spectral characteristics of aerosol single scattering albedo over the Bay of Bengal inferred from shipborne measurements. *Geophysical Research Letters*, 35(10), 1–5.

Nizar, S. and Dodamani, B. M. (2019). Spatiotemporal distribution of aerosols over the Indian subcontinent and its dependence on prevailing meteorological conditions. *Air Quality, Atmosphere and Health*, 12(4), 503–517.

Pai, D. S., Sridhar, L., Rajeevan, M., Sreejith, O. P., Satbhai, N. S., and Mukhopadyay, B. (2014). Development of a new high spatial resolution (0.25×0.25) Long Period (1901-2010) daily gridded rainfall data set over India and its comparison with existing data sets over the region. *Mausam*, 65(1), 1–18.

Panicker, A. S., Pandithurai, G., and Dipu, S. (2010). Aerosol indirect effect during successive contrasting monsoon seasons over Indian subcontinent using MODIS data. *Atmospheric Environment*, 44(15), 1937–1943.

Patra, P. K., Behera, S. K., Herman, J. R., Maksyutov, S., Akimoto, H., and Yamagata, T. (2005). The Indian summer monsoon rainfall: Interplay of coupled dynamics, radiation and cloud microphysics. *Atmospheric Chemistry and Physics*, 5(8), 2181–2188.

Penner, J. E., Charlson, R. J., Schwartz, S. E., Hales, J. M., Laulainen, N. S., Travis, L., Leifer, R., Novakov, T., Ogren, J., and Radke, L. F. (1994). Quantifying and Minimizing Uncertainty of Climate Forcing by Anthropogenic Aerosols. *Bulletin of the American Meteorological Society*, 75(3), 375–400.

Platnick, S., Meyer, K. G., King, M. D., Wind, G., Amarasinghe, N., Marchant, B., Arnold, G. T., Zhang, Z., Hubanks, P. A., Holz, R. E., Yang, P., Ridgway, W. L., and Riedi, J. (2017). The MODIS Cloud Optical and Microphysical Products: Collection 6 Updates and Examples from Terra and Aqua. *IEEE Transactions on Geoscience and Remote Sensing*, 55(1), 502–525.

Pope, C. A., Burnett, R. T., Thurston, G. D., Thun, M. J., Calle, E. E., Krewski, D., and Godleski, J. J. (2004). Cardiovascular Mortality and Long-Term Exposure to Particulate Air Pollution. *Circulation*, 109(1), 71–77.

Prasad, A. K., Singh, R. P., and Kafatos, M. (2006). Influence of coal based thermal power plants on aerosol optical properties in the Indo-Gangetic basin. *Geophysical Research Letters*, 33(5), 3–6.

Prasad, S. and Gupta, R. K. (1998). Estimation and evaluation of Aerosol Optical Depth using NOAA AVHRR data. *Advances in Space Research*, 22(11), 1525–1528.

Prijith, S. S., Aloysius, M., and Mohan, M. (2013). Global aerosol source/sink map. *Atmospheric Environment*, 80, 533–539.

Prospero, J. M. (2002). Environmental characterization of global sources of atmospheric soil dust identified with the NIMBUS 7 Total Ozone Mapping Spectrometer (TOMS) absorbing aerosol product. *Reviews of Geophysics*, 40(1), 1002.

Quan, J., Gao, Y., Zhang, Q., Tie, X., Cao, J., Han, S., Meng, J., Chen, P., and Zhao, D. (2013). Evolution of planetary boundary layer under different weather conditions, and its impact on aerosol concentrations. *Particuology*, 11(1), 34–40.

Rajeev, K., Nair, S. K., Parameswaran, K., and Raju, C. S. (2004). Satellite observations of the regional aerosol distribution and transport over the Arabian Sea, Bay of Bengal and Indian Ocean. *Indian Journal of Marine Sciences*, 33(1), 11–29.

Rajeev, K., Ramanathan, V., and Meywerk, J. (2000). Regional aerosol distribution and its long-range transport over the Indian Ocean. *Journal of Geophysical Research: Atmospheres*, 105(D2), 2029–2043.

Ramachandran, S. and Cherian, R. (2008). Regional and seasonal variations in aerosol optical characteristics and their frequency distributions over India during 2001–2005. *Journal of Geophysical Research*, 113(D8), D08207.

Ramanathan, V., Chung, C., Kim, D., Bettge, T., Buja, L., Kiehl, J. T., Washington, W. M., Fu, Q., Sikka, D. R., and Wild, M. (2005). Atmospheric brown clouds: Impacts on South Asian climate and hydrological cycle. *Proceedings of the National Academy of Sciences*, 102(15), 5326–5333.

Ramanathan, V., Crutzen, P. J., Kiehl, J. T., and Rosenfeld, D. (2001). Atmosphere: Aerosols, climate, and the hydrological cycle. 294(5549), 2119–2124.

Rashki, A., Kaskaoutis, D. G., Mofidi, A., Minvielle, F., Chiapello, I., Legrand, M., Dumka, U. C., and Francois, P. (2019). Effects of Monsoon, Shamal and Levar winds on dust accumulation over the Arabian Sea during summer – The July 2016 case. *Aeolian Research*, 36, 27–44.

Rolph, G., Stein, A., and Stunder, B. (2017). Real-time Environmental Applications and Display sYstem: READY. *Environmental Modelling & Software*, 95, 210–228.

Rosenfeld, D. (1999). TRMM observed first direct evidence of smoke from forest fires inhibiting rainfall. *Geophysical Research Letters*, 26(20), 3105–3108.

Saavedra, S., Rodríguez, A., Taboada, J. J., Souto, J. A., and Casares, J. J. (2012). Synoptic patterns and air mass transport during ozone episodes in northwestern Iberia. *Science of the Total Environment*, 441, 97–110.

Sahu, S. K., Schultz, M. G., and Beig, G. (2015). Critical pollutant emissions from the Indian telecom network. *Atmospheric Environment*, 103, 34–42.

Sarangi, C., Tripathi, S. N., Kanawade, V. P., Koren, I., and Sivanand Pai, D. (2017). Investigation of the aerosol-cloud-rainfall association over the Indian summer monsoon region. *Atmospheric Chemistry and Physics*, 17(8), 5185–5204.

Satheesh, S. K., Krishna Moorthy, K., Suresh Babu, S., Vinoj, V., and Dutt, C. B. S. (2008). Climate implications of large warming by elevated aerosol over India. *Geophysical Research Letters*, 35(19), 1–6.

Sayer, A. M., Hsu, N. C., Bettenhausen, C., and Jeong, M.-J. (2013). Validation and uncertainty estimates for MODIS Collection 6 "Deep Blue" aerosol data. *Journal of Geophysical Research: Atmospheres*, 118(14), 7864–7872.

Schaap, M., Apituley, A., Timmermans, R. M. A., Koelemeijer, R. B. A., and de Leeuw, G. (2009). Exploring the relation between aerosol optical depth and PM 2.5 at Cabauw, the Netherlands. *Atmospheric Chemistry and Physics*, 9(3), 909–925.

Schmit, T. J., Griffith, P., Gunshor, M. M., Daniels, J. M., Goodman, S. J., and Lebair, W. J. (2017). A Closer Look at the ABI on the GOES-R Series. *Bulletin of the American Meteorological Society*, 98(4), 681–698.

Schmit, T. J., Gunshor, M. M., Menzel, W. P., Gurka, J. J., Li, J., and Bachmeier, A. S. (2005). Introducing the next-generation advanced baseline imager on GOES-R. *Bulletin of the American Meteorological Society*, 86(8), 1079–1096.

Schwartz, S. E. (1996). The whitehouse effect—Shortwave radiative forcing of climate by anthropogenic aerosols: an overview. *Journal of Aerosol Science*, 27(3), 359–382.

Shir, C. C. (1973). A Preliminary Numerical Study of Atmospheric Turbulent Flows in the Idealized Planetary Boundary Layer. *Journal of the Atmospheric Sciences*, 30(7), 1327–1339.

Sikka, D. R. (2002). Developments in tropospheric aerosols studies in India. *Indian Journal of Radio and Space Physics*, 31(6), 391–403.

Singh, R. P., Dey, S., Tripathi, S. N., Tare, V., and Holben, B. (2004). Variability of aerosol parameters over Kanpur, northern India. *Journal of Geophysical Research: Atmospheres*, 109(D23), 1–14.

Small, J. D., Jiang, J. H., Su, H., and Zhai, C. (2011). Relationship between aerosol and cloud fraction over Australia. *Geophysical Research Letters*, 38(23), 1–7.

Srivastava, N., Satheesh, S., Blond, N., and Moorthy, K. K. (2016). Anthropogenic aerosol fraction over the Indian region: model simulations versus multi-satellite data analysis. *International Journal of Remote Sensing*, 37(4), 782–804.

Stein, A. F., Draxler, R. R., Rolph, G. D., Stunder, B. J. B., Cohen, M. D., and Ngan, F. (2015). NOAA's HYSPLIT Atmospheric Transport and Dispersion Modeling System. *Bulletin of the American Meteorological Society*, 96(12), 2059–2077.

Steinfeld, J. I. (1998). Atmospheric Chemistry and Physics: From Air Pollution to Climate Change. *Environment: Science and Policy for Sustainable Development*, 40(7), 26–26.

Struthers, H., Ekman, A. M. L., Glantz, P., Iversen, T., Kirkevåg, A., Seland, Ø., Mårtensson, E. M., Noone, K., and Nilsson, E. D. (2013). Climate-induced changes in sea salt aerosol number emissions: 1870 to 2100. *Journal of Geophysical Research: Atmospheres*, 118(2), 670–682.

Su, T., Li, Z., and Kahn, R. (2018). Relationships between the planetary boundary layer height and surface pollutants derived from lidar observations over China: Regional pattern and influencing factors. *Atmospheric Chemistry and Physics*, 18(21), 15921–15935.

Sweeney, M. R., McDonald, E. V., and Etyemezian, V. (2011). Quantifying dust emissions from desert landforms, eastern Mojave Desert, USA. *Geomorphology*, 135(1-2), 21–34.

Tanner, P. A. and Law, P. T. (2002). Effects of synoptic weather systems upon the air quality in an Asian Megacity. *Water, Air, and Soil Pollution*, 136(1-4), 105–124.

Tripathi, S. N., Dey, S., Chandel, A., Srivastava, S., Singh, R. P., and Holben, B. N. (2005). Comparison of MODIS and AERONET derived aerosol optical depth over the Ganga Basin, India. *Annales Geophysicae*, 23(4), 1093–1101.

Tripathi, S. N., Pattnaik, A., and Dey, S. (2007). Aerosol indirect effect over Indo-Gangetic plain. *Atmospheric Environment*, 41(33), 7037–7047.

Twomey, S. (1977). The Influence of Pollution on the Shortwave Albedo of Clouds. *Journal of the Atmospheric Sciences*, 34(7), 1149–1152.

Venkataraman, C., Habib, G., Kadamba, D., Shrivastava, M., Leon, J. F., Crouzille, B., Boucher, O., and Streets, D. G. (2006). Emissions from open biomass burning in India: Integrating the inventory approach with high-resolution Moderate Resolution Imaging Spectroradiometer (MODIS) active-fire and land cover data. *Global Biogeochemical Cycles*, 20(2).

Wang, C. (2004). A modeling study on the climate impacts of black carbon aerosols. *Journal of Geophysical Research: Atmospheres*, 109(D3), n/a–n/a.

Wang, J. (2003). Intercomparison between satellite-derived aerosol optical thickness and PM 2.5 mass: Implications for air quality studies. *Geophysical Research Letters*, 30(21), 2095.

Wang, X., Wang, K., and Su, L. (2016). Contribution of Atmospheric Diffusion Conditions to the Recent Improvement in Air Quality in China. *Scientific Reports*, 6(1), 36404.

Washington, R., Todd, M., Middleton, N. J., and Goudie, A. S. (2003). Dust-Storm Source Areas Determined by the Total Ozone Monitoring Spectrometer and Surface Observations. *Annals of the Association of American Geographers*, 93(2), 297–313.

Wooster, M. J., Roberts, G., Perry, G. L., and Kaufman, Y. J. (2005). Retrieval of biomass combustion rates and totals from fire radiative power observations: FRP derivation and calibration relationships between biomass consumption and fire radiative energy release. *Journal of Geophysical Research Atmospheres*, 110(24), 1–24.

Xu, W. Y., Zhao, C. S., Ran, L., Deng, Z. Z., Liu, P. F., Ma, N., Lin, W. L., Xu, X. B., Yan, P., He, X., Yu, J., Liang, W. D., and Chen, L. L. (2011). Characteristics of pollutants and their correlation to meteorological conditions at a suburban site in the North China Plain. *Atmospheric Chemistry and Physics*, 11(9), 4353–4369.

Yin, L., Du, P., Zhang, M., Liu, M., Xu, T., and Song, Y. (2019). Estimation of emissions from biomass burning in China (2003-2017) based on MODIS fire radiative energy data. *Biogeosciences*, 16(7), 1629–1640.

Zhao, C., Wang, Y., Yang, Q., Fu, R., Cunnold, D., and Choi, Y. (2010). Impact of East Asian summer monsoon on the air quality over China: View from space. *Journal of Geophysical Research*, 115(D9), D09301.

Zheng, X. Y., Fu, Y. F., Yang, Y. J., and Liu, G. S. (2015). Impact of atmospheric circulations on aerosol distributions in autumn over eastern China: observational evidence. *Atmospheric Chemistry and Physics*, 15(21), 12115–12138.

Zhou, M., Laszlo, I., Liu, H., Zhou, M., Laszlo, I., and Liu, H. (2018). Preliminary Evaluation of GOES-16 ABI Aerosol Optical Depth Product. *AGU Fall Meeting Abstracts*, 2018, A51G–2229.

Ziomas, I. C., Melas, D., Zerefos, C. S., Bais, A. F., and Paliatsos, A. G. (1995). Forecasting peak pollutant levels from meteorological variables. *Atmospheric Environment*, 29(24), 3703–3711.

LIST OF PUBLICATIONS/ CONFERENCE PAPERS

Journal Publications

- *Satellite-Based Top-Down Lagrangian Approach to Quantify Aerosol Emissions over California. Quarterly Journal of the Royal Meteorological Society Vol-136, Issue-729,Pages:1626-1635. Nizar, S. & Dodamani, B.M., 2020*

- *Spatiotemporal distribution of aerosols over the Indian subcontinent and its dependence on prevailing meteorological conditions. Air Quality, Atmosphere & Health, 12(4), 503-517. Nizar, S. & Dodamani, B.M., 2019*

Conference Proceedings

- *Spatio-temporal distribution of rainfall and aerosols over urban areas of Karnataka. In Remote Sensing of Clouds and the Atmosphere XXIII (Vol. 10786, p. 107860U). (Nizar, S. & Dodamani, B.M., 2018)*

- *Pathak, A. A., Nizar, S., & Dodamani, B. M. (2018, June). Trends in Agro-Meteorological Parameters as Groundwater Exploitation Indicators. In IOP Conference Series: Earth and Environmental Science (Vol. 167, No. 1, p. 012004).(A. A. Pathak et al., 2018)*